Title
Characterization of the Interface between the Mouse Mammary Epithelium and its Microenvironment during Morphogenesis

Author
Brownfield, Douglas Glenn

Publication Date
2011

Peer reviewed|Thesis/dissertation

Characterization of the Interface between the Mouse Mammary Epithelium and its Microenvironment during Morphogenesis

By

Douglas Glenn Brownfield

A dissertation submitted in partial satisfaction of the requirements for the degree of

Joint Doctor of Philosophy

with University of California, San Francisco

in

Bioengineering

in the

Graduate Division

of the

University of California, Berkeley

Committee in Charge:

Professor Mina Bissell, Co-Chair
Professor Daniel Fletcher, Co-Chair
Professor Tejal Desai
Professor Terry Machen

Fall 2011

Abstract

Characterization of the Interface between the Mouse Mammary Epithelium and its Microenvironment during Morphogenesis

by

Douglas Glenn Brownfield

Joint Doctor of Philosophy in Bioengineering with UCSF

University of California, Berkeley

Professor Mina Bissell, Co-Chair

Professor Daniel Fletcher, Co-Chair

In characterizing the interface between the mammary epithelium and the microenvironment, it is necessary to first study specific components individually before interpreting the results in a larger context. With this in mind, the cell-cell component of the interface was first studied with respect to self-organization. Since initial experiments showed significant variance in size and morphology, a unique methodology was employed combining a micropatterning approach that confined cells to a cylindrical geometry with an algorithm to quantify changes of cellular distribution over time in order to measure the ability of different cell types to self-organize relative to each other. Using normal human mammary epithelial cells enriched into pools of the two principal lineages, luminal and myoepithelial cells, experiments demonstrated that bilayered organization in mammary epithelium was driven mainly by lineage-specific differential E-cadherin expression, but that P-cadherin contributed specifically to organization of the myoepithelial layer. Disruption of the actomyosin network or of adherens junction proteins resulted in either prevention of bilayer formation or loss of preformed bilayers, consistent with continual sampling of the local microenvironment by cadherins. Together these data show that self-organization is an innate and reversible property of communities of normal adult human mammary epithelial cells.

Next, the cell-extracellular matrix (**ECM**) component was considered, focusing on the role of extracellular stiffness in both functional differentiation as well as branching morphogenesis. Since functional differentiation of the mammary epithelium involves the production of milk proteins such as caseins, a fluorescent reporter construct with the mouse β-casein promoter was used as a metric for functional differentiation. This system was used for studies in which extracellular stiffness was tightly controlled and cellular stiffness measured and demonstrated a strong association between extra- and intracellular elasticity as well as functional differentiation in mammary epithelial cells (**MEC**s). A benchmark for biomimetic intracellular elasticity

was empirically determined via atomic force microscopy (**AFM**) measurements on normal mammary epithelium and used in subsequent experiments as a marker for the range of normal intracellular elasticity. The results established that maintenance of β-casein expression required both laminin signaling and a 'soft' extracellular matrix, as is the case in normal tissues in vivo, and biomimetic intracellular elasticity, as is the case in primary mammary epithelial organoids. Conversely, two hallmarks of breast cancer development, stiffening of the extracellular matrix and loss of laminin signaling, led to the loss of β-casein expression and non-biomimetic intracellular elasticity. Extracellular stiffness was further plummeted with respect to branching morphogenesis by utilizing a three-dimensional culture model composed of type collagen-I. AFM was used to measure local stiffness of matrices either at invasive fronts or away from cell clusters and found the average stiffness at invasive fronts was nearly half the average measurement far from cell clusters. Further mechanistic studies demonstrated the local softening was MMP-dependent and necessary at sufficient extracellular stiffness to permit branching. Taken together, these results demonstrate that extracellular stiffness is a critical cue of the cell-ECM interface that can regulate various processes.

Finally, from studying extracellular stiffness at the cell-ECM interface [1, 2], it became apparent that matrix organization was critical during branching in collagen I matrices. Initial time course studies demonstrated that local, cellular contractions via the actomyosin machinery generated aligned collagen I tracks at invasive fronts that the multicellular branch co-orient with. Further work, using a novel approach to aligning three-dimensional matrices, demonstrated that aligned collagen I matrices provided a strong directional cue during branching and that cellular machinery for co-orientation was independent from the actomyosin machinery previously mentioned. Orientation analysis in extracted mammary glands provided strong evidence that pre-oriented collagen I tracks exist in the fat pad prior to onset of branching morphogenesis. Moreover, the orientation of the mammary epithelial tree formed during branching morphogenesis is uni-axially biased and co-oriented with the collagen I tracks previously described. Taken together, this study strongly implies the possibility that the fat pad encodes the orientation of the epithelial tree well before branching morphogenesis. Combining the findings from both cell-cell and cell-ECM centric studies gives a greater appreciation for the complexity of decision-making taken on by the epithelium as well as how it must query and alter its interface with the microenvironment during development.

Table of Contents

Table of Figures

Table of Tables

Table of Equations

Nomenclature

7 S	N-terminal cysteine-rich domain
AJ	adherens junction
AFM	atomic force microscopy
BSA	bovine serum albumin
CFP	cyan fluorescent protein
COL	triple-helical domain
CRM	confocal reflection microscopy
CV	coefficient of variation
DAPI	4',6-diamidino-2-phenylindole
DG	dystroglycan
DMEM	Dulbecco's modified eagle medium
DNA	deoxyribonucleic acid
ECM	extracellular matrix
EGF	epidermal growth factor
En	entactin
ER	endoplasmic reticulum
FA	focal adhesion
F-actin	filamentous actin
FACIT	fibril associated collagens with interrupted triple helices
FACS	fluorescence-activated cell sorting
FITC	fluorescein isothiocyanate
FX	focal complex

GH	growth hormone
HMEC	human mammary epithelial cell
HNK-1	human natural killer-1
IGFI	insulin-like growth factor 1
LEP	luminal epithelial cell
LG	laminin globular domain
LM1	laminin $\alpha 1\beta 1\gamma 1$
LN	laminin N-terminal domain
MT	magnetic tweezers
MEC	mammary epithelial cell
MEP	myoepithelial cell
MLCK	myosin light chain kinase
MMP	matrix metalloproteinase
mRNA	messenger ribonucleic acid
NC	nontriple-helical C-terminal domain
Nd	nidogen
OI	osteogenesis imperfecta
OT	optical tweezers
PBS	phosphate buffered saline
PDMS	polydimethylsiloxane
PE	phycoerythrin
SED	spondyloepiphyseal dysplasia congenital
SEM	scanning electron microscopy

TCP tissue culture plastic

TDLU terminal ductal lobular unit

TEB terminal end bud

TGFβ transforming growth factor beta

TFM traction force microscopy

TRP transient receptor potential

Symbols

α	cantilever tip half angle
c	collagen concentration
D	differential intensity
d	deflection
E	Young's modulus
ε	mesh size
F	punch load
F_{el}	elastic force
I_n	pixel intensity
k	spring constant
L_e	length between entanglements
δ	indentation
υ	Poisson ratio
x	distance
z	piezo position

Acknowledgements

My training and work during my graduate career would not have been possible without a veritable plethora of people who assisted me in a great number of ways, starting with my family and friends as well as the great people in the Bissell Laboratory and UC Berkeley. Specifically I would like to thank Mina Bissell and Dan Fletcher for mentoring me, the NSF and NIH for funding me. Former and previous lab members that trained and supported me, such as Mark Labarge, Jordi Alcaraz, Celeste Nelson, Genee Lee, Rana Mroue, Kandice Tanner, Aaron Boudreau, Jimmie Fata, Saori Furata, Jamie Bascom, Alvin Lo, Rick Schwartz, and Keith Vann. I have these people and others to thank for their time and patience that took in working with me. I would like to acknowledge the administrative staff of my lab as well as in the Joint Graduate Group in Bioengineering for there never ending supply helpfulness and positivity as well as all the amazing facilities managers, such as Holly Aaron at the Molecular Imaging Center and Michelle Scott who runs the LBNL FACS facility. A great deal of my momentum to complete this degree arises from all the interesting conversations and support from friends and fellow graduate students at UCB and for that I am thankful, especially to Robin Held and Weston Whitaker, who went up and beyond in helping me on this project.

I want to thank everyone who made getting this degree possible, including all the fantastic teachers I had growing up at Barbers Hill, Tulane, as well as Baylor College of Medicine (especially Gayle Slaughter!). The last acknowledgement is to my family whose support is the main reason why I am where as well as who I am today. Thank you, I am eternally grateful.

Curriculum Vitae

Douglas Glenn Brownfield

Life Sciences Division
Lawrence Berkeley National Laboratories
One Cyclotron Road, MS 977R222G
Berkeley, CA 94720
(510) 684-7861
dbrownfi@gmail.com

Education

August 2005 - Present — **University of California, Berkeley** (UCB)
University of California, San Francisco
Joint Graduate Group in Bioengineering
Ph.D., Bioengineering, minor in Management of Technology

August 2001 - July 2005 — **Tulane University**, New Orleans, LA
Department of Biomedical Engineering
B.S., Biomedical Engineering
"Quantification of atherosclerotic lesions using Magnetic Resonance Imaging"

Employment History

December 2005 – Present — **Mina J. Bissell** Ph.D., Distinguished Scientist
Daniel A. Fletcher Ph.D., Faculty Scientist
Lawrence Berkeley National Laboratories, Berkeley, CA
Life Sciences Division
Graduate student

May 2004 – August 2005 — **Joel D. Morrisett** Ph.D., Professor
Baylor College of Medicine, Houston, TX
Department of Biochemistry
Consultant/ Summer intern

May 2003 – August 2003 — **Margaret A. Goodell** Ph.D., Professor
Baylor College of Medicine, Houston, TX
Stem Cells and Regenerative Medicine Center
Summer intern

Teaching Experience

Fall 2007 — **Optics and Microscopy**, UCB
Daniel A. Fletcher Ph.D., Professor

Led discussion sections, graded coursework, and developed the final project

Awards and Honors

- National Science Foundation Graduate Research Fellow (2006)
- Graduate Research and Education in Adaptive Bio-Technology Grant Finalist (2009)
- Biomedical Engineering Honors Program, Magna Cum Laude (2005)
- Baylor College of Medicine's Summer Medical and Research Training internship (2003, 2004)
- Tulane University Distinguished Scholar Award (2001)
- Citizen's Scholarship Foundation Award (2001)
- Teagle Foundation Scholar (2001)
- Warren Petroleum Scholar (2001)

Achievements and Technical Skills

- Invented a method of aligning collagen matrices for 3D culture assays
- Maintained and isolated tissue from normal and transgenic mice strains
- Developed novel fluorescent probes for detecting collagen
- Developed a method for analyzing angular orientation of branching structures
- Developed a method for quantifying fiber orientation
- Generated novel recombinant tools to study mechanisms of branching in 3D culture
- Developed a method to quantify degree of sorting between populations in 3D culture
- Investigated mechanical properties of different human mammary epithelial cell types
- Characterized mechanical properties of biological matrices

Cytometry & Microscopy: Advanced training on an 8-color FACS sorter, advanced user of Zeiss 710 LSM for live and fixed sample imaging, two-photon imaging, long (~3 day) time-lapse of 3D embedded cultures, FRET, photoablation, photoactivation, and atomic force microscopy

In vivo: Maintenance of normal and transgenic strains, mammary gland extraction, isolation of mammary epithelial tissue for 3D culture studies and primary cell isolation, mammary anlagen removal for cleared fat pad cell injection studies

Cell culture: Maintenance of human and murine cell lines as well as primary cultures, 3D embedded culture assays, plasmid transfection, lenti/retro/adeno-viral transduction as well as subsequent antibiotic selection and FACS sorting

Computation: Matlab (image transformation, analysis, and modeling), ImageJ, Java (macros/plugins for ImageJ), Multitime (Zeiss plugin), SigmaPlot, Graphpad prism, Imaris, FACSDiva, Autocad, Comsol Multiphysics

Molecular: PCR (reverse transcription, site-directed mutagenesis, complex overlap-extension), general plasmid construction (fusion proteins, his/myc/etc tagging, Cre/Lox recombination systems, shRNA and miRNA) and optimization, lenti/retro/adeno-viral production, mRNA isolation/cDNA conversion for qPCR, protein expression and purification, fluorophore conjugation, preparatory ultracentrifugation, Western blot analysis, immunofluorescence (OCT and paraffin), and immunoprecipitation

Publications

Brownfield D, Venugopalan G, Lo AT, Fletcher DA, Bissell MJ. "Directional patterning of the mammary epithelium utilizes Fascin1-dependent sensing of the pre-established collagen microenvironment." In preparation.

Alcaraz J, Mori H, Ghajar C, **Brownfield D**, Galgoczy R and Bissell MJ. "Collective epithelial cell invasion overcomes mechanical barriers of collagenous extracellular matrix by a narrow tube-like geometry and MMP14-dependent local softening." *Integr. Biol.*, 2011 Oct13; Epub ahead of print.

Chanson L*, **Brownfield D***, Garbe JC, Kuhn I, Stampfer MR, Bissell MJ, Labarge MA. "Self-organization is a dynamic and lineage-intrinsic property of mammary epithelial cells." *PNAS*. 2011 Feb 22; 108(8):3264-9. *Authors contributed equally to publication.

Alcaraz J, Xu R, Mori H, Nelson CM, Mroue R, Spencer VA, **Brownfield D**, Radisky DC, Bustamante C, Bissell MJ. "Laminin and biomimetic extracellular elasticity enhance functional differentiation in mammary epithelia." *EMBO J*. 2008 Nov 5; 27(21):2829-38.

Martin K, **Brownfield D**, Karmonik C, Sanford L, Torres L, Insull W, Morrisett J. "Short-term tracking of atherosclerosis in operated and unoperated human carotid arteries by high resolution magnetic resonance imaging." *World J Surg*. 2007 Apr; 31(4):723-32.

Interests

Homebrewing (Belgian and American ales), SCUBA, skiing, and hiking

Chapter 1 – Hypothesis and Specific Aims

1.1 Introduction

For over 400 years, the mammary gland has fascinated biologists and inspired scientific research. Besides being responsible for milk production, the mammary gland is distinct in that it undergoes the majority of its development postnatally, making it a model amenable to cell and developmental biologists for studying aspects of plasticity and morphogenesis. Much work has shown the importance of the extracellular matrix during various steps in mammary development as well maintenance of a normal, nonmalignant phenotype. In recent years, particular focus has given on the mechanical properties of the microenvironment, demonstrating the need for different approaches in attaining further mechanistic insight regarding the interface between the mammary epithelium and the surrounding microenvironment.

Several questions remain regarding the development and maintenance of the mammary gland, particularly around how the epithelium interprets the extracellular milieu. A few questions of particular interest for this dissertation are 1) How do the main epithelial lineages sort into a bilayer? 2) How does the epithelium interpret exogenous mechanical cues? 3) How does the epithelium interpret differences in extracellular matrix organization? To answer such questions, new techniques and quantitative methods need to be developed; either because current experimental models have limitations hindering deeper mechanistic studies or that simply the necessary materials do not exist.

1.2 Objective

This dissertation seeks to both develop and employ new methods to study the interface between the microenvironment and the epithelium. Within this dissertation, three main hypotheses exist and each will be the focus of subsequent chapters. To start, we first characterized the interface between the different epithelial lineages of mammary gland, each are intimate components of one another's microenvironment, especially in maintaining a normal, polarized structure. We hypothesize that cell sorting within the resting human mammary epithelium is lineage dependent. Specific Aim A details the approach that was developed in testing this hypothesis as well as further work in determining a molecular mechanism as well as the dynamic nature of self-organization. Next we progressed into studying the role of the extracellular matrix stiffness during normal mammary development. To that end, we hypothesize that extracellular stiffness has a dynamic and reciprocal relationship to both functional differentiation and branching morphogenesis. Specific Aim B details the collaborative approach we chose to measure and modulate extracellular stiffness in pre-existing culture models for studying functional differentiation and branching morphogenesis of the mammary gland. Finally, from the previous study, we began to appreciate the role of extracellular matrix organization during branching morphogenesis. We hypothesize that the orientation of the mammary epithelium is determined by pre-oriented type I collagen tracks that impart directional cues during branching morphogenesis. Specific Aim C

explains the novel methods for characterizing mammary gland orientation as well as determining molecular mechanisms for directional determinacy using three-dimensional culture models.

1.3 Specific Aims

1.3.1 Specific Aim A – Characterization of the lineage-dependent sorting between human mammary epithelial cells.

In this aim, we sought to observe and quantify the sorting of different human mammary epithelial cells (**HMEC**s). Towards that end, we developed a method to extract different epithelial lineages from normal human mammary tissue as well as a three dimensional culture model to visualize and quantify sorting between lineage mixtures. From there we crafted experiments to determine which cell surface molecules are involved in lineage-specific sorting. Further characterization was carried out to test the role of cellular stiffness in sorting, as well as to test whether regulators of the actomyosin cytoskeleton were also implicated in self organization. Finally, experiments to discern between mechanisms necessary for the establishment versus maintenance of sorting were carried out.

1.3.2 Specific Aim B – Characterization of the extracellular stiffness in mammary gland development.

For this aim, the goal was to determine the impact of extracellular stiffness in various stages of mammary gland development. First we measured stiffness in various extracellular matrices as well as cellular stiffness of different mammary epithelial cell lines. To observe differences in functional differentiation, we observed changes in milk expression in attached, floated, and variable stiffness states. Next, we wished to observe differences of branching with respect to type I collagen stiffness as well observe local changes in stiffness during branching. In looking for a molecular mechanism, we utilized various tools to determine the role of matrix degradation in modulating stiffness during this process.

1.3.3 Specific Aim C – Characterization of matrix organization during branching morphogenesis.

The final aim involves probing the role of matrix organization during branching morphogenesis. Partially inspired from results from the previous aim, we wished to observer the orientation of the type I collagen as well as epithelium within the fat pad at different stages of branching. Furthermore, we developed a three dimensional culture branching model for testing the sensitivity to matrix alignment. Finally, we focused upon experiments to indicate particular cellular machinery involved in sensing and following type I collagen tracks.

1.4 Organization

This document outlines three focused yet interlocking studies that, taken together, shed light on how the mammary epithelium interprets its microenvironment during its development. As such, these studies separate nicely into individual chapters detailing how the study was conceived, developed, and executed towards characterizing each interface as well as ascertaining possible underlying molecular regulators.

Chapter 2

The first chapter gives a general review of relevant literature, both classic and current. As this dissertation details work that is highly interdisciplinary, the introduction will have three main parts. A significant portion of said introduction focuses around the organization, development, and disease of the mammary gland, both human and mouse. This information should be useful to those with little background in this field, both for development as well as cancer progression and will be relevant for all chapters. The next section covers key extracellular matrix proteins, specifically laminin and collagen, which are studied within Chapter 4 and 5 of this dissertation. Characteristics such as structure, function, expression, previous relevant work, and disease implications will be introduced. The final section will go over all relevant methods for mechanical characterization as well as fabrication, optical, and quantitative techniques as generally needed and taken together are relevant for all chapters. Background from the mammary gland, cellular biology, as well as cellular mechanics field provides the motivation for all subsequent chapters.

Chapter 3

This is the first chapter delving into our experimental work. We start with a smaller, more focused introduction and methodological description, a format that will be repeated in Chapter 4 and Chapter 5. Here we give a detailed description of how cells are isolated from reduction mammoplasties and sorted by known lineage markers. Initial attempts using previously existing models for cell sorting were attempted and were found not amenable to quantitative analysis. A novel method using microfabrication technologies to stamp microwells was developed and yielded better results, much more amenable to quantification. Coupling FACs analysis to determine relative amounts of proteins on the cell surface with inhibitor studies; we are able to conclude that lineage-dependent sorting occurs via differing levels of E-cadherin and that regulators of the actomyosin skeleton play different roles in establishment and maintenance of the sorted phenotype.

Chapter 4

Chapter 4 focuses upon the role of extracellular matrix stiffness on two stages of mammary gland development. Initially, we sought to measure differences in stiffness of the various extracellular matrices as well as mammary epithelial cell lines and tissues. From there we modulated extracellular stiffness in a variety of ways and measure the

effect on functional differentiation via changes in milk production. We found that there is an optimum amount of laminin as well as stiffness for maximum functional differentiation and that differences between cell lines could be from differential expression of integrins. The second half focuses on differences of stiffness during branching within type I collagen matrices. We were able to observe that mammary epithelial cells require proteins capable of degrading type I collagen to locally soften the matrix and that the inherent stiffness of the matrix affected the efficiency of branching.

The final experimental chapter focuses on the role of extracellular matrix organization during branching morphogenesis. Specifically, we develop a novel probe to visualize type I collagen in the mammary gland, and find pre-oriented tracks of type I collagen prior to the start of branching. This orientation aligns to the epithelial orientation observed by the end of branching morphogenesis, indicating these tracks play a role in determining the final architecture of the gland. A novel three dimensional culture model was developed to determine a causative role of type I collagen fiber orientation to branching orientation. Further work demonstrates the role of known filopodial components in sensing matrix organization as well as the role of the actomyosin machinery in generating local areas of alignment.

Chapter 5

In this chapter we summarized the conclusions from the previous 3 key chapters and dissect key points as well as areas that need further study. Potential future directions will be brought up and discussed.

Chapter 2 – Background and significance

While the past century of scientific inquiry into the development and maintenance of life on various size and time scales has garnered a great deal of knowledge, the answers of many broader questions remain: What are the principles underlying tissue generation? Once generated, how is that specificity maintained? What is the overlap between such mechanisms? In attempting to answer these questions, biologists have found the mammary gland useful for its unique characteristic of undergoing the majority of its development postnatally. Below is a fairly succinct background regarding the structure, function, development, and disease of the mammary gland. Since this dissertation will also focus on the extracellular matrix, a background section regarding the discussed components is also listed with necessary information regarding structure, function, and known regulation. Finally, critical bits regarding cellular mechanics will be given for readers that are unfamiliar the methods and key literature in the field that also motivates the work with this dissertation.

2.1 – The mammary gland

2.1.1 - Morphology

The adult, virgin mammary gland can be divided into two main compartments: the ectodermally-derived epithelium with its arboreal architecture whose purpose is the production and transport of milk; and the mesodermally-derived stroma, which encapsulates and interacts with the epithelium. Within the epithelium, two epithelial subtypes exist: luminal cells which are cuboidal that are known to undergo functional differentiation upon pregnancy and secrete key components of milk into the ductal lumens; myoepithelial cells are basal, that is they separate luminal cells from the stroma, and form a mesh-like basket which assists in milk delivery during lactation by contracting the epithelium, schematically shown in Figure 2.1. The synchronized contractions of the myoepithelium is induced by suckling and leads to the concentration of milk into the main ducts and terminating at the nipple, except in the case of monotremes, the group of mammals that lay eggs. Throughout the epithelium, both in its resting and pregnant state, there exists an apical-basal polarity, characterized by the lumen as the innermost layer followed by luminal cell layer and finally the myoepithelial layer. Of course, the epithelium is tubular, with the polarized configuration forming ducts for milk collection, while the terminating ends give rise to lobular structures defined as terminal ductal lobular units (**TDLU**s) that will beget alveolar buds during that are the main secretory alveoli during lactation.

The stroma is rich in its diversity of cell types that comprise it, with the main component being adipocytes, giving the non-epithelial component of the mammary gland its name, the fat pad. Fibroblasts, vascular and neural cell types play an integral role in the development and maintenance of the mammary gland as well. The stromal component comprises 80% of the volume of the human breast [3]. Subtle differences exist between the stromal compositions of the mammary gland of different species. The most pertinent to note would be that the mouse mammary gland is composed from a

higher percentage of fat cells when compared to the human breast, which is has a higher amount of non-fat stroma, such as fibroblasts and extracellular matrix.

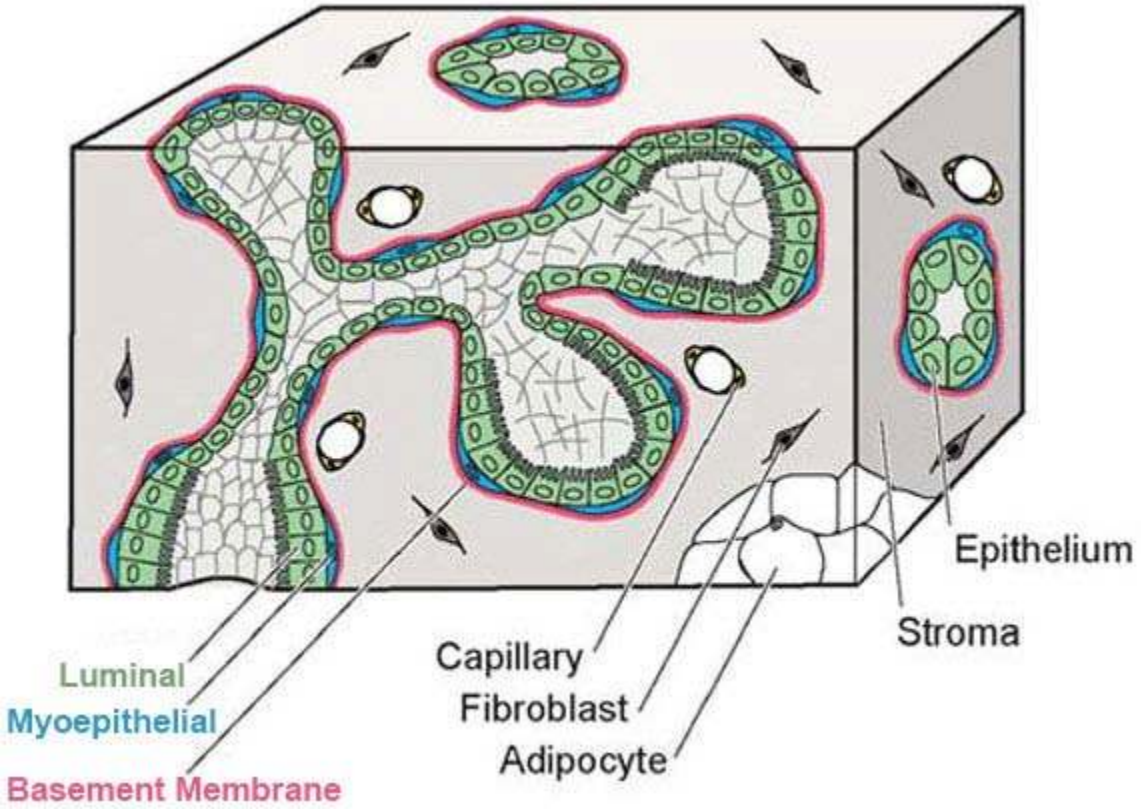

Figure 2.1. Schematic of the mammary gland and its components. The epithelium consists of a luminal epithelial layer surrounded by a mesh-like layer of myoepithelial cells and basement membrane. A fibrous stroma encapsulates the epithelium and connects it to the adjacent fatty stroma (figure adapted from [4]) .

2.1.2 – Development

Mammary Embryogenesis

As first observed in 1933[5], the initiation of the mammary gland appears in 10-11 day embryos as a distended single-layer ectoderm, referred to as the mammary streak, that runs between the anterior and posterior limb bud on either side. By day 12, embryos show what is then referred to as a mammary bud, when the initial rudiment begins to form several layers of epidermal cells; creating more of a lens-like morphology which distinguishes is from the surrounding embryonic tissue. A bit of controversy occurred over the mechanism of bud formation, with the initial explanation relying on unequal cell proliferation within the mammary line. However, in 1950 quantitative experiments demonstrated a relative decrease in proliferation when compared to the surrounding epidermal tissue, suggesting proliferation was insufficient in regulating such a dramatic change in morphology [6]. Finally, the prevailing postulation in the field, that substantial cell migration explained the shape change, was confirmed in 1978 via scanning electron microscopy (**SEM**) in the rabbit mammary gland, suggesting that

epidermal cell migration played a fundamental role in various stages of mammary gland embryogenesis [7]. By the 14th day of gestation, the lens-like structure of the primary mammary tissue takes on a more bulb morphology, best characterized by a narrow neck pointing into the mesenchyme, with irregular-shaped cells filling the central portion.

A distinctive change in mammary development occurs between male and female embryos by day 13-14, a time in which sexual differentiation occurs in the gonads of males as well as the production of androgen in the testes. Fetal androgen causes an inhibition of growth of the mammary sprout, as seen by a loss in volume and change from round to spindle epithelial morphology. A burst of the epithelial stalk is typically seen in the male mammary bud by day 15 due to extreme narrowing, leaving the residual rudiment separated from the epidermis and buried in the fat pad as a blind duct. There are variations by strain and species to the degree of mammary gland formation in males, where within some mice strains half the male mice completely lack mammary glands. Alternatively, the mammary glands of male rats develop similarly to females but have no external connection to the epidermis.

For the female counterparts, there is a lack of sexual differentiation as well as slower growth, deemed the resting phase, that lasts from day 11 to 16 of gestation. From late day 16 to 17 of gestation, the sprout undergoes a substantial increase in proliferation, leading to an elongated morphology. This sprout grows rapidly away from the epidermis into the fat pad precursor tissue, within which it branches. In the time window of day 17 until birth, a progression of branching occurs, resulting in the initial mammary tree of 15-20 ducts. This arboreal architecture is maintained from birth until puberty, with the majority of mammary gland growth being isometrically in the stromal compartment. The embryonic stages and differences by sex of mammary gland development are depicted below in Figure 2.2.

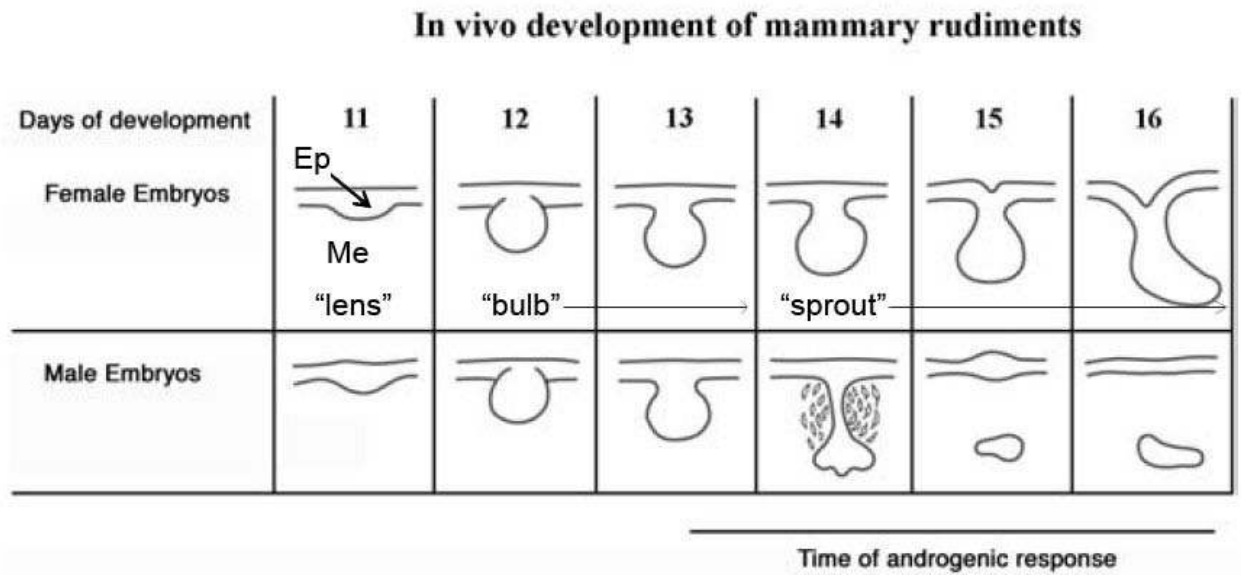

Figure 2.2. Stages of embryonic mammary gland development, indicating how the epithelium (Ep) interfaces with the mammary mesenchyme (Me). Differences between the male and female embryo progression are also depicted (adapted from [8]).

Postnatal Mammary Development

Starting from puberty, 3-4 weeks after birth for the mouse, end buds reappear at the termination points of neonatal epithelium. From there, both rate and amount of branching growth dramatically increases [9] and becomes allometric. For rats, it has been shown that the occupied area of the fat pad by the mammary gland increases 1.13 and 3.92 times faster than the body surface area between 10 and 20 and 23 and 40 days of age, respectively [10]. The period in mammary development is referred to as branching morphogenesis and is initiated by mammotrophic signals from the hypothalamic-ovarian-pituitary axis [11]. As is the case in the growth of other tubular branched tissues [12], the epithelium elongates as they invade into an adipocytes-rich stroma from the bulbous structures, named terminal end buds (**TEB**s), located at the ductal forefront [13]. Epithelial-stromal crosstalk necessary during branching morphogenesis is co-regulated both by growth hormone (**GH**) activation of stromal insulin-like growth factor 1 (**IGFI**) as well as ovarian estrogen mediated release of epithelial amphiregulin [14]. As these swollen TEBs fill the fat pad, spacing of the epithelial tree is determined by a series of bifurcations that evenly space out the ducts. Separate from this process is what is referred to as secondary and tertiary branching, that occurs from lateral bud sprouting that occurs well after initial branching has ceased in the vicinity [15, 16]. Branching morphogenesis ends as the epithelium reaches the edges of the fat pad, a mechanism that is at least partially mediated by transforming growth factor beta (**TGFβ**) signaling [14].

Once formed, the adult female mammary gland undergoes cyclic remodeling concomitantly with the reproductive cycle. Lobuloalveologenesis, a rapid increase in polarized alveoli, occurs during the murine diestrus, with the human analog occurring at the luteal phase [17]. Besides morphological differences, this phase also displays increases in cell proliferation and death, which reach their apex at diestrus. Lateral branching during this period has the added steric hindrance of deposited ECM and must engage and promote locale remodeling on the microenvironment.

Both progesterone and pituitary-derived prolactin are critical in conducting mammary epithelial differentiation during pregnancy [18, 19]. In response to the postcoitum maintenance of the corpus luteum, progesterone levels rise. Resulting from these changes is a dramatic increase in epithelial proliferation and differentiation, approximately ~100 fold increase in cell number. Differentiation leads to a furthering of polarization and secretion during a mere 19 days of gestation in mice. Within this phase, the adipocyte to epithelial cell number dramatically drops, furthering the expansion of the parenchyma. The transition from pregnancy to lactation involves a good number of hormones, though the best indicator is a drop in progesterone, which causes a promotion of myoepithelial contraction for milk ejection. Systemic maintenance of this state has been demonstrated to occur through new-born suckling [20, 21]. The final stage is involution, which when either studied through forced or natural weaning, is characterized by rapid loss of about 50%-80% of the differentiated epithelium. This process seems highly dependent on cell death pathways and occurs quickly, within 1 week [22]. Milk stasis initiates the first step in involution, in which it is

mechanically triggered and reversible [23]. The second, more permanent step involves the specified disassembly of lobuloalveolar structures as well as degradation of the surrounding ECM [24, 25]. The deflated alveoli form cords which overall return the mammary gland morphologically to its pregestation state. During this second step, many extracellular proteases are expressed to remodel the microenvironment which ultimately leads to a restoration of the adipocyte compartment.

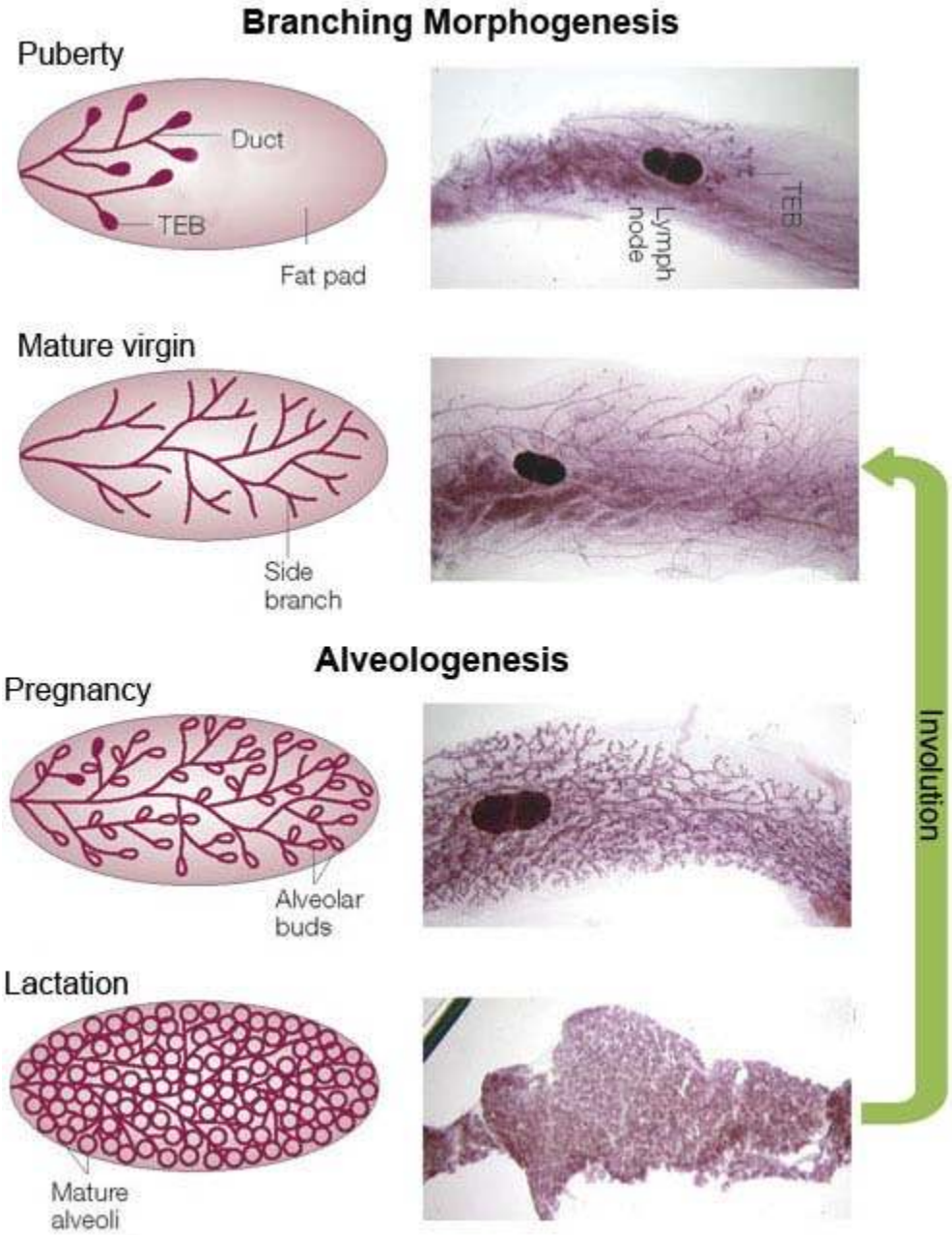

Figure 2.3. Schematic and wholemounts at different postnatal mouse mammary gland states adapted from [26]. During puberty, hormone production accelerates ductal outgrowth, forming a regularly spaced system of ducts. Upon pregnancy, hormones increase alveologenesis. During lactation, alveoli are fully matured and the luminal cells synthesize and secrete milk into the lumina. Afterwards, dramatic alveolar regression occurs during involution that reverts the gland to a state similar to the mature virgin.

2.2 – The extracellular matrix

Originally thought only to house the cellular components of various tissues[27], the ECM continuum of secreted factors that makes up the acellular fraction of the microenvironment has been shown to direct aspects of cellular behavior. The ECM usually is quite diverse in composition, with large macromolecules like collagens, fibronectin, and laminins as well as polysaccharides such as the glycosaminoglycan, hyaluronan. One key study demonstrated that deoxyribonucleic acid (**DNA**) synthesis within endothelial cells was intimately related to the degree of spreading and attachment to a given surface [28]. The common ECM component, Collagen, has also been shown with various cell types, such as myoblasts and corneal epithelium, to be critical in dictating aspects of morphology, cell-cell interaction, and differentiation [29, 30]. Of important note for this dissertation is the study using mammary epithelial cells (**MEC**s) derived from pregnant or lactating mice [31] in which a failure to respond to lactogenic hormones and produce milk proteins was observed upon growth on tissue culture plastic (**TCP**). However, when cultured upon floating collagen gels, thought to more accurately mimic the mammary gland microenvironment, MECs dramatically increased in both response to cues and secretion of milk proteins. Because of these and other studies, the perception of the ECM and microenvironment changed from a mere scaffold to a key component for bidirectional crosstalk. Specifically, the nuclear compartment interacts with the cytoskeletal compartment which interacts with the membrane compartment which interacts with the extracellular world. Moreover, components of the ECM can signal and alter aspects of the cell-interior components and conversely, the cell can secrete and remodel the ECM. Taken together, the perception changed to one now commonly referred to as "dynamic reciprocity" [32]. Below is a somewhat brief introduction to the main ECM components discussed in the dissertation, collagen I and laminin.

2.2.1 – Collagens

Categorization and Structure

The initial appreciation for collagens arose from their structural role, particularly type I collagen in tendons, ligaments, skin, and bone, as well as type II in hyaline cartilage, not to mention type IV collagens in the basement membranes of various tissues. Although collagens make up a superfamily of ECM molecules that is diverse in structure as well as in tissue type, all must fulfill the following criteria [33]: (a) The native protein must contain at least one triple-helical domain, formed by three subunits (α-chains) each containing a $(Gly\text{-}X\text{-}Y)_n$ repetitive sequence motif. (b) The protein must aggregate into supramolecular structures, such as fibers, filaments, or networks. (c) The protein must contribute to the three-dimensional extracellular continuum, directly or otherwise. While many encoded molecules fit this classification, differences in exon structure allows further classification of collagens, as depicted in Table2.1 below, into fibrillar, FACIT, and basement membrane collagens.

In the case of fibrillar collagens, the triple helical domain accounts for almost the whole length of the molecule. This family includes five different molecular types (I, II, III, V, and XI) which contain subunits (α-chains) encoded by at least nine different genes. Within every α-chain is more than three-hundred repeats of $(Gly\text{-}X\text{-}Y)_n$ motif bordered with short nontriplet sequences, referred to as telopeptides, on either end of the glycine rich domain. The supramolecular aggregates of fibrillar collagen members typically occur as a triple helix containing more than one type of collagen [34]. Because of such heterotypic states, collagen fibrils are arranged in different patterns depending on tissue type, such as parallel bundles in tendon, criss-crossing layers in cornea, and spiraled structures in lamellar bone. The heterotypic fibrils with type I, III, and/or V collagens are predominantly found in mesenchymal tissue such as skin, tendon, ligaments, and bone, while types II and XI mainly reside within hyaline cartilage as well as vitreous body of the eye. Cells engage collagen fibers through membrane bound receptors, such as integrins, that either directly or indirectly binds ECM molecules [35].

	Gene Locus	Chain Designation	Chromosomal Location	Reference
Fibrillar	COL1A	1α1(I)	17q21.3-q22	[36]
	COL1A	2α2(I)	7q21.3-q22	[37]
	COL2A	1α1(II)	12q13-q14	[38]
	COL3A	1α1(III)	2q24.3-q3117	[39]
	COL5A	1α1(V)	9q34.3	---
	COL5A	2α2(V)	2q24.3-q31	[40]
	COL5A	2α2(V)	---	---
	COL11A1	α1(XI)	1p21	[41]
	COL11A2	α2(XI)	6p212	[42]
FACIT	COL9A1	α1(IX)	6q12-q14	[43]
	COL9A2	α2(IX)	---	---
	COL9A3	α3(IX)	---	---
	COL12A1	α1(XII)	---	---
	COL14A1	α1(XIV)	**---**	**---**
Short Chain	COL8A1	α1(VIII)	3q11.1-q13.2	[44]
	COL8A2	α2(VIII)	1p.32.3-p34.3	[45]
	COL10A1	α1(X)	6q21-q22	[46]
Basement Membrane	COL4A1	α1(IV)	13q33-q34	[39]
	COL4A2	α2(IV)	13q33-q34	[47-49]
	COL4A3	α3(IV)	---	---
	COL4A4	α4(IV)	2q35-2q37.1	---
	COL4A5	α5(IV)	Xq22	[50]

Table 2.1. Various collagen families, detailing name, chain type, location on the chromosome, as well as underlying reference, adapted from [51].

In the case of type I collagen, the composition is two α1(I) and one α2(I) chain, each chain type is the product of gene, located on chromosome 17 and 7, respectively. Like the majority of fibrillar collagens, the gene contains over 50 exons and there is a stunning amount of similarity of arrangement between exons in the coding region for the triple-helical domains [52] which is independent of species or fibrillar collagen type. It is commonly thought that the triple-helical domains evolved from repeated duplications of an exon unit of 54bp [53]. For most cases of osteogenesis imperfecta (**OI**), characterized by defective connective tissue and brittle bones [54], as well as certain cases of Ehlers-Danlos syndrome, characterized by hyperextension and osteoarthritis [55], the cause is a mutation (deletion or substitution) in type I genes [56, 57], Ehlers-Danlos type IV showing specific mutations in the α1(III) gene [58]. Another, more rare disease known as spondyloepiphyseal dysplasia congenital (**SED**) has been shown to caused by mutations in the α1(II) gene [59, 60], leading to skeletal abnormalities and in most cases, dwarfism. Regardless of type, fibrillar collagens polymerize into fibrils that reinforce the ECM [61, 62]. A 300nm long rod-like fibers overlap with one another with their ends of about 30nm and arrange in a quarter-staggered aggregates, forming bands detectable bv electron microscopy of 67nm, as depicted in Figure 2.4.

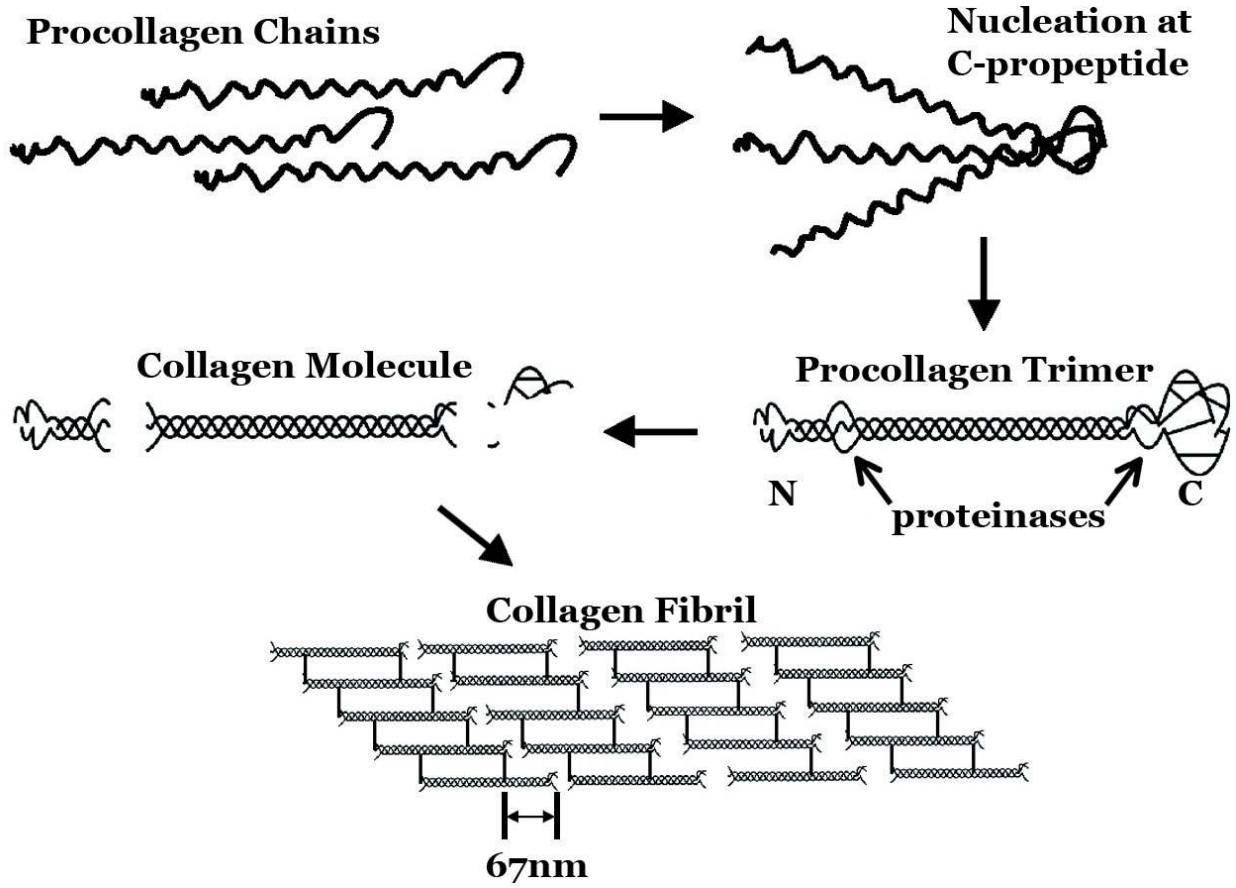

Figure 2.4. Schematic of the process by which collagen fibrils are formed adapted from [63]. Procollagen is made in the endoplasmic reticulum (**ER**), propeptide interactions initiate folding into a rod-like triple-helix. Removal of the N- and C-propeptides from procollagen occurs after exit from the Golgi and allows for self-assembly into fibrils. Links between triple-helical collagen molecules in fibrils stabilize the fibril.

Another family of collagens is the basement membrane collagens, which form a network with one another as well as other basement membrane components, such as laminin, nidogen, and heparin sulfate proteoglycan [64-66]. The genes of this family are thought to have arisen from duplications of a common precursor gene. Basement membrane collagen molecules, also referred to as type IV molecules, also form heterotrimers like fibrillar collagens, but are composed of two α1(IV) and one α2(IV) chain and as expected are the main collagenous component of most basement membranes. Both chain types are around 1,700 amino acid residues long and contain three distinct domains: a cysteine-rich (**7 S**) domain, the obligatory central triple-helical domain, and a non-helical C-terminal domain (**NC1**) [66]. The mechanism and morphology of type IV molecule networks are quite different from their fibrillar counterparts, different molecules are covalently crosslinked within laterally localized 7 S domains as well as by end-to-end associations through NC1 domains [65]. Further network structuring is achieved through tangential links across triple-helical domains.

The final collagen family is the fibril associated collagens with interrupted triple helices (**FACIT**) group. The proposed purpose of this collagen family is to link fibrillar collagens to other ECM macromolecules [67, 68]. This family's collagen structure is dramatically different from the previous two; specifically the molecules contain two or more short triple-helical domains connected by non-helical sequences. Three main collagens of this group are type IX, XII, and XIV, which are made from five different polypeptide chains. Type IX collagens are heterotrimers comprised of an α1(IX), α2(IX), and α3(IX) chains of 84, 160, and 68kDa, respectively [69]. Each molecule contains three triple-helical domains (**COL**) that are flanked by nontriple-helical (**NC**) regions which contain cysteinyl residues that form disulfide bridges across subunits. Of note for type IX is that the α2(IX) chain serves as a proteoglycan core protein around the NC3 domain [69]. The type IX macromolecule is expressed in the hyaline cartilage where it attaches to fibrillar collagens, though it has also been found in the cornea of chickens [67]. Two other FACIT collagens, type XII and XIV, are homologous but distinct homotrimeric molecules, with each subunit consisting of ~220kDa. Each chain contains two COL domains separated by a NC of at least 40 amino acid residues followed by a large NC domain of at least 1,500 amino acid residues. Together, these chains create a macromolecule of a cruciform shape, with the long NC domains creating three of the four extensions [70-75].

Fibril Synthesis

The synthesis of collagen molecules is comprised of six main steps, the majority of which is depicted from Figure 2.4. The first step is the expression of messenger ribonucleic acid (**mRNA**) for each collagen subunit. An approximate total of 34 genes encoding collagen subunits have been discovered. Next, the exiting mRNA enters the cytoplasm to be translated by ribosomes. After the process of translation, the N-terminus of the collagen peptide sequence is recognized by the ER, which directs the molecule into the ER for post-translational modifications, the molecule is now known as a pre-pro-peptide. From here, three modifications transform the alpha peptide to procollagen: 1) The N-terminal signal peptide is cleaved from the molecule, 2)The

enzymes prolyl hydroxylase and lysyl hydroxylase hydroxylate prolines and lysines, respectively, to assist in attaching α-chains to one another, 3) Glycosylation of hydroxylysine groups, thus allowing for the three α-chains to twist and form a triple-helix. The molecule is now referred to as procollagen and is composed of a center twisted region flanked by two loose ends. The procollagen is packaged into a transfer vesicle destined for the golgi apparatus. The fourth step occurs once inside the golgi apparatus, in which oligosaccharides are attached to the molecule before secretion into the extracellular space. The next step is the enzymatic cleavage of the loose ends on the N and C-terminus by collagen peptidases. The final step involves lysyl oxidase, which creates aldehyde groups on lysines and hydroxylysines, allowing for covalent bonding between tropocollagen molecules, successfully polymerizing into fibrils.

2.2.2 – Laminins

Structure and Function

Laminins are a key component of the ECM in almost every animal tissue. A family of glycoproteins, the standard laminin macromolecule, which varies between 400-800kDa, is the product of a heterotrimeric amalgamation of one each of the possible five α, four β, and three γ chains which co-join through a similar coil-coil domain [76, 77]. There is an inherent restriction to the possible combinations of heterotrimers that can form from the charged residues of the coil-coil domain residing in the heptad repeats, allowing only the following combinations: laminins-111 (i.e. α1β1γ1), 121, 211, 213, 221, 311, 312, 321, 332, 411, 421, 422, 423, 511, 521, and 523 [76, 78, 79]. Generally, the laminins mainly separate from one another by composition of the shorter arms of the cruciform macromolecule as specificity or affinity for other ECM molecules or cell surface receptors, depicted in Figure 2.5. Laminins are secreted into the extracellular space, where they then can self-assemble, bind various ECM molecules and cell surface receptors, affect cell differentiation, and maintain tissue phenotype. Laminins are found in the basement membrane and as such bind with a variety of basement membrane molecules, such as collagen IV (previously mentioned), nidogens (entactins), proteoglycans (perlecan, agrin, and bamacan), which also forms complexes with fibronectin and growth factors [80-83]. A brief list of cellular receptors for laminins includes the various β1 integrins, β4 integrins, and dystroglycan (**DG**).

A highly similar feature within all laminin chains is a tandem distribution of globular, rod-like and coil-coil domains, with the last serving the purpose of joining the three chains properly. While the N-termini of the short arm chains have the greatest amount of sequence homology, the majority of diversity between laminin isoforms lies within arm length and domain number of the short arms. These differences are the basis for subgroup designation of laminins, with laminins 1-4, 12 having full complements of domains in each short arms while laminins 6-9 have several truncations in α-subunit but have complete β and γ arms. Modifications during translation as well as secretion can direct proteolytic cleavage upon the G domain as well as short arms of most laminins [84-86]. Interestingly, such proteolysis doesn't cause complete cleavage and may be key in modulating integrin-dependent migration [87, 88].

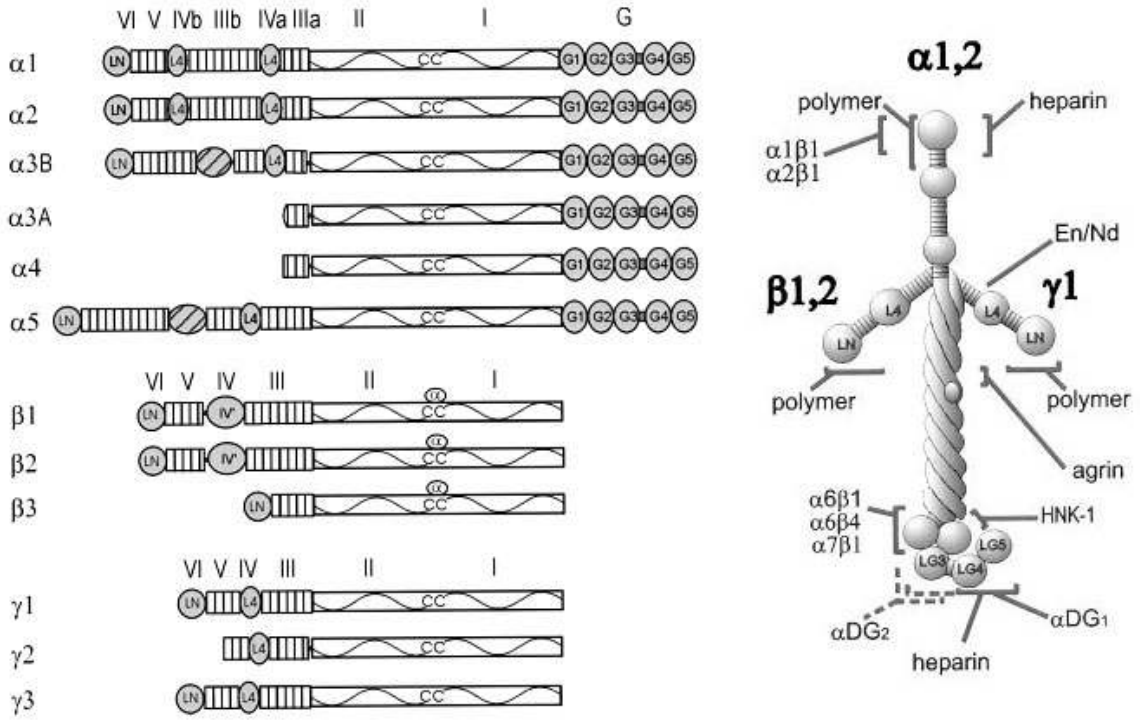

Figure 2.5. Structure of motifs from the various laminin chains as well as the classical macromolecule, adapted from [89]. Each laminin subunit is made from tandem arrays of globular and rod-like motifs. The N-terminal (**LN**, domain VI) and internal short arm globular (L4, domain IV) modules are indicated by ovals. Rod-like epidermal growth factor (**EGF**) repeats are shown as vertical rectangles, while coiled-coil (cc) forming domains are shown with horizontal rectangles containing a wavy line. The C-terminal globular G-repeat (**LG**) modules are indicated as circles. Also shown is the classic cruciform structure of laminin 1 as well as known binding sites for various molecules, such as entactin/nidogen (**En/Nd**) and human natural killer-1 (**HNK-1**).

With regard to embryogenesis, the main laminin expressed is laminin-1 at the earliest stages [90-94]. As early as the blastocyst, the α1 chain is then expressed in a variety of different areas later in development but disappears soon afterwards [84, 95-99]. The N-terminal domains of the short arms are involved in a calcium-dependent reversible polymerization [100-102]. When purified, laminin self-assembles at concentrations around 70-140nM, although this critical concentration is dramatically lower with tissues when laminin interacts with lipid layers during this process [103]. While laminins are able to associate with lipids, the more feasible situation is that they interact with membrane bound receptors. Certain molecules can affect laminin polymerization, such as heparin which binds to G domains, bridging between laminin molecules [104]. Laminin-1 also associates with the ECM molecule nidogen-1 with a relatively high affinity though noncovalent interaction between laminin's rod domain γ1-III (corresponding to the amino acid sequence NIDPNAV) with the C-terminal globule LG3 of nidogen [105, 106]. It is commonly thought that nidogen acts as a tether the surrounding basement membrane, since it has been demonstrated to bind to type IV collagen, perlecan, and fibulin-1, thus stabilizing membrane organization [106-110].

Besides interacting with other ECM molecules, laminin-1 can bind to many cell surface receptors. Of particular note is the amino-terminal of α-chain, which contains

regions that interact with integrins α1β1 and α2β1 which are known to have broad specificity, binding to other ECM molecules like collagens [111-115]. The G domain of laminin interacts with integrins α6β1, α7β1, and α6β4 as well as with α-dystroglycan, a subunit of the dystrophin-glycoprotein complex (**DGC**) [116-121]. Interestingly, integrin α6 has specificity for certain laminin family members [122]. In studying binding sites on laminin molecules, key peptide sequences (e.g., YIGSR, IKVAV, LRE, SINNNR) have been discovered corresponding to domain regions that are critical in mediating cellular interactions [123-127]. However, much controversy grew from these studies, surrounding from the perspective that most of the laminin functions depend on protein conformation, such as with laminin-4 where the amino acid triplet LRE from laminin β2 subunit inhibited axon growth while the full form, in which the LRE is buried, promoted outgrowth [123, 127]. Such differences can be perceived as a discrepancy, but further thought on the complexity of this molecule leads some to believe that laminin-4 could provide a context-dependent signal, in this case mediated by laminin degradation. Laminin-1 has been proposed to be involved in the development of organs such as the lung, kidney, gut, and certain neural circuitry [125, 128-132].

2.3 – Cellular mechanics

As early as 1892 [133] it was postulated that mechanicals forces played a crucial role in biological processes. In this particular case, it was thought that physical loading mediated trabeculae formation and shape in bone development and that is persisted after recovery from fracture [133]. During this era it was also proposed that mechanical forces guided morphological changes in tissues and organs during embryogenesis [134, 135]. Besides the most obvious examples of mechanical forces of biological processes, such as breathing, heart and cardiovascular function, as well as physical exercise, concepts from the past era inferred the possibility of mechanics playing a critical role on the cellular scale. With the technological advances of the past century, scientists and mechanobiologists have found that forces can regulate such cellular processes as proliferation, differentiation, and migration.

2.3.1 – Current understanding

Perhaps not so surprisingly, much work in the field of mechanobiology focuses on applying exogenous forces onto tissue or cultures of bone and vasculature. Attempts to mimic mechanics underlying physical exercise in bone in vitro have shown increases in proliferation, osteogenic differentiation, as well as deposition of bone ECM [136-139]. Experiments in which mechanical stretching representative of pulsatile blood was employed shows dramatic changes in endothelial and smooth muscle cell signaling, proliferation, and release of inflammation factors [140-144].

However, much knowledge has been gathered observing the endogenous mechanical behavior various cell types. The earliest and most telling result can from an experiment in which cells were cultured on a soft substrate, thus allowing these nonmuscle cells to deform and wrinkle the substrate's surface [145, 146]. While this

result was initially controversial, it led to two main points: 1) Almost every cell generates intracellular forces that can be felt by the surrounding microenvironment; 2) these forces are critical for biological processes such as mitosis, migration, and differentiation [147, 148]. Before delving deeper into this topic, the cellular components involved in force generation must be described.

The Cytoskeleton

The cytoskeleton is a highly dynamic and complex scaffold that is fundamental in mechanical force transmission and generation [149]. The main cytoskeletal elements are actin (6nm diameter), intermediate filaments (10nm), and microtubules (23nm), all of which form polymeric structures spanning relatively long regions of a given cell. Monomeric actin in certain contexts can polymerize into filamentous actin (**F-actin**) that when co-formed with myosin molecules, generate contractions. For intermediate filaments, such as vimentin, keratin, and lamin, monomers connect into filaments that tether cellular components like the nucleus and Golgi together, increasing structural integrity. Microtubules arise from the polymerization of tubulin monomers and take the form of hollow tubes that act as tracks for certain motor proteins like kinesins and dyneins [150]. The cytoskeleton and other components within the cytoplasm do not exist in a vacuum but a continuum with the extracellular milieu. The actomyosin cytoskeletal component directly attaches to different parts of the cell membrane as well as with the nucleus [151]. The cytoskeleton assists in connecting the cell membrane bound components to the ECM by bundling at certain surface regions named focal adhesions (**FA**s). Exogenous force applied through this ECM-FA linkage would likely result in deformation of both the ECM architecture as well as the cytoskeleton, not to mention the FA itself. However, it is important to keep in mind the reciprocal nature of this interaction, as forces are generated in the contraction of actomyosin components or the polymerization/depolymerization of microtubules [152, 153]. A given FA is the result on an orchestrated process, starting as a nascent consisting of integrin clusters which either get recycled within a minute or mature into larger clusters deemed Focal Complexes (**FX**s), of which only a small number assembler into their larger FA counterparts [154-156].

Mechanotransductive components

Mechanotransduction between the various biological components has been observed. Starting from the most external, the ECM, forces can unfold quaternary domain-domain structures as well as unstable domains in the case of fibronectin [157]. In the case of TGF-β, application of mechanical force has been shown to expose cryptic sites for binding cellular receptors [158]. Regarding intracellular mechanotransduction, loss of the nuclear scaffold proteins, lamin and nesprin, affects cellular force transduction [159, 160]. A recent study demonstrated a general increase in cytoskeletal tension via an increase of exposed cryptic cysteines mediated by type II myosin contractions [161]. FA proteins, such as talin and p130cas, also have been shown to undergo force-induced unfolding [162, 163], though the contribution to cell signaling remains to be demonstrated. However, mechanotransduction via cell surface receptors

has been shown successfully in ion channels and integrins as well changes in the resulting signaling [149, 164, 165]. In the case of stretch-activated ion channels, forces alter conformation of transient receptor potential (**TRP**) family of channels which leads to a quick calcium influx (<4ms) [166]. Much work has shown interesting interactions between forces and adhesion formation/maturation [167]. Force mediated exposure of binding and/or phosphorylation sites on talin, paxillin, and p130cas that stabilizes nascent adhesions into FXs, and at higher forces matures FXs into FAs [162, 163, 168, 169]. The converse has been shown, in which myosin II is inhibited decreasing tension and a simultaneous disassembly of FAs [170, 171].

Since the mechanotransductive aspects of adhesions occur at the cell-ECM and/or cell-cell interface, varying aspects of the microenvironment, such as density, stiffness, and organization alters the context with which the force is perceived. Previous work with increasing ECM density, ECM stiffness, or RhoA-mediated myosin II activity has shown a decrease in apoptosis and an increase in proliferation [172-174]. Tissue stiffening has also been shown to regulate tumor proliferation, progression, and metastasis while tissue softening related to increased angiogenesis [175-178]. Regarding the cell-cell interface, adherens junctions (**AJ**s) are clusters of cadherins that are properly poised to be mechanosensors between cells. The cytoplasmic regions of AJs are attached to cortical actin filaments via protein complexes partly composed of vinculin, p120, alpha and beta catenin [179]. Exogenous force has been shown to grow AJ size and number while actomyosin-mediated contractions also reinforce AJs, purportedly this feedback is to protect from cell rupture [180-182]. A veritable cornucopia of molecules have been reported within the AJ to be mechanoresponsive, from force-induced unfolding of alpha catenin exposing vinculin binding sites to AJ clustering modulating the balance between Rac and Rho GTPase signaling [183-185]. Recent work has included the aspect of tissue geometry in the spatial control of both cell-cell and cell-ECM mechanotransduction, indicating a patterning role during morphogenesis [186, 187]. Taken together, these studies demonstrate the ubiquitous nature of mechanical forces in modulating biological systems

2.3.2 – Experimental approaches

Measuring cell traction

Initial studies utilized soft substrates, specifically thin silicone membranes, to observe mechanical behaviors of single cells, though was unable to quantify forces [145]. Recent work makes use of traction force microscopy (**TFM**), a method that uses fluorescent microbeads embedded in a polyacrylamide matrix for accurately tracking deformations from adherent cells and calculating cell generated forces [188-190]. Issues underlying the chemistry of crosslinking of hydrogels, mainly inadvertent changes of surface hydration, chemistry, and adhesiveness, has led others to use elastomeric cantilever posts to quantify cell forces on soft surfaces [191, 192]. With either method, the main observations have been that cellular tension increases with substrate stiffness and cells constantly apply tensile forces towards its centroid [188, 191, 193].

Surface restriction and pharmacologic inhibitors

Another critical technology for studying mechanotransduction has been microfabrication, which has allowed scientists to restrict cell spreading and migration, demonstrating the role of surface restriction on growth arrest and differentiation [194]. Combined with the previously mentioned micropost technology was able to demonstrate that surface restriction limited the ability of cells to generate traction forces [191], inferring a mechanoregulated loop between spreading and proliferation [174]. Another tool for parsing out mechanisms of mechanotransduction is pharmacologic inhibitors for molecules such as myosin light chain kinase (**MLCK**, inhibitors ML-7 & ML-9), Rho GTPase (C3 botulim exotoxin), Rho-associated coiled-coil containing protein kinase (**ROCK**, inhibitor Y27632), as well as actin (latrunculin & cytochalasin D). Of course, these have been used in combination and surface restriction is not limited to only two dimensions, such is in a study detailing the mechanisms behind lineage specific sorting of human mammary epithelial cell types [195].

Local force application

A significant amount of work has utilized methods in which local applications of force on single sites of adhesion can be finely exerted, such as magnetic tweezers (**MT**s), optical tweezers (**OT**s), and atomic force microscopy (**AFM**). While MTs can exert forces between 0.05pN-150pN and have been used to study molecules as well as transmembrane integrins [149, 162, 196, 197], OTs range from 0.1-100pN and have been used to study motor proteins such as kinesin, myosin, and dynein [198-200] as well as observe cytoskeletal stiffening from restraining forces [201]. AFM has been readily adopted for its wide range of force application of 5-10,000 pN to study protein unfolding as well as whole cell and even cell-cell mechanics [202-206]. Briefly, AFM utilizes piezoelectric elements that facilitate tiny but accurate and precise movements of a cantilever, the deflection of which can also be measured by the concomitant deflection of a laser beam reflecting off the cantilever onto a photodiode. In short, AFM is useful in determining mechanical properties of cells as well as biological matrices.

Chapter 3 – Lineage dependent sorting

3.1 - Introduction

In characterizing the interface between the microenvironment and the mammary epithelium, it is necessary to assess the cell-cell component. Besides the necessity of proper junction formation and localization for epithelial polarization and milk production, the cell-cell interface is critical in tissue repair within adult tissues. Most mammalian adult tissues are replenished and repaired throughout life by reservoirs of stem cells. As new somatic cells replace old ones or build new tissue, organization and architecture must be maintained. The alternative, loss of organization in adult tissues, is associated with cancer and other diseases. The goal of this work was to determine key factors of the cell-cell interface in proper mammary tissue assembly. Lineage-specific progenitors or their differentiated progeny must have a means to reach their ultimate site of residence within the adult tissue. The robust ability to organize cells into tissues is marked from conception: Heterogeneous aggregates of dissociated cells from embryonic tissues, suspended in gels or hanging droplets or on agarose-coated plates, self-organize into semblances of the original tissues [207-211]. The mechanisms governing self-organization during developmental morphogenesis [212-215] are likely conserved in the maintenance of organization in adult tissues. Here we use normal human mammary epithelial cells (**HMEC**) as a model to determine how organized states are preserved in normal adult epithelia.

3.2 - Methods

Cell Culture

HMEC strains were established and maintained according to previously reported methods [216, 217]. Briefly, a pre-stasis cell strain was derived from reduction mammoplasty tissue from a 21-year-old woman (specimen no. 184) with no detectable breast epithelial cell pathology. The fresh surgically removed tissue was processed for separation of epithelial organoids from stromal components. Purified epithelial clusters, named organoids, were stored frozen in liquid nitrogen until primary cultures were initiated and strains isolated. Cells were maintained in M87A medium and used for assays at fourth and fifth passages; the pre-stasis strain 240L was the only strain used for self-organizing and binding assays.

Flow Cytometry Sorting and Assays

HMEC at fourth or fifth passage were trypsinized and resuspended in medium. For enrichment of luminal epithelial cells (**LEP**s) and myoepithelial cells (**MEP**s), anti–CD227- fluorescein isothiocyanate (**FITC**) (clone HMPV; BD) or anti–CD10-Phycoerythrin (**PE**) (clone HI10a; BioLegend) was added to the medium at 1:50 for 25 min on ice. HMEC then were washed in phosphate buffered saline (**PBS**) and fluorescent-activated cell sorted (**FACS**) on a FACS Vantage DIVA (BD) into individual

medium. E-cadherin expression on LEP and MEP populations was measured by addition of anti–E-cadherin-A647 (clone 67A4; Biolegend) to the above mixture at 1:50.

Microwell Self-Organization Assay

Micropatterned substrata were made according to Tan et al. [218]. Briefly, polydimethylsiloxane (**PDMS**) microwell arrays were formed by curing prepolymer with base:cure ratio of 10:1 (Sylguard 184) against a prepatterned master. The arrays of wells were peeled away and were cut into 1-cm^2 pieces that were affixed with a few microliters of uncured PDMS to the bottom of a 24-well plate (Mitek). Plates with microwells were ultraviolet (**UV**) light oxidized for 7 minutes (UVO-Cleaner 42; Jelight Co.), blocked with 2 mg/mL bovine serum albumin (**BSA**) (Sigma) for 1 hour under vacuum, and rinsed with PBS and M87A.

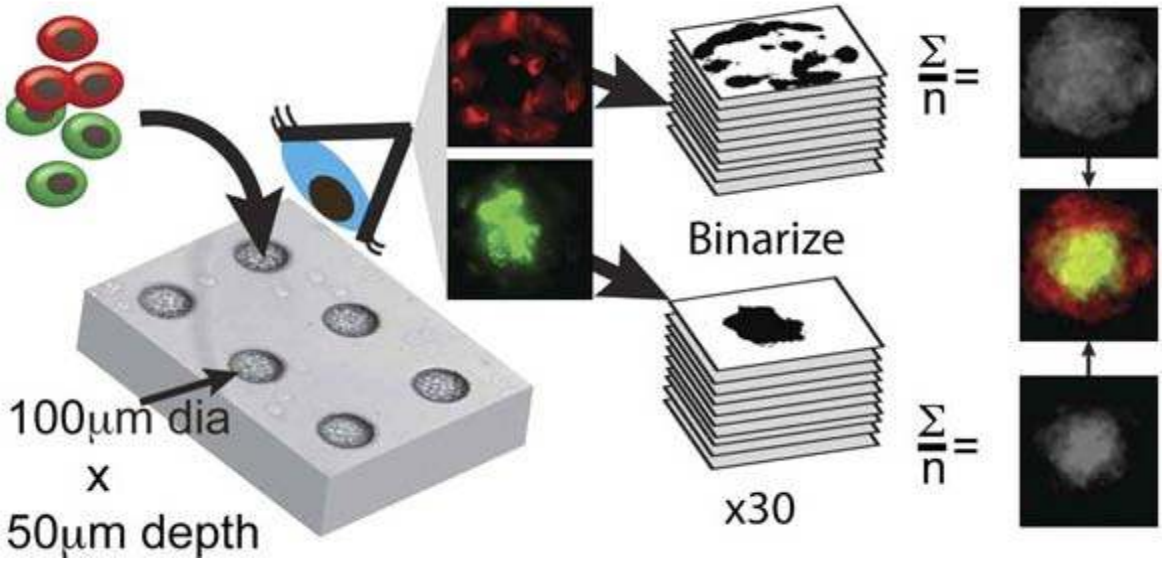

Figure 3.1. Schematic of microwell assay and subsequent analysis. MEPs and LEPs are labeled, red and green accordingly, mixed and placed into microwells. Confocal images (blue eyeball) are taken at the midsection of 30 microwells and an average map of LEP and MEP localization is generated.

All self-organizing experiments were conducted with HMEC strain 240L. Flow cytometry-sorted HMEC were stained with CM-DiI, SP-DiOC18(3), or DiIC18(5)-DS (Invitrogen), used at 1:1,000 in PBS for 5 min at 37 °C followed by 15 min at 4 °C. Cells were washed extensively with medium after staining. Dye-stained HMEC were mixed at a ratio of 1:1 (LEP:MEP) or 1:1 (randomly stained green:red HMEC cultures) and resuspended in M87A at 1x10^6 cells/mL. Inhibitors were added to the cell suspensions just before HMEC were introduced into the wells and were allowed to load for 30–60 minutes. Excess cells were washed away with medium; inhibitors then were added to the medium after excess cells were washed away and at every medium change: anti–E-cadherin (100 μg/mL clone HECD-1; Invitrogen); anti–E-cadherin (100 μg/mL clone HECD-1; Invitrogen); anti–P-cadherin (100 μg/mL clone NCCCAD-299; Abcam); recombinant human (rh)E-cadherin-Fc (recEcad, 100 μg/mL;R&D Systems); rhVE-cadherin (100 μg/mL; R&D Systems); Y27632 (10 μM; Calbiochem); or ML-7 at 3 μM

(Calbiochem). The microwell assay as well as subsequent analysis is depicted in Figure 3.1. HMEC were imaged at 0, 24, or 48 hours with a spinning disk confocal microscope (Carl Zeiss). Red and green fluorescence channels in images taken at the ~25 μm z-axis positions of 30 wells from each condition at each time point were binarized using a threshold function, merged into a z-stack, and then averaged using ImageJ software (National Institutes of Health). Gray-scaled average images corresponding to LEP and MEP were merged into a single image with red or green look-up tables applied to each average image. Heat maps were normalized to the highest intensity value and were used to quantify sorting using the expression:

$$D(x) = \log_2\left(\sum_1^{360} \frac{I_{LEP}(x)}{I_{MEP}(x)}\right)$$

Equation 3.1

Where D is the differential, expressed as the base two log of the averaged ratio of LEP over MEP intensity, I, as a function of distance from center, x. A script was written using MATLAB (Mathworks) to plot differential intensity as a function of the distance from the center and to compute the average plot from θ of 1–360° as depicted in Figure 3.2.

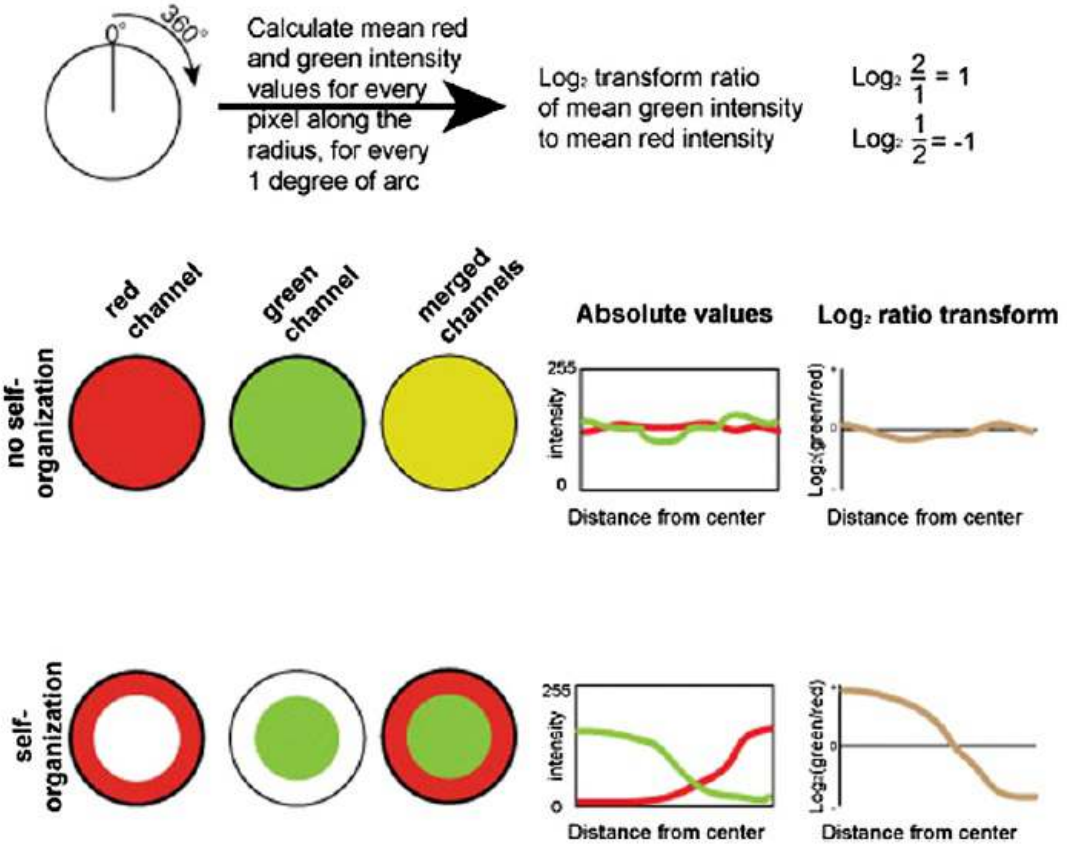

Figure 3.2. Depiction of method for transforming localization maps. Assuming radial symmetry, the average normalized pixel intensity is calculated as a function of distance from the microwell's center. This method allows for easy comparisons of sorting.

Atomic Force Microscopy

Once samples were equilibrated to 25°C, cell deformity was measured, and stiffness was calculated as previously described [2]. Briefly, cantilever deflections are measured as a function of extension height with a constant, low (< 400nm/s) extension rate using a pyramid punch and analyzed using a Hertzian mechanics model [203, 219, 220], which assumes a material that is homogeneous, isotropic, linear-elastic solid that is undergoing a small strain. Under these assumptions, indentation δ can be related to punch load F by:

$$\delta^2 = \frac{4F(1-\upsilon^2)}{3E\tan\alpha}$$

Equation 3.2

While the piezo position, z, is related to deflection, d, as:

$$z = z_0 - (d - d_0) - \left(\frac{4k(1-\upsilon^2)(d-d_0)}{3E\tan\alpha}\right)^{1/2}$$

Equation 3.3

Where k is the spring constant, υ is the Poisson ratio (~0.5) and α is the cantilever tip half angle. Knowing these constants the data can be fit to the Hertz model allowing for the calculation of contact point (z_0, d_0) and Young's modulus, E. The resulting data were plotted using Prism (GraphPad Software) (n = 45).

Statistics

E-cadherin images and atomic force microscopy were analyzed using the Kruskal–Wallis test and Dunn's test for multiple comparisons, using a 95% confidence interval. Differences between first and third thirtiles of $\log_2$ (mean green fluorescence/ mean red fluorescence) per pixel plotted as a function of distance from the center were analyzed by one-way ANOVA, using Bartlett's test for equal variance and followed by a Tukey's test for multiple comparison using a 99.9% confidence interval. Statistics were computed with Prism (GraphPad Software, Inc.).

3.3 – Results

3.3.1 – Quantification of self-organization between HMEC lineages

The mammary gland undergoes cycles of proliferation and involution, showing as much as a 10-fold expansion in preparation for lactation followed by return to normal size. During these processes, the precise bilayered branching organization throughout the gland is maintained; secretory luminal epithelial cells (LEPs) line the lumen,

surrounded by a layer of contractile myoepithelial cells (MEPs) that are adjacent to the basement membrane. We hypothesized that mammary epithelial cells possessed lineage-specific intrinsic abilities to self-organize into domains of lineage specificity. Such a mechanism would help explain how, for instance, the mammary stem cell-enriched zone in the ducts [221] is maintained separately from the rank-and-file LEPs and MEPs, and how LEPs and MEPs form and maintain bilayers.

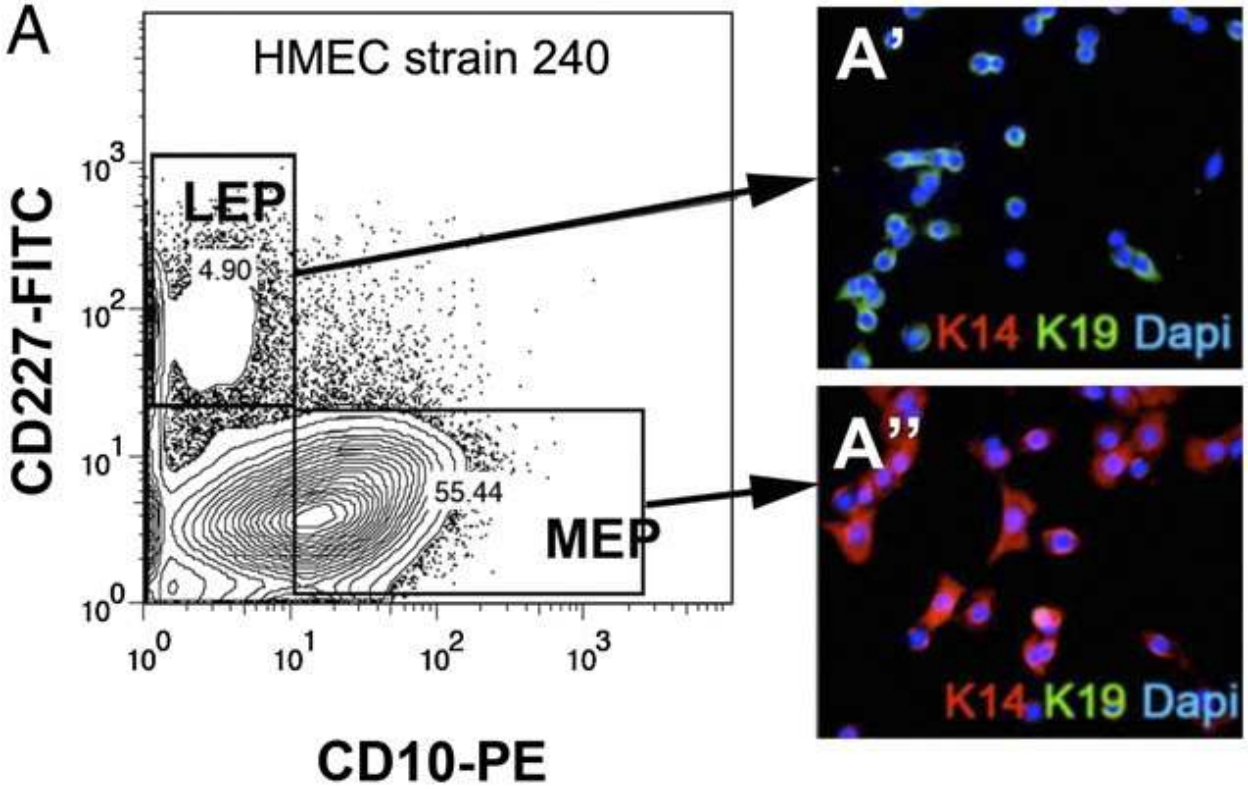

Figure 3.3. Flow cytometry analysis of fourth-passage finite-lifespan HMEC strain 240L reveals distinct populations of the two principal somatic epithelial lineages of mammary gland: MEPs, defined here as CD227−/CD10+, and LEPs, defined as CD227+/CD10− (A′ and A′′). Immunofluorescence of sorted cells for MEP and LEP markers K14 (red) and K19 (green), respectively, verified that (A′) CD227+ LEPs were K14−/K19+, and (A′′) CD10+ MEPs were K14+/K19−. Nuclei were counterstained with 4',6-diamidino-2-phenylindole (**DAPI**) (blue).

The phenomenon of self-organization has not been well studied in humans, perhaps because of the challenges of working with primary materials and a paucity of tractable culture systems for maintaining cell types from normal adult tissues. To facilitate a quantitative understanding of those processes in an adult epithelial tissue, we used a robust cell culture system that enables culture of pre-stasis normal HMEC obtained from reduction mammoplasties for 40–60 population doublings while maintaining both the LEP and MEP lineages [216]. Flow cytometry-enriched cells from both lineages were placed in arrays of micropatterned microwells, where their distributions were tracked over time to generate a dynamic understanding of lineage-specific self-organizing behavior.

We first used a classical self-organization assay to determine whether different lineages of cultured HMEC derived from reduction mammoplasty possessed an intrinsic ability to form bilayered structures. Subpopulations of LEPs and MEPs, defined as CD227+/CD10−/keratin 19 (K19)+/keratin 14 (K14)− and CD227−/CD10+/K19−/K14+, respectively [221], were enriched by FACS from heterogeneous normal finite lifespan HMEC [216] at passage 4 or 5 as depicted in Figure 3.3. The two lineages were labeled with long-lasting fluorescent membrane dyes of different wavelengths, mixed together, and then were suspended in hanging droplets. The formation of cores of LEPs surrounded by MEPs, similar to their organization in vivo, was observed over 48 hours. However, the considerable variation in aggregate size, shape, and focal planes precluded a quantitative understanding of the phenomenon.

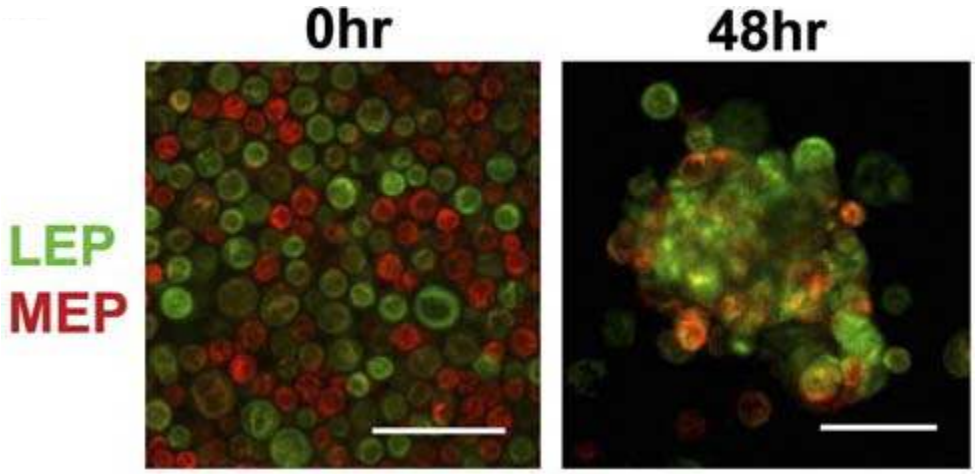

Figure 3.4. Images of mixtures of fluorescently labeled LEPs (green) and MEPs (red) suspended in hanging droplets and imaged with a confocal microscope just after mixing at 0 hour (Left) and at 48 hour (Right). (Scale bars: 20 μm.)

Therefore, a microwell culture platform was engineered that confined the HMEC mixtures to a 3D cylindrical geometry, which enabled quantification of lineage distributions over time as depicted on Figure 3.1. Representative optical sections of mixed LEPs and MEPs in microwells, taken at mid-depth (~25 μm) at 0 and 48 hours, suggest self-organization had occurred, as compared with mixtures of arbitrarily labeled HMEC cultures as seen in Figure 3.5, where heat maps also show the lineage distributions over time, suggesting that in a majority of microwells MEPs formed a ring surrounding cores of LEPs as early as 24 hours, and lasted for at least 48 hours. A 1:1 ratio of LEPs to MEPs was determined empirically to provide the most clearly separable distributions, as compared with ratios of 1:2 or 1:3. Using relatively more LEPs than MEPs (e.g., in a ratio of 2:1 or 3:1) was difficult due to the paucity of LEPs. Arbitrarily labeled HMEC cultures, mixed at a 1:1 ratio, showed overlapping distributions of cells that did not resolve into distinct populations. Quantification of the heat maps confirmed that a core of LEPs surrounded by MEPs was observable as early as 24 hours, and showing as much as a fourfold difference in LEP:MEP ratios at the core versus the periphery by 48 hours ($P < 0.001$). By contrast there was no difference in ratios at the

core and the periphery of the arbitrarily labeled HMEC controls at any time point as shown in Figure 3.5. Inflections in the graphs sometimes were observed toward the peripheral regions because of imperfect registration of the well images. Taken together, these results indicate that self-organizing is an innate property of the LEP and MEP HMEC lineages.

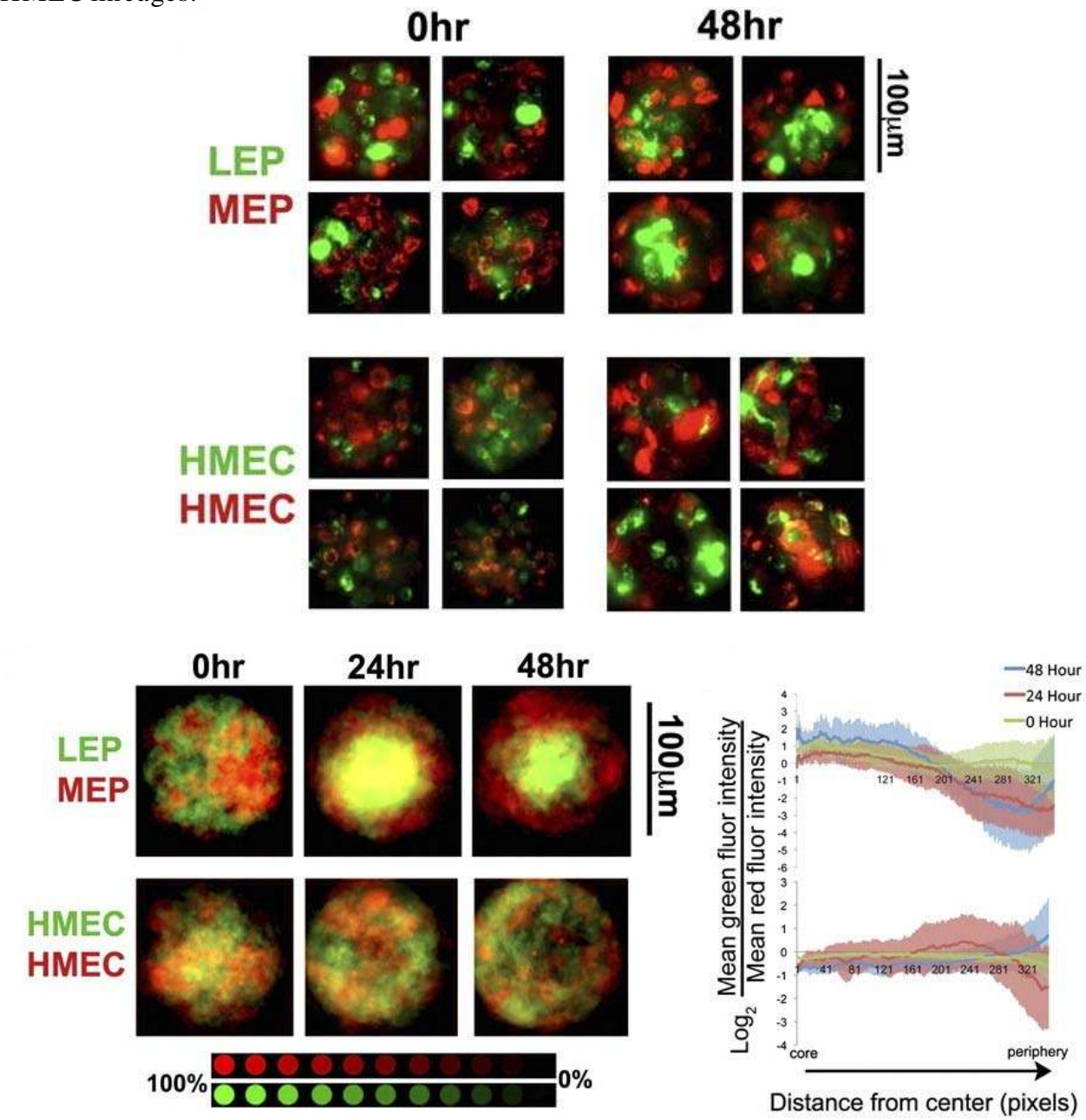

Figure 3.5. Representative fluorescence images of LEP (green) and MEP (red) in four different microwells at 0 and 48 hours and of controls, which were heterogeneous HMEC arbitrarily labeled with red or green labels. Distribution maps of LEP (green) and MEP (red) or control mixtures at the 0, 24, and 48 hours. Quantification of heat maps in showing mean distribution of red and green pixels along the radius around 360° of arc at three time points. Green lines show 0 hours, red lines show 24 hours, and blue lines show 48 hours. Standard deviation is shown by the lightly shaded regions of colors corresponding to each line.

3.3.2 - Levels of E-cadherin expression are lineage specific

Self-organizing behavior has been ascribed to disparate adhesive properties among the participating cells in embryonic progenitors from the three germ layers, in cancer cell lines, and in fibroblasts engineered to express cell–cell adhesion molecules (the differential adhesion hypothesis, reviewed in [213, 214]). Cadherin cell–cell adhesion molecules, particularly E-cadherin, play key roles in tissue morphogenesis during vertebrate gastrulation [222]. Quantification of images of fluorescently immunostained tissue sections of normal mammary gland from two individuals revealed that more E-cadherin protein was present at the borders between two LEPs than at the borders between a LEP and a MEP ($P < 0.001$) as shown in Figure 3.6. Flow cytometry measurements of E-cadherin surface protein levels were made on LEPs and MEPs as well. In HMEC strains at fourth passage from six individuals, a reproducible pattern was observed, whereby more E-cadherin was detected on LEPs than on MEPs as depicted on Figure 3.6. The lineage specific expression levels of E-cadherin made it an attractive candidate for further testing of the differential adhesion hypothesis as it pertains to self-organization among HMEC.

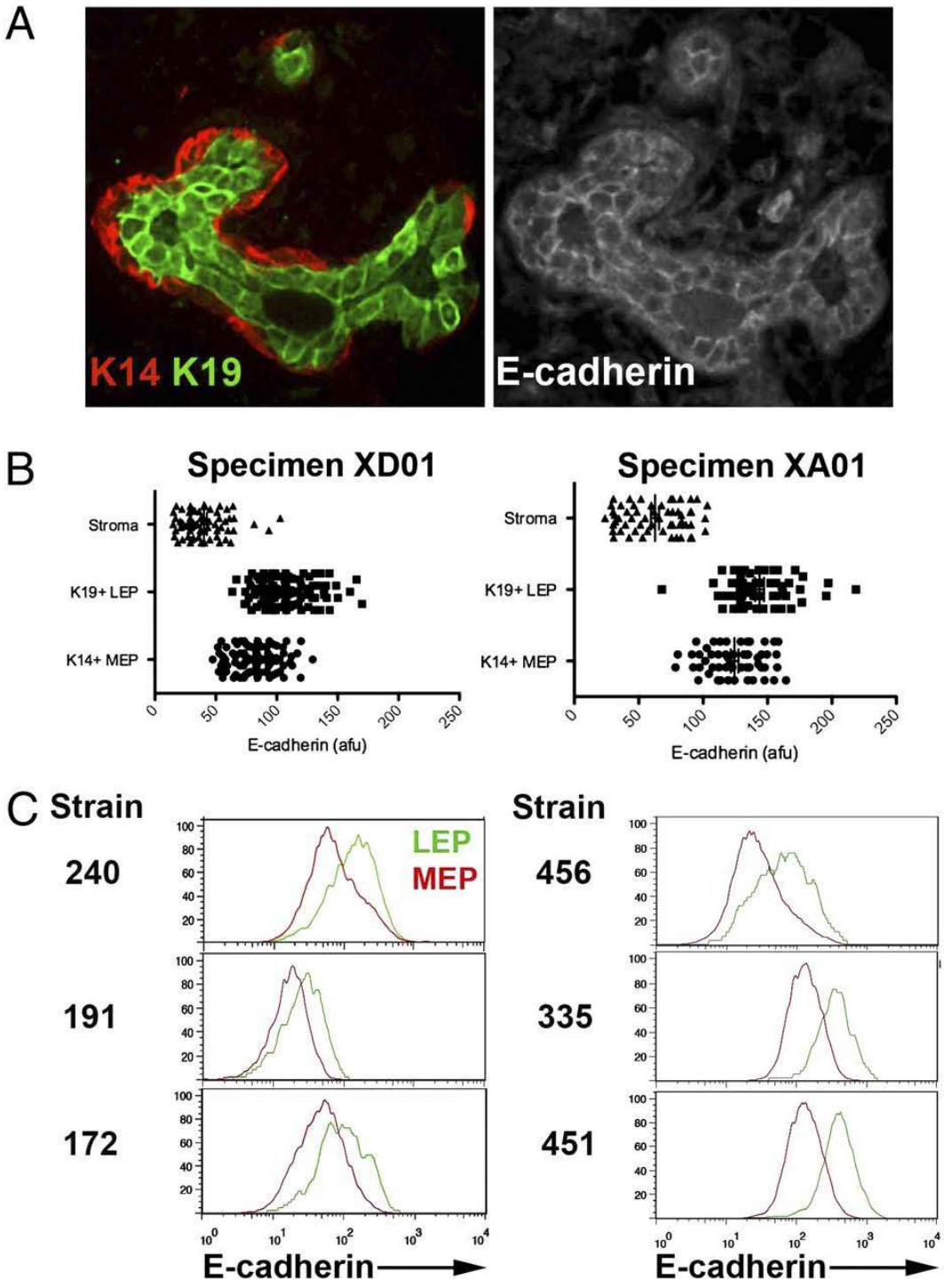

Figure 3.6. A tissue section from a normal mammary gland, triple-immunostained to show (Left) the MEP and LEP markers K14 (red) and K19 (green), respectively, and (Right) E-cadherin. (B) Dot plots show image quantification from two individuals, XD01 and XA01, of E-cadherin protein levels at the border between two LEPs and at the border between a LEP and a MEP cell and background fluorescence as measured on stroma, which does not express E-cadherin (Stroma). Measurements are expressed in arbitrary fluorescence units (afu), n = 100 for each cell type collected from at least three sections.

3.3.3 - Identification of adhesion molecules that drive epithelial sorting

To determine whether cadherins played a functional role in the self-organization of LEPs and MEPs, inhibitors of E-, P-, and VE-cadherin were added to the medium of the microwell assay to antagonize those specific cell–cell interactions. P-cadherin is expressed by MEPs in vivo but not by LEPs [223]. VEcadherin is expressed by endothelial cells but not by epithelial cells [222] and was used as a control for potential effects of heterotypic cadherin interactions [224]. Each of the putative inhibitors was added at the beginning of the experiment and was refreshed every 24 hours with medium changes.

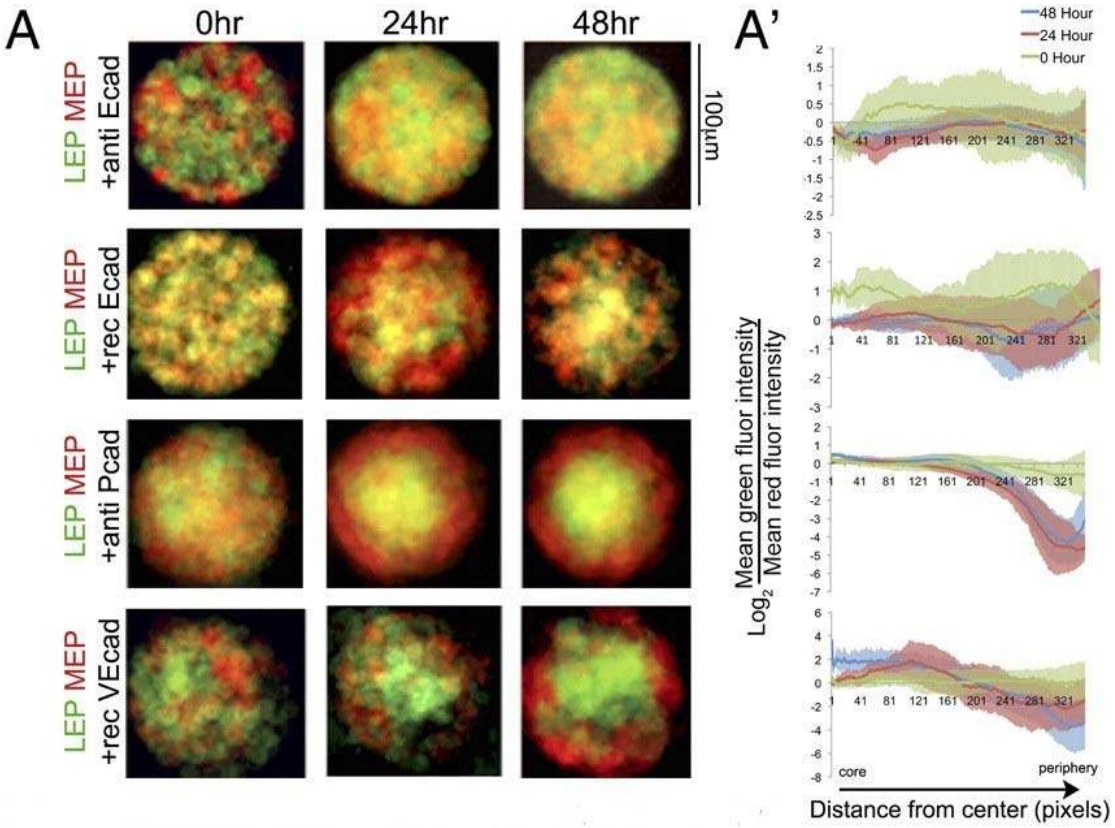

Figure 3.7. E-cadherin–containing junctions are required for self-organizing. (A) Maps of HMEC lineage distributions over time in the presence of E-, P-, or VE-cadherin–blocking agents (anti–E-cadherin, recombinant (rec)E-cadherin, anti–P-cadherin, or recVE-cadherin); LEP are green, and MEP are red. (A') Quantification of heat maps, showing changes in mean distribution of red (MEP) and green (LEP) pixels along the radius around 360° of arc at three time points. Green lines show 0 hour, red lines show 24 hours, and blue lines show 48 hours. SD is shown by the lightly shaded region of color corresponding to each line

An antibody that blocked E-cadherin, and recombinant E-cadherin fused to the human IgG-Fc region (recEcad), prevented self-organizing of LEPs and MEPs. Quantification of the heat maps did not reveal differences in LEP:MEP ratios at the core and periphery in Figure 3.7. An antibody that blocked P-cadherin did not abolish sorting, because a core enriched for LEPs was surrounded by MEPs ($P < 0.001$).

However, quantification revealed that there were more MEP at the core [hovering around a ratio of 1:1] than in untreated LEPs and MEPs, which usually showed about a twofold enrichment of LEPs at the core such as in Figure 3.5. Those data suggest that LEPs organization at the core is unaffected by P-cadherin antibodies, whereas the MEPs were relatively more challenged in their journey to the periphery. Recombinant VE-cadherin IgG-fusion protein (recVEcad) did not prevent organizing as can be seen on Figure 3.7. These data suggested that differential levels of E-cadherin at the surfaces of LEPs and MEPs were the principle drivers of self organization and thus were the focus of the majority of subsequent studies. However, these data also show that P-cadherin plays a more lineage-restricted role in MEP self-organizing.

3.3.4 - Self-organization requires the actomyosin network.

Previous studies of mammary epithelial morphogenesis have implicated profound roles for the actomyosin regulatory network in normal morphogenesis [225, 226]. We therefore examined the impact on HMEC self-organization of the actomyosin network inhibitors ML-7, a myosin light-chain kinase (MLCK) inhibitor [227], and Y27632, a Rho kinase (ROCK) inhibitor that blocks both ROCK1 and ROCK2 [228]. Inhibitors were added at the beginning of the experiment and were refreshed every 24 hours with medium changes. Analysis of LEPs and MEPs distributions over 48 hours revealed that both inhibitors prevented self-organization; there were no differences in lineage distribution between the core and peripheral regions as shown in Figure 3.8.

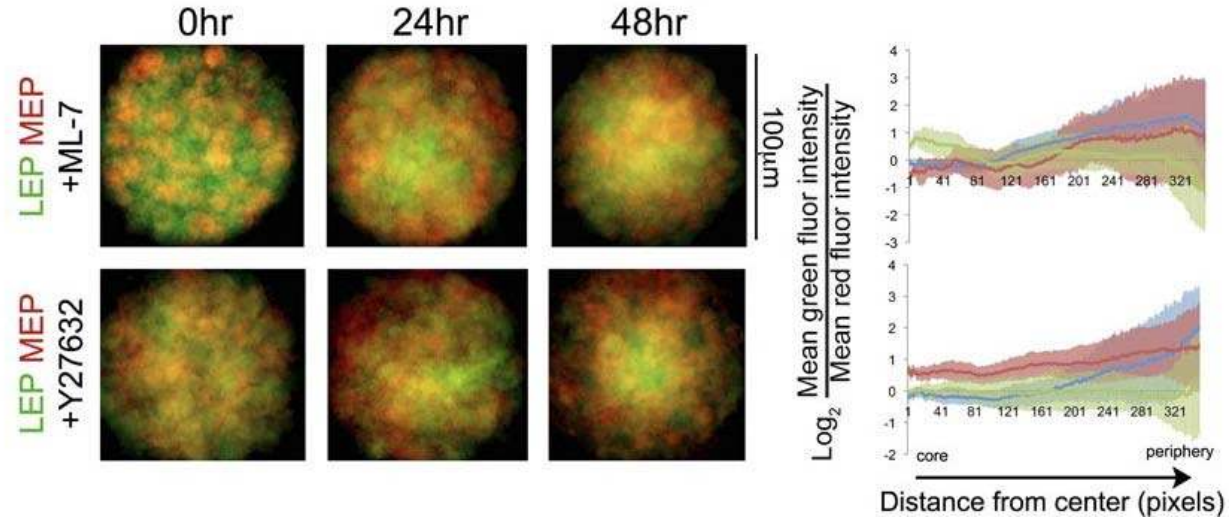

Figure 3.8. The cytoskeleton regulatory molecules ROCK and MLCK are required for self-organization. LEP (green) and MEP (red) distributions in the presence of the MLCK inhibitor ML-7 or the ROCK inhibitor Y27632. Quantification of heat maps, showing changes in mean distribution of red (MEP) and green (LEP) pixels along the radius around 360° of arc at three time points. Green lines show 0 hour, red lines show 24 hours, and blue lines show 48 hours. SD is shown by the lightly shaded region of color corresponding to each line.

Modulation of the actomyosin network also is known to cause changes in the elasticity and cortical tension of cells. Self-organization studies of germline progenitor cells dissociated from zebra fish embryos suggested that differential actomyosin-dependent cell-cortex tension was a crucial component of self-organization in that system [212], in which stiffer cells organized to the inside and were surrounded by softer cells, and disruption of the stiffness relationship by actomyosin network inhibitors led to deficits in self-organization. Using an atomic force microscope, we measured the elasticity of untreated and inhibitor treated MEPs and LEPs. Although untreated MEPs tended to be stiffer than LEPs, that difference became significant only in the presence of the inhibitors ($P < 0.001$), as shown in Figure 3.9. While MEP stiffness was unaffected by ML-7 and by Y27632, both inhibitors caused softening of LEPs. In HMEC the actomyosin network inhibitors increased the magnitude of the difference in elasticity between LEPs and MEPs but did not alter their relative elasticity (i.e., LEPs always were softer than MEPs), suggesting that in this system self-organization was not driven by differential elasticity.

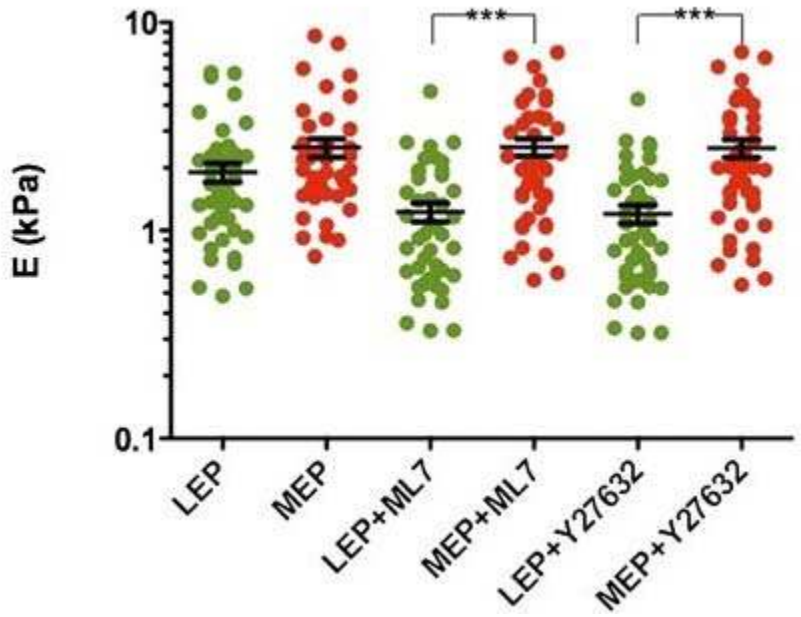

Figure 3.9. Atomic force microscopy measurements of LEP and MEP in the presence of ML-7 and Y27632. The graph represents elasticity (kPa) values for 45 cells per condition; the interior line represents mean elasticity values; error bars show SE. Strain 240L at fourth passage was used for all experiments.

3.3.5 – Regulators of the actomyosin network revealed self-organization is dynamic and reversible

How did the actomyosin inhibitors upset the self-organizing mechanism? We investigated whether the actomyosin inhibitors affected expression or binding activities of E-cadherin in HMEC. Addition of ML-7 or Y27632 to the HMEC culture medium did not change lineage-specific differences in E-cadherin expression as measured via flow

cytometry; invariably, LEPs expressed more E-cadherin than did MEPs as seen on Figure 3.10. The ability of rec-Ecad simply to bind surfaces of HMEC in suspension also was measured by flow cytometry. Binding of recEcad did not occur in Ca2+-free medium or when HMEC were preincubated with an E-cadherin–blocking antibody. A 6-hour pretreatment with Y27632 or ML-7 did not prevent recEcad binding. Therefore, neither differential expression levels of E-cadherin nor its ability simply to bind other E-cadherin molecules at the surface was impacted by ML-7 or Y27632.

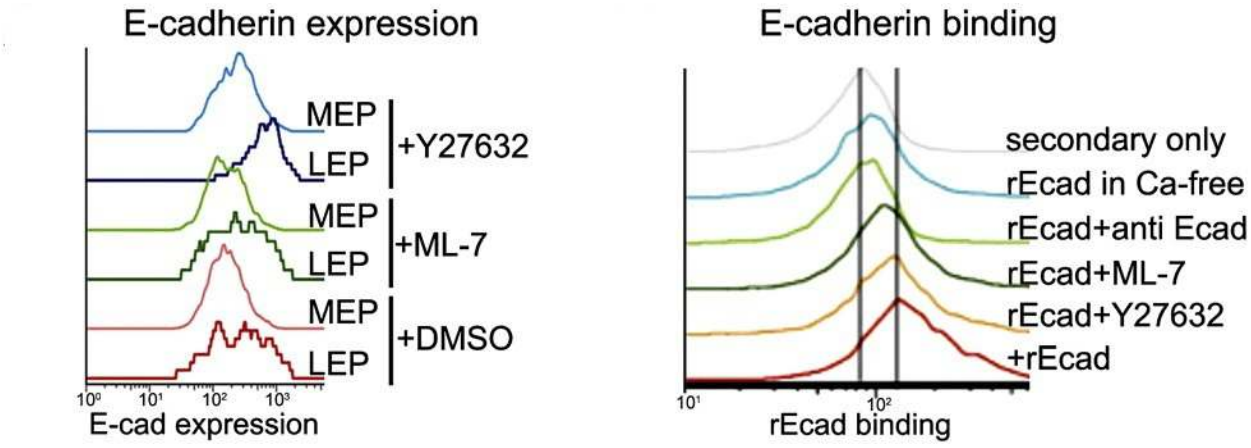

Figure 3.10. Self-organization among luminal and myoepithelial cells is driven by E-cadherin activity. E-cadherin protein expression at the surface of LEPs and MEPs in the presence of ML-7 or Y27632, as measured by flow cytometry. Flow cytometry analysis of recombinant E-cadherin (rEcad) binding to HMEC cell surfaces.

Because of the central importance of the cytoskeleton in adherens junction regulation, we considered the possibility that the actomyosin inhibitors modulated the ability of E-cadherin junctions to mature or remodel [229], thereby impacting HMEC organization. Disruption of MLCK would prevent proper localization of myosin IIA to the E-cadherin junction, disrupting E-cadherin clustering and decreasing homophilic adhesion [180]. Conversely, mature adherens junctions were unable to break down and recycle in the presence of Y27632 in HCT116 and MDCK epithelial cell lines [230]. Those reports predicted that ML-7 would ablate already-organized HMEC structures, whereas Y27632 would preserve them. Accordingly, ML-7 or Y27632 was added to mixtures of LEPs and MEPs in the microwell assay, either just after cells were added to wells at the start of the assay (0 hour) or after 24 hours, when the DMSO controls already started to show signs of organization. In contrast to the experiments shown in Figure 3.10, in which the inhibitors were refreshed every 24 hours, in these experiments the inhibitors were added a single time, with the expectation, based on empirical findings that the inhibitor's activity would begin to weaken by 48 hours. This protocol tested the reversibility of the system, because in one condition sorting would be prevented from the beginning and then gradually would be unleashed, and in the second condition sorting would be allowed to get underway before perturbation by the inhibitors after 24 hour. Both inhibitors, when added at 0 hour, prevented self-organization through the 24-hour time point, but as the inhibitors' activity diminished significantly, differences in LEP:MEP ratios in the core and at the periphery were

observed by 48 hours ($P < 0.01$) as shown in Figure 3.11. The unique phenotypes of each inhibitor were revealed when they were added after the assay had been underway for 24 hours. Before addition of the inhibitors, the LEP were enriched at the core and were surrounded by peripheral MEPs ($P < 0.001$). When measured at 48 hours, addition of ML-7 had obliterated organization, eliminating any difference in the distributions of the lineages (P = ns), whereas Y27632 had preserved the self-organized LEP cores that were encircled by MEPs ($P < 0.001$). As a whole, these observations are consistent with the following model: ML-7 prevented adherens junction formation or maturation, and breaking the adherens junctions prevented cells from self-organizing and caused dissolution of already organized structures. Conversely, Y27632 prevented adherens junction recycling, so the cells could not let go of one another to sample the surrounding microenvironment. Thus, both establishing and maintaining organized states are dynamic and reversible processes.

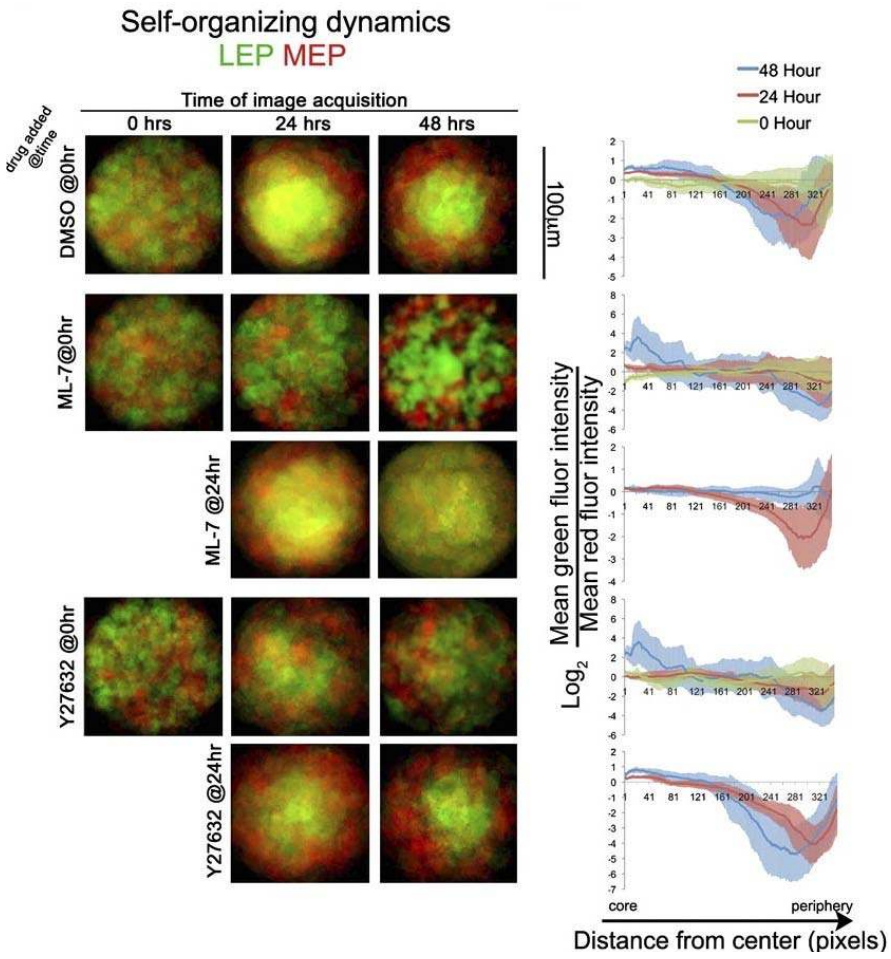

Figure 3.11. Impact on self-organization over time (time points: 0, 24, and 48 hours) when the inhibitors ML7 and Y27632 were added at 0 or 24 hours. Quantification of heat maps showing changes in mean distribution of red (MEP) and green (LEP) pixels along the radius around 360° of arc at three time points: green lines show 0 hour, red lines show 24 hours, and blue lines show 48 hours. SD is shown by the lightly shaded region of color corresponding to each line. Strain 240L at fourth passage was used for all experiments.

3.4 - Discussion

Here we demonstrated that self-organization of mammary epithelial cells is a lineage-specific process that is principally E-cadherin driven; however, P-cadherin also may play a role in organizing the MEP layer. Unaltered normal finite-lifespan HMEC and the microwell assay were used together with recombinant proteins and antibodies that blocked specific adherens junction proteins. The elegant proof-of-principal experiments, which that showed differential levels of cell–cell adhesion molecules can drive self-organizing, were performed using fibroblasts and other immortal cell lines that were engineered to express different levels of adherens junction proteins. It is remarkable, given the undoubted complexity of the LEP and MEP cell surfaces, that E-cadherin plays so central a role in the process of self-organization in those cells. It has been hypothesized that self-organizing is not simply the result of differential levels of cadherin expression or of binding affinities, but rather that adhesion energy and the ability to remodel cell–cell junctions are crucial determinants [231].

Dynamic analysis of HMEC in the microwell assay platform in the presence of actomyosin inhibitors provided support for that hypothesis in the context of mammary gland (Figure 3.11). Elegant time-lapse imaging studies of mouse mammary organoid morphogenesis also revealed that the actomyosin inhibitors Y27632 and ML-7 disrupted the clean bilayered organization [226], but not to the catastrophic extent observed in the HMEC microwell assay. Because the mouse mammary organoids were developed in vivo, a number of additional cellular interconnectivities crucial for tissue stability may have formed that were absent in our recombined system. Although we focused on cell–cell E-cadherin junctions, other adhesive and physical interactions, such as desmosomal interactions between LEPs and MEPs [232], undoubtedly are important in maintaining mammary gland organization and bear further dissection. Cell–ECM interactions also will likely affect sorting in vivo. Because the microwell assay uses a nonfouling coating to prevent cell adhesion, the adherens junction proteins may have had a more pronounced effect on self-organizing than they would have had in the presence of ECM.

Atomic force microscopy analysis of LEP and MEP on plastic dishes indicated that LEP tended to be softer than MEP. However, a cultured murine epithelial cell line became less stiff in contact with laminin-111, a principal component of basement membrane, than when in contact with plastic [2]. Therefore, MEPs in vivo may be less or equally as stiff as LEPs because of their direct contact with basement membrane. Future iterations of the microwell platform will help elucidate more of the factors involved in making stable and organized tissues.

Studying self-organizing behavior of a human epithelium generally is challenging because results cannot be extrapolated easily to in vivo conditions. However, observations of breast cancer pathogenesis suggest the basic mechanisms described here are important for maintaining mammary gland organization. E-cadherin expression and localization frequently are misregulated in breast cancers [233-235], and loss of E-cadherin is a hallmark of the epithelial-to-mesenchymal transition, which is associated with invasive and aggressive breast cancer [236]. The mechanisms governing self-

organization also are important in the context of regenerative tissue maintenance. As MEPs and LEPs are produced anew by mammary progenitor cells in vivo, they must adopt their appropriate place within the tissue, or, alternatively, the progenitors must be able to move to receive instructive microenvironments that direct cell-fate decisions [237]. Understanding tissue self-organization mechanisms may help explain how stem cell differentiation and maintenance of tissue architecture in adults are coordinated.

Loss of organization is a principle feature of cancers; therefore it is important to understand how normal adult multilineage tissues, such as bilayered secretory epithelia, establish and maintain their architectures. The self-organization process that drives heterogeneous mixtures of cells to form organized tissues is well studied in embryology and with mammalian cell lines that were abnormal or engineered. Here we used a micropatterning approach that confined cells to a cylindrical geometry combined with an algorithm to quantify changes of cellular distribution over time to measure the ability of different cell types to self-organize relative to each other. Using normal human mammary epithelial cells enriched into pools of the two principal lineages, luminal and myoepithelial cells, we demonstrated that bilayered organization in mammary epithelium was driven mainly by lineage-specific differential E-cadherin expression, but that P-cadherin contributed specifically to organization of the myoepithelial layer. Disruption of the actomyosin network or of adherens junction proteins resulted in either prevention of bilayer formation or loss of preformed bilayers, consistent with continual sampling of the local microenvironment by cadherins. Together these data show that self-organization is an innate and reversible property of communities of normal adult human mammary epithelial cells. This chapter attempts to meet the first aim of the dissertation, which is to characterize lineage-dependent sorting between human mammary epithelial cells. While much work is left to be conducted, the chapter demonstrates the role of E-cadherin in mediating lineage-dependent sorting as well as infers that different regulators of the actomyosin complex play separate roles in formation and maintenance of self-organization. Now that the cell-cell aspect of the microenvironment has been studied, the next section of the dissertation will cover work on the cell-ECM component of the microenvironmental interface.

Chapter 4 – Characterization of cell-ECM interface during mammary development

4.1 - Introduction

In studying the interface between the epithelium and the ECM, it becomes obvious that the surrounding microenvironment undergoes dramatic organizational changes. Besides changes in composition, the epithelium has been shown to directly remodel the surrounding matrix via matrix metalloproteinases (**MMP**s) as well as crosslinking enzymes. Still, more work is required to decipher how contextual differences within the extracellular environment are discerned by cells, as it is instrumental to understanding development and disease. Recent studies have highlighted the importance of extracellular stiffness and organization on malignancy [175] and metastasis [238] as well as characterized key regulators of the cellular response to extracellular cues [239]. What requires further elucidation is the role of extracellular matrix organization during development. The goal of this chapter is to pursue both Aim B and Aim C in characterizing the role of matrix stiffness and organization, respectively, in mammary gland development.

In addressing Aim B, ECM stiffness and composition is first studied with respect to functional differentiation [2]. Models for functional differentiation typically quantify expression of milk proteins; such is the case for the following mechanistic studies. Previous studies have shown the ECM component, laminin-111 (**LM1**), is necessary to induce polarity and acinar morphogenesis [240] and, together with lactogenic hormones, is required for b-casein expression in MECs [241, 242]. Additionally, tissue elasticity is thought to be maintained by a mechanical homeostatic mechanism largely determined by the reciprocal mechanochemical interactions between cells and their surrounding ECM. Using a quantitative and comprehensive approach, we unraveled the intimate interrelationship among LM1 binding, ECM stiffness, cell shape and cell stiffness. The results show that variations of these properties to those comparable with normal physiological conditions may be linked to proper functional differentation.

Next, both Aim B and Aim C is pursued in the context of branching morphogenesis [1], a form of cohesive and guided multicellular movement observed in a variety of physiologic processes including tissue repair, blood vessel formation, and morphogenesis of organs such as the lung, kidney, pancreas, salivary gland, and mammary gland [15, 243]. Using a three-dimensional model for mammary epithelial branching, biophysical mechanisms employed to overcome mechanical barriers as well as determine direction are studied. A novel method for orienting collagen matrices was developed and employed in mechanistic studies as well as in vivo studies conducted to determine the organization of the endogenous collagen matrix.

4.2 – Methods

Cell culture, lentivirri and inhibitors

SCp2 [244] and EpH4 [245] were propagated in growth medium supplemented with 2% fetal bovine serum and gentamicin. Unless noted otherwise, cells were seeded at a density of ~10,000 cells/cm^2 on top of different substrata in growth medium supplemented with hydrocortisone (1 mg/ml) (Sigma). After 4 hours, cells were treated with differentiation medium consisting of Dulbecco Eagle's minimal essential medium (**DMEM**) variant DMEM/F12, insulin, gentamicin, hydrocortisone and prolactin (3 mg/ml). Cell mechanics and β-casein expression were probed 24 and 48 hours after adding differentiation medium, respectively. To pre-round cells in the absence of exogenous ECM signaling, cells were cultured on the nonadhesive substratum poly-HEMA (Sigma) [246]. EpH4 cells were transfected with a plasmid containing 16 concatenated copies of the mouse β-casein promoter fused to a sequence encoding cyan fluorescent protein (**CFP**) using Lipofectamine 2000 (Invitrogen). To screen for positive clones, 2% Matrigel (BD Biosciences) diluted in differentiation medium (~15–200 mg/ml) was added to cells 24 hours after plating on glass.

When using the mouse mammary epithelial cell line EpH4 [245] for branching studies, cultures were maintained in DMEM/F12 supplemented with 10% fetal bovine serum and gentamicin. Lentiviral constructs, such as containing Elongation factor 1α (EF) promoter driving mYPET-RhoA^{T17N} as well as CMV driven Fascin-1 were constructed via standard molecular techniques. To generate shRNA constructs, forward and reverse oligonucleotides were annealed to generate a double-stranded DNA oligonucleotide, which was ligated into BamH1/EcoR1 site of pGreen puro lentiviral vector (System Biosciences). Lentivirus production and transduction of target cells were conducted following the guideline by the manufacturer. Briefly, lentivirus vector and packaging plasmid mix (System Biosciences) were transfected into 293FT cells (Invitrogen) using Lipofectamine® 2000. After 48 hours, medium was harvested, filtered and used to infect target cells with the addition of polybrene (10 μg/ml). After 24 hours medium was replaced and at 72 hours post-infection puromycin (5 μg/ml) was added for selection and maintained throughout the culturing period. Y27632 (Tocris, Avonmouth, UK) was used at 5μM; ML-7 (Calbiochem, San Diego, CA) was used at 1μM; Blebbistatin (Calbiochem, San Diego, CA) was used at 20μM.

Preparation of 3D collagen-I gels

Acid-soluble collagen-I (Cellagen IAC-50, Koken) was neutralized on ice by mixing gently 8 volume (vol) with 10X 1 : 1 DMEM/F12 (1 vol) and 0.1N NaOH (1 vol) to obtain a 4 mg/ml collagen solution. Depending on the experiment, collagen solution was diluted in DMEM/F12 to obtain the desired final concentration (1–4 mg/ml). Desired volumes of collagen solutions at final concentrations were incubated at 37˚C for 30 min to allow gelation, and immediately hydrated with DMEM/F12. In some experiments, collagen gels were incubated with 100 mg/ml bacterial collagenase (Sigma).

Preparation of substrata

For AFM experiments, 100 ml of ECM solutions were added to glass-bottomed culture dishes (MatTek) and incubated for 30 minutes at 37˚C to allow gelation unless otherwise indicated. Biological gels included Matrigel, LM1 (incubated overnight) (Trevigen) and neutralized COL-I (2 or 3 g/l) (ICN Biomedicals) mixed with increasing concentration of LM1. Traditional 2D substrata included uncoated borosilicate glass coverslips and polystyrene, referred to as glass and plastic, respectively. In the floating gel assay, gels containing 40% LM1 and 60% COL-I (3 g/l) were detached from the container edge with a spatula, whereas the gel centre remained attached to the underlying substratum for AFM measurements. The polyacrylamide gel assay was performed as described elsewhere [247]. Briefly, different volumes of 30% w/v acrylamide and 2% w/v bis-acrylamide solution (Bio-Rad) were mixed to form gels attached to a glass coverslip, with Young's modulus comparable to normal rodent mammary tissue, average tumours or stiffer [175]. Gels were subsequently coated with 40 mg/cm^2 human fibronectin (BD) to facilitate cell adhesion.

AFM elasticity measurements

We used a stand-alone AFM (Bioscope, Veeco) coupled to an inverted microscope as described in detail elsewhere [248, 249]. In brief, force measurements were conducted using low spring constant cantilevers (k=0.03 N/m) (Microlever, Veeco). For cell measurements, the tip was positioned above the central part of the cell and approached to the cell surface using a stepping motor. Following the initial tip contact with the cell surface, three force versus piezo displacement recordings (F–z curves) were acquired at moderate loading force (~1nN) and low speed (~5 μm/s). A similar procedure was used to probe the elasticity of the substrata. Young's modulus, E, and sample indentation d were computed from F–z curves as described elsewhere [248]. Recordings from cells subjected to d larger than 15% of the total height were discarded to rule out any artifactual contribution from the underlying substratum. Data from cells or gels that yielded irreproducible E values (coefficient of variation (**CV**) higher than 15%) were also discarded. E data were screened for outliers using Chauvenet's criterion. Application of these selection criteria led to ≤15% discarded elastic moduli from either gels or cells. All mechanical data are given as mean ± s.e. and were calculated from at least nine measurements for each independent experiment (n≥2).

Rheometry measurements

The bulk elasticity of biological gels prepared as in AFM experiments was assessed by measuring the complex modulus at low frequencies (~1 Hz) using a parallel plate rheometer (Paar Physica MCR 300, kindly provided by Professor K Healy at UCB). Data are given as mean ± s.e. and were calculated from at least six repeated measurements for each independent experiment (n≥2).

Branching assay and Collagen alignment

Both aggregates of EpH4 cells as well as tissue explants from 10 week Balb/c mice were used for the branching assay in three-dimensional collagen matrices. EpH4 aggregates were generated by plating cells on nonadhesive, polyHEMA (Sigma) coated wells for 48 hours [246]. Organoids were isolated as previously described [250], where the mammary gland is minced and the epithelium separated in steps of digestion and centrifugation. Type I collagen matrices was prepared from acid-soluble rat tail collagen (BD Biosciences) to a final concentration of 3mg/ml, with organoids or aggregates added to the final concentration of 1 per 1 μl. Gelation of 300μl collagen matrices in either 48 well plates or PDMS chambers with exact dimensions occurred for 45 minutes at 37°C. To induce branching, DMEM/F12 media supplemented with ITS-PS (1% insulin/transferrin/selenium/penicillin/streptomycin, Sigma) and 9nM bFGF (R&D Systems). Media was replaced every 2 days.

To align collagen matrices, PDMS wells were fabricated from an acrylic master with dimensions matching a 48 well plate at a ratio of 10:1 of base:cure (Sylguard). The wells were then removed and UV oxidized for 7 minutes (UVO-Cleaner42, Jetlight Co.), rinsed with distilled H_20 under vacuum overnight, and dried. To generate an axial alignment with 3D collagen matrices, the PDMS wells were stretched prior to addition of collagen using custom acrylic frames and steel pins (McMaster-Carr). After gelation the pins are removed, generating a uniaxial compression of 10% strain.

Sample preparation, labeling, and microscopy

To visualize collagen remodeling during branching, EpH4 cells were seeded in No. 1.5 thickness borosilicate chamber slides (Nalge Nunc International) within 3 mg ml1 collagen-I gels mixed with 2%(v/v) DQ-Collagen (type I Collagen; Invitrogen) of identical concentration. Images were acquired after 4 days of branching induction with a LSM 710 laser-scanning confocal microscope (Zeiss) using a LD C-Apochromat 40x water immersion objective. DQ-Collagen was excited with a 488 nm laser and emitted signal was captured from 493–582 nm. Image stacks of 50 mm total depth and 1.1 mm slice thickness were obtained, and each image was line averaged over 2 scans. Brightfield images were captured concurrently. Collagen-I fibers in cell-free gels were visualized by CRM by exciting collagen with a 488 nm laser and collecting the reflected signal at the same wavelength. To assess nuclear distribution in branching MECs, cells were fixed, permeabilized and stained with DAPI and phalloidin (Invitrogen) as previously described,20 and image stacks were collected using either the 40x or a 20x water immersion objective.

Whole mounts were prepared as described. Mammary glands were extracted from Balb/c, B6C3Fe a/a-Col1a2^{oim}/J, and B6;129S4-Col1a1^{tm1Jae}/J mice strains. To visualize collagen organization within the fat pad, a fluorescent probe was generated as previously described [251, 252]. Briefly, a his-tagged collagen binding protein (CNA35)

from *Staphylococcus aureus* was expressed in an E.Coli strain, purified, and conjugated to Alexa Fluor 564 following the manufacturer's instructions (Invitrogen). Confocal images were taken using a Zeiss 710, visualizing collagen via reflection. Otherwise, a Zeiss Axiovert spinning disk was used to track migration. Brightfield images were taken using a Zeiss Axiovert and whole mount images were taken using a stereoscope.

Image and Data analysis

To determine orientation of the mammary epithelium, a custom Matlab (Mathworks, Natick, MA) script was used to segment traces performed in ImageJ (NIH), measuring orientation every 50 microns. Branch orientation from in culture experiments was simpler to calculate, where direction was measured from the aggregate/organoids geometric center to branch end via ImageJ, with 50 aggregates/organoids measured per condition, totally to 150-250 branches per condition. Collagen orientation was measured via fast fourier transform (FFT) analysis previously described [253].

4.3 - Results

4.3.1 – Characterization of epithelial stiffness

To estimate the elasticity of fully differentiated MECs in vivo, we isolated milk-synthesizing primary mammary organoids from early pregnant mice and cultured them on top of Matrigel in differentiation medium for 24 hours. Matrigel is a suitable substratum because it is rich in LM1 and exhibits physiologically similar elastic modulus, as measured by AFM and rheometry and shown in Table 4.1. Since mammary organoids (**MO**s) in culture are heterogeneous in size, elasticity of both small- and medium-sized organoids as measured, which typically contain about a dozen or several dozen cells, respectively. Irrespective of size, cells within the organoids exhibited comparable average elastic moduli between 400 and 800 Pa as seen in Figure 4.1. We used this range as a reference for physiologically similar range of cellular elasticity throughout this work (horizontal dashed lines).

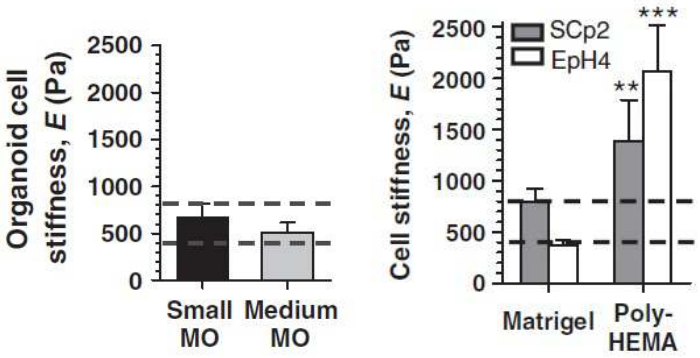

Figure 4.1. Stiffness of mammary epithelial components. Organoids have similar stiffness regardless of size, which is comparable to the mammary epithelial cell lines SCp2 and EpH4 when cultured on Matrigel.

The two mammary cell lines, SCp2 and EpH4, have been used extensively to study functional differentiation of MECs in culture [244, 245]. The elastic moduli of either single SCp2 or EpH4 cells cultured on top of Matrigel for 24 hours fell within the physiological range defined by cells in mammary organoids as seen above in Figure 4.1. As MECs exhibit a round morphology both in vivo and when exposed to LM1 in culture [254], it is possible that their similar elastic moduli is due to the round shape per se [255].

Sample	Tissue or substratum		Single cells[a]
	E_{AFM} (Pa)[b]	E_{bulk} (Pa)[c]	E_{AFM} (Pa)[b]
Normal mammary tissue	n.a.	170 ± 30[d]	
Average mammary tumour	n.a.	4050 ± 940[d]	
Mammary organoids on Matrigel	120 ± 20	n.a.	600 ± 200
Matrigel	120 ± 20	220 ± 10	700 ± 100
Laminin-111	110 ± 30	n.a.	730 ± 110
Laminin-111+collagen I (2 g/l) (40:60% v/v)	72 ± 8	150 ± 40	600 ± 90
Collagen I (2 g/l)	290 ± 100	240 ± 40	400 ± 100
PolyHEMA	n.a.	n.a.	1700 ± 300
Borosilicate glass (2D)	n.a.	63 10^9[e]	1300 ± 200
Data are mean ± s.e.; n.a., not available.			
[a]Mean of all cell lines.			
[b]Young's modulus measured by AFM.			
[c]Young's modulus measured with a rheometer.			
[d]From [175]			
[e]According to the manufacturer's instructions.			

Table 4.1. Stiffness of epithelial cells, tissues, and extracellular matrices.

4.3.2 - Extracellular stiffness modulates cellular stiffness and β-casein expression

As normal mammary tissue is soft as seen in Table 4.1, it was possible that strong functional differentiation in culture could be altered by modulating the elasticity of the substrata towards one that mimics normal tissue. Accordingly, two culture assays were used that allow accurate control of extracellular stiffness well beyond physiological values while maintaining biochemical signaling constant [256]. EpH4 cells were plated on top of polyacrylamide gels exhibiting elastic moduli either close to mammary tissue (referred to as 'soft'), comparable with or even higher than mammary tumours (referred to as 'stiff'). After 24 hours after plating on the stiffer substrata, cells displayed spread morphology and less of a physiological elasticity as seen in Figure 4.2. To induce β-casein, cells were overlaid with 2% Matrigel diluted in differentiation medium. In agreement with the first assay, stiffer substrata downregulated β-casein transcription, measured by the fluorescence of cells transfected with a construct containing 16 concatenated copies of the mouse b-casein gene promoter driving cyan fluorescent protein (**CFP**) expression as depicted in Figure 4.2. These findings support our

hypothesis and indicate that LM1-dependent functional differentiation is modulated by the extracellular elasticity.

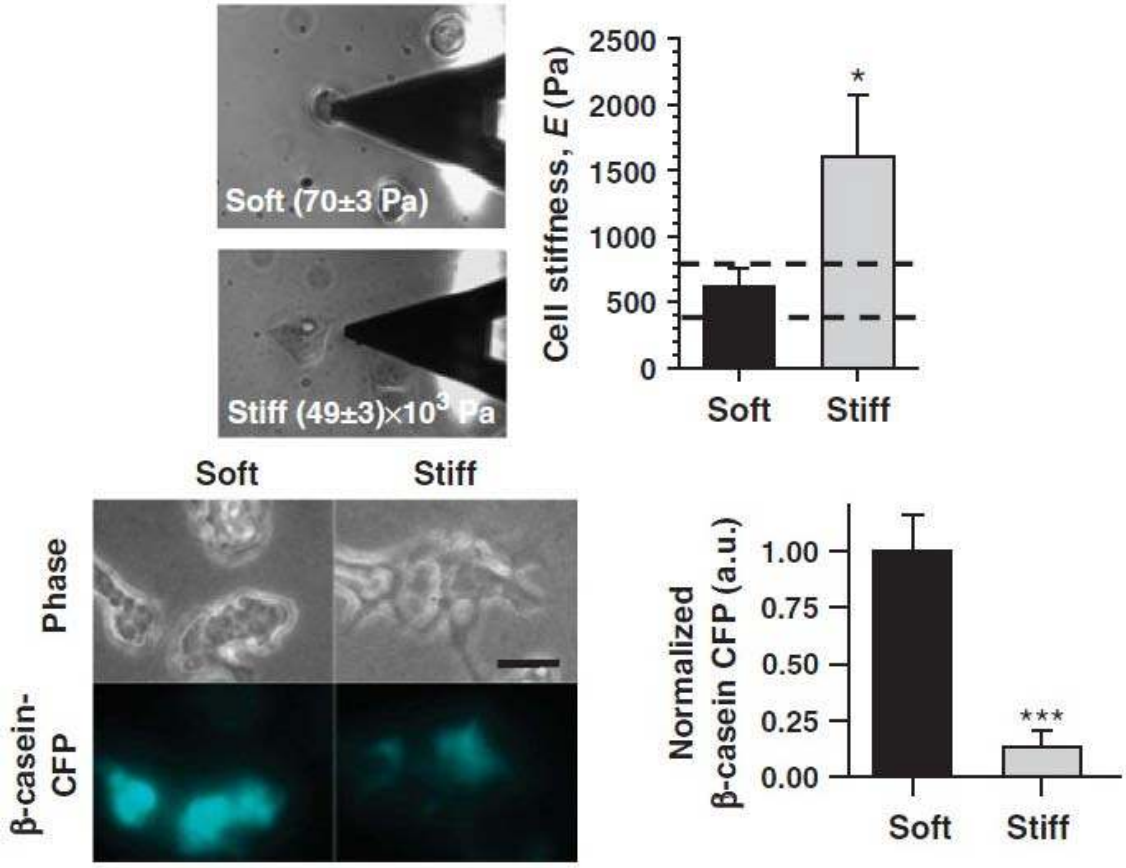

Figure 4.2. Extracellular stiffness modulates cellular stiffness as well as β-casein expression. Phase images show an increase in spreading on the stiffer substrate as well as AFM measurements demonstrating a concomitant increase in cellular stiffness. Fluorescent imaging shows an increase of β-casein expression on softer substrates. *P<0.1 and ***P<0.01 were determined by two-tailed Student's t-test, adapted from [2].

4.3.3 - LM1 signaling regulates cellular elasticity as well as β-casein expression

Mammary epithelial cells in vivo are in contact with a basement membrane, a specialized ECM rich in LM1 that physically separates mammary epithelium from the stroma; the latter is rich in COL-I [238] and contains much less LM1 [257]. During tumour cell invasion, the integrity of the basement membrane is often compromised [258] and MECs can contact the stroma directly. To investigate how this loss of LM1 signaling affects functional differentiation and the mechanical properties of MECs, we examined SCp2 and EpH4 cells plated on top of LM1 gels mixed with increasing ratio of COL-I (2 g/l). As little as 10% LM1 was sufficient to maintain β-casein expression as well as physiological extra- and intracellular elasticity demonstrated in Figure 4.3. Interestingly, reducing LM1 concentration below 10% led to a dramatic downregulation

of β-casein expression as well as a decrease in β-casein promoter activity, non-physiological cellular elasticity and a sudden increase in the gel's elastic moduli as depicted in Figure 4.3. Both SCp2 and EpH4 cells exhibited a similar relative downmodulation of β-casein as the COL-I/LM1 ratio increased. Moreover, SCp2 cells appeared stiffer on softer gels, thereby revealing a strong non-linear relationship between extra- and intracellular elasticity in these cells, and confirming that our methodology to probe cell mechanics with AFM was not biased by the stiffness of the underlying substrata. These experiments reveal that at a concentration of 10% or above, LM1 signaling is dominant over COL-I signaling, and that COL-I-dependent loss of β-casein expression is associated with non-physiological extra- and intercellular elastic moduli.

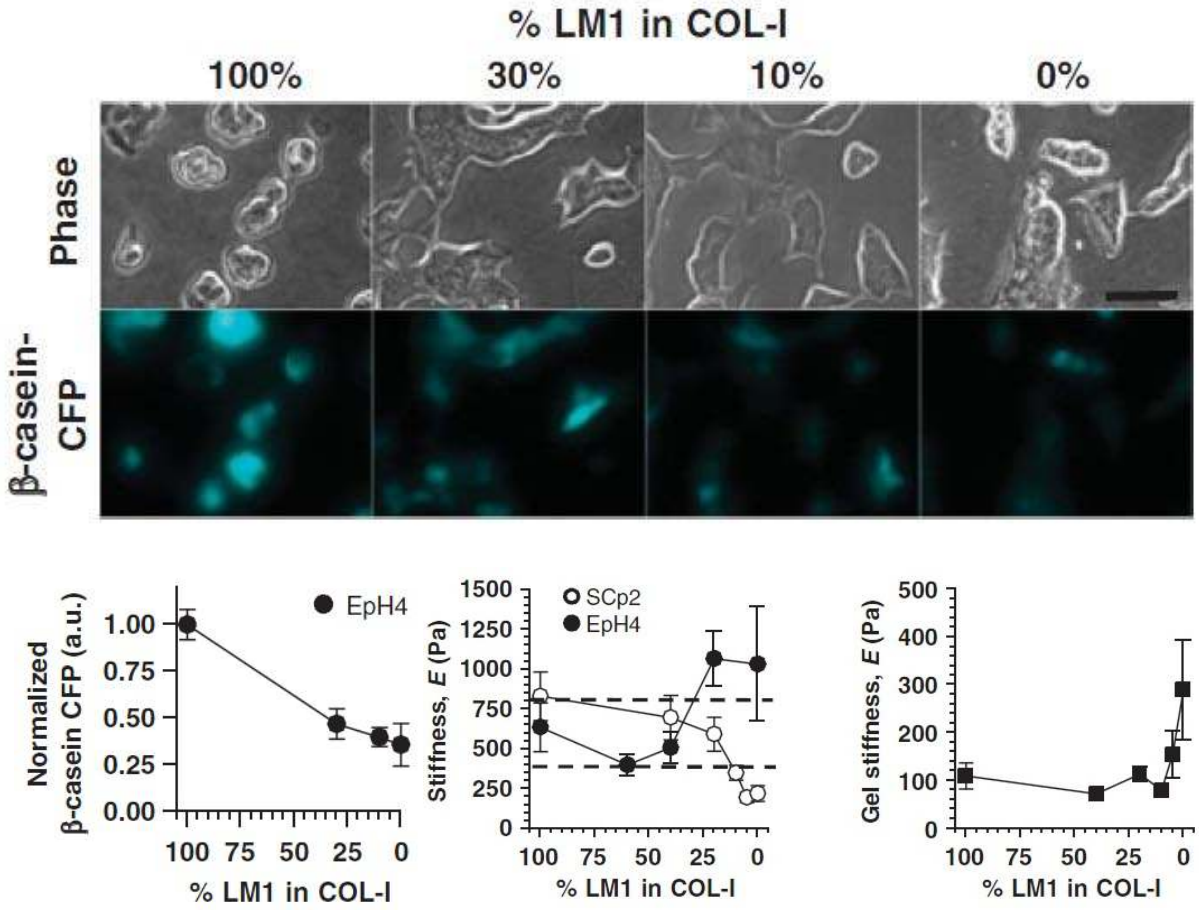

Figure 4.3. Loss of LM1 signaling downregulates b-casein expression and induces non-physiological cellular elasticity and morphology in SCp2 and EpH4 MECs. β-casein expression of MECs cultured on top of COL-I (2 g/l) gels mixed with decreasing concentrations of LM1, with visualization and corresponding quantification of fluorescent intensity. Elastic moduli of MECs exhibited non-physiological elasticity for LM1 concentrations below 10%, with the elastic moduli of SCp2 being lower while EpH4 was higher. Note the non-linear relationship between these two properties. The range of elasticity as a function of %LM1, showing a relatively small increase below 10%. Adapted from [2].

4.3.4 – Branching MECs soften the ECM through local proteolytic degradation

In the context of mammary branching morphogenesis, previous studies reported an absolute requirement for MMPs in branching of MECs in collagenous gels [15, 259]. Accordingly, it is conceivable that MECs could minimize resistance further by locally degrading the ECM, thereby down-regulating E of the collagenous gel at invasive fronts. To test this hypothesis, we used AFM to measure locally E of gels either at invasive fronts or >100 μm away from cell clusters in the absence or presence of the broad spectrum MMP inhibitor GM6001 (40 μM) as illustrated in Figure 4.4. Only the closest invasive bodies to the gel surface (<25 μm in depth) were considered to guarantee that our AFM measurements were not biased by large differences in the depth of the cell clusters within the gel. We found that the average E at invasive fronts was nearly half the average E measured far from cell clusters as seen in Figure 4.4. Furthermore, this dramatic ECM softening at the edge of invasive bodies was abrogated with GM6001, thereby supporting our hypothesis that ECM softens locally at invasive fronts, and that this softening is driven by MMP-dependent local degradation.

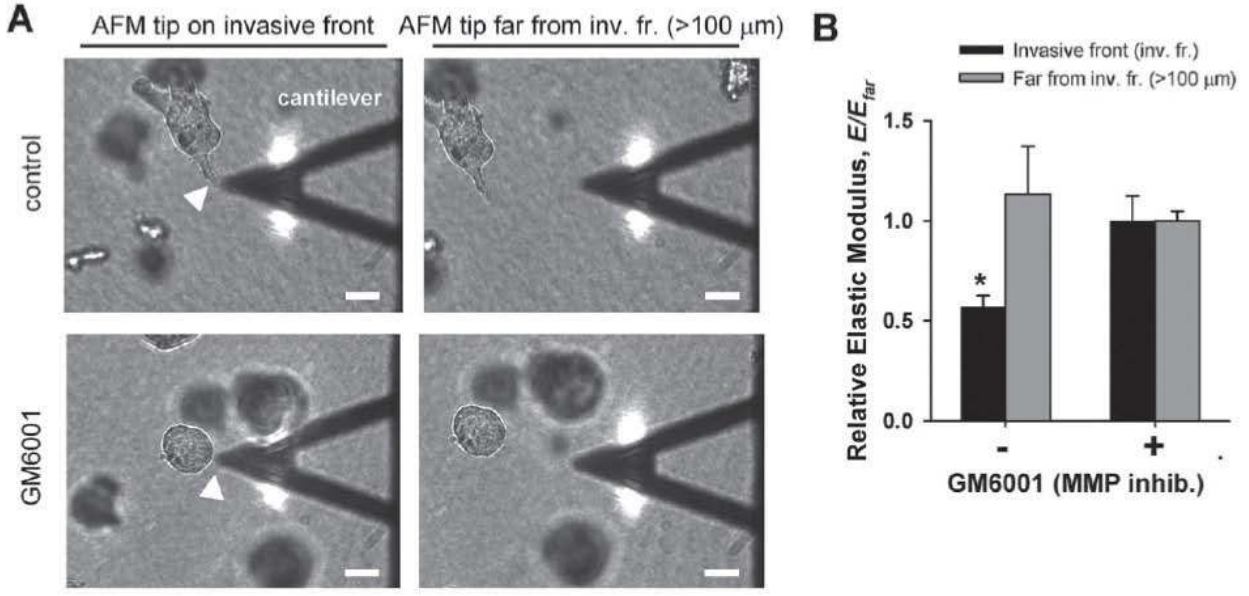

Figure 4.4. Assessment of local ECM degradation and softening at invasive fronts by AFM and confocal microscopy. (A) Representative bright-field images illustrating the spatial localization of the AFM measurements. For each cell cluster, the tip of the AFM cantilever was positioned at the very edge of either an invasive tubule (top left) or a non-invasive cluster (bottom left), the corresponding E was measured, and normalized afterwards with respect to E measured far (>100 μm) from the cell cluster (E_{far}) (right images). White arrow points to an invasive front (top left image) or an edge of a non-invasive cluster (bottom left image). Scale bars correspond to 40 μm. (B) Normalized E data obtained in the absence or presence of GM6001. *P < 0.05 between normalized data obtained at the cell cluster edge or far from it. Scale bars correspond to 20 μm.

To analyze the extent of this local collagenous degradation, branching experiments were conducted with cell clusters embedded in regular collagen-I mixed with dye quenched collagen (DQ-Collagen), which enables direct visualization of collagen filaments by fluorescence microscopy owing to the large number of fluorescent dyes present along the DQ-Collagen. Representative confocal images and corresponding bright field images of branching MECs are shown in Figure 4.5. The white arrows in the left panel point to an area void of DQ signal located at the very front of an invasive body. Such areas void of DQ-signal were consistently observed at invasive fronts, whereas they were barely observed and randomly distributed in non-branching clusters or in clusters treated with GM6001. Morphometric analysis of the areas void of DQ-signal revealed an average width of 25–40 μm, which is slightly larger than the depth of invasive bodies probed with AFM. These findings indicate that the local ECM softening measured at invasive fronts spatially matched the appearance of areas void of fluorescent signal, which is indicative of degradation of filamentous collagens.

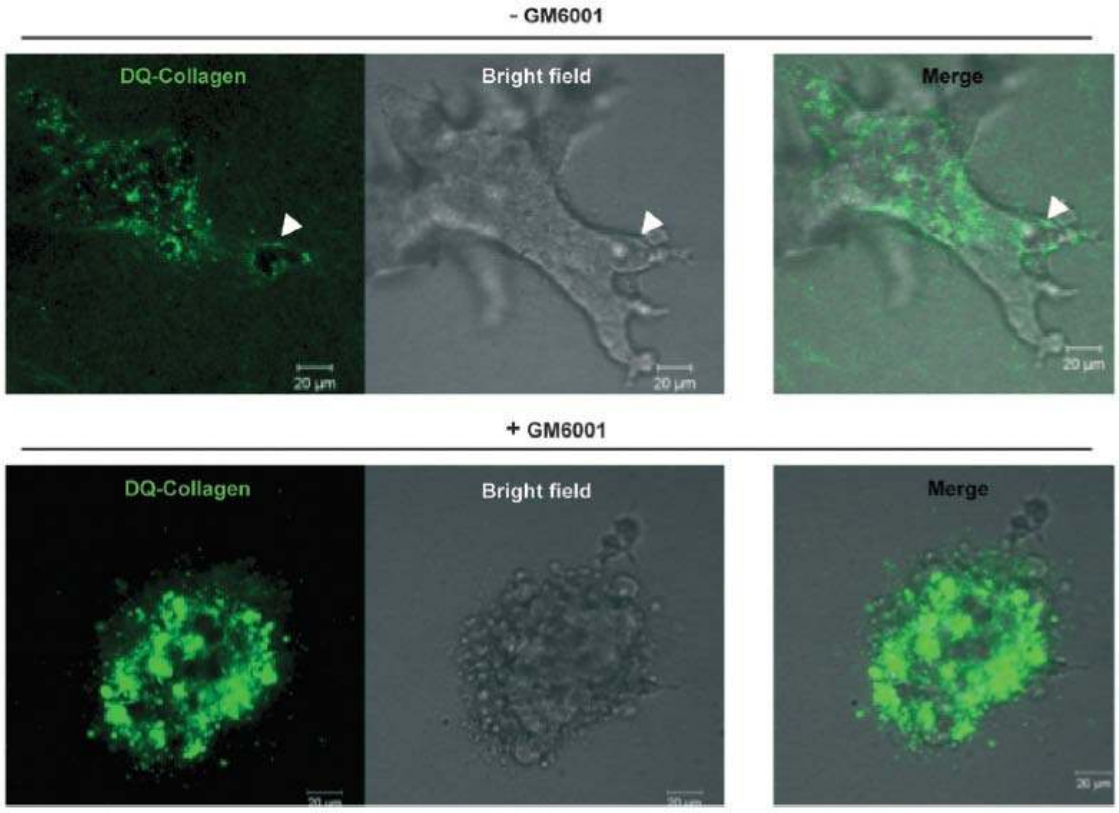

Figure 4.5. Confocal sections (left images) showing collagen filaments surrounding the middle of a cell cluster embedded in 3D collagen-I gel containing fluorescent DQ-Collagen and untreated (top images) or treated (bottom images) with GM6001. Corresponding bright field and merged images are shown in the middle and right of each panel. The arrows (top left) point to an area void of DQ-Collagen fluorescence in the untreated cells, whereas such void areas were absent or randomly distributed in GM6001 treated cells, adapted from [2].

4.3.5 - Relationship between matrix degradation and elasticity

To understand quantitatively how local collagen degradation (i.e., reduction in concentration) leads to gel softening, two complementary experiments were conducted. First, we treated a cell-free 3 mg/ml collagen-I gel with exogenous bacterial collagenase for up to 60 minutes. This enzymatic degradation induced a dramatic disappearance of collagen filaments as revealed by confocal reflection microscopy (**CRM**) as depicted in Figure 4.6. Concomitantly we also measured how collagenase altered the mechanics of the gel and found a five-fold decrease in E as measured by AFM. Therefore, as in our branching assay, we observed that collagenase-dependent gel softening was associated with loss of reflective signal indicative of degradation of collagen filaments. Second, we measured E on gels prepared at different collagen concentrations, from 1 to 4 mg/ml and observed a marked gel stiffening with increasing as see in Figure 4.6.

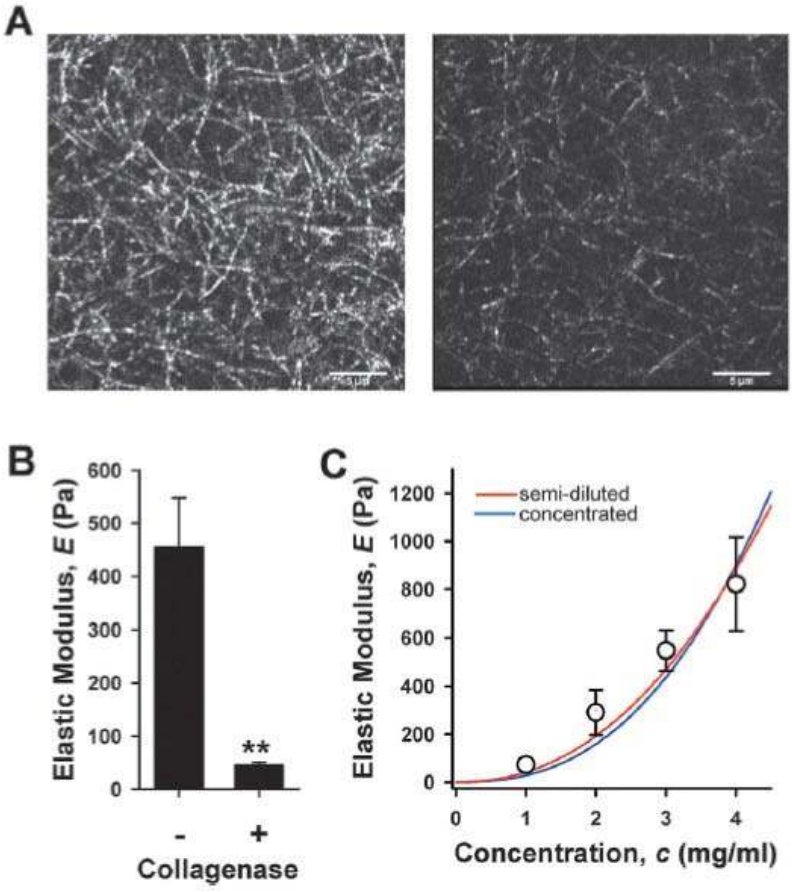

Figure 4.6. Structural and elastic properties of cell-free collagen-I gels untreated or treated with exogenous collagenase. (A) Representative confocal sections of collagen filaments obtained by CRM corresponding to an untreated or a collagenase treated (up to 60 minutes) 3 mg/ml collagen-I gel. Scale bars correspond to 5 μm. (B) E of untreated or collagenase treated collagen-I gels measured by AFM. **P<0.01. (C) E of different concentrations of cell-free collagen-I gels measured by AFM. Data were fitted to semiflexible polymer models corresponding to semi-diluted (red) or concentrated (blue) gels.

Current models of semiflexible polymers, which were developed to describe the mechanical characteristics of filamentous proteins entangled without permanent crosslinks, predict that E depends on the average length between entanglements (L_e), the average mesh size or void length between filaments (ε), and collagen concentration (c) [260]. We conducted a morphometric analysis of CRM images of cell-free collagen gels with Image J and estimated L_e ~2 μm and ε ~0.8 μm, thereby suggesting that our collagen gel could be modeled as a semiflexible semi-diluted polymer. Consistently with this morphometric analysis, we found a slightly better fitting of E vs. c data for semi-diluted (r^2=0.97) instead of concentrated (r^2 = 0.94) crosslinking as seen in Figure 4.6. These data reveal that reduction of collagen concentration by collagenolytic degradation is an efficient strategy to soften a collagenous gel, and highlight the suitability of current models of semiflexible polymers to describe E versus c data for collagen gels.

4.3.6 – Local matrix alignment and co-orientation occurs during branching and is mediated by ROCK

Previous work has shown the dynamic and reciprocal relationship between matrix stiffness and the branching epithelium. However, in performing experiments on ECM stiffness in which the collagen was visualized, it became obvious that matrix organization was profounding modified during branching. In order to study the interaction of the branching epithelial with the surrounding collagen and the subsequent changes in ECM organization, we embedded mammary explants in three-dimensional collagen type I matrices. Explants were induced to branch and visualized via bright field while the matrix was visualized via confocal reflection microscopy. Interestingly, significant matrix remodeling occurred within 48 hours of branching, with proximal to branch sites showing the most profound alterations of alignment, as illustrated in Figure 4.7.

In order to quantify matrix orientation, Fast Fourier Transform (**FFT**) analysis was employed. Following a given area of the matrix before and after the approach of an epithelial branch, a dramatic increase in matrix alignment was observed at the tip, the direction perceived to be the branching direction. Measuring branch orientation in culture from the explant base to tip, we found that most branches co-orient with the axis of alignment of the proximal collagenous matrix, as seen in Figure 4.7. In order to determine mechanism of local matrix alignment in culture, the activation of ROCK was inhibited via Y27632 (20μM) and a time course of the collagen matrix conducted. While such a high concentration of the inhibitor dramatically reduced branching, filopodia were still observed interacting with the surrounding collagen matrix. However, no significant change in matrix orientation was observed in a comparable time-point of the control. This result strongly infers the role of actomyosin machinery in locally orienting the matrix via cellular contraction.

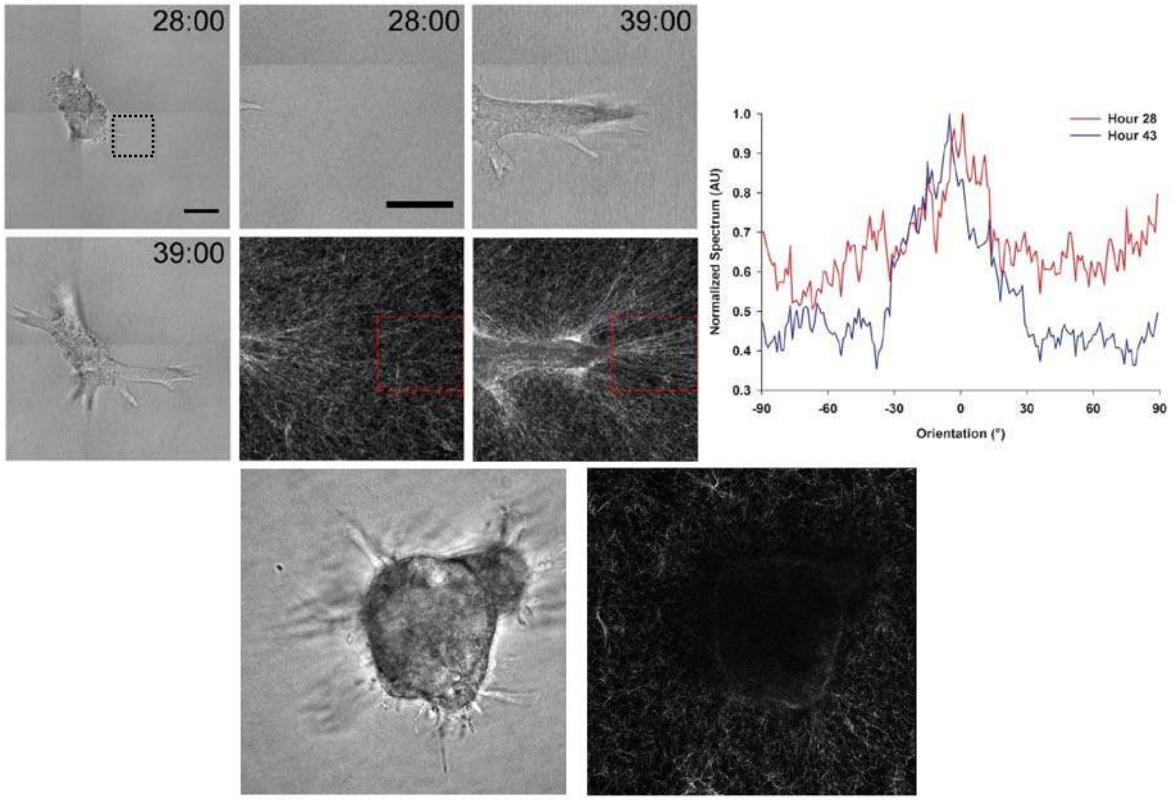

Figure 4.7. Local collagen matrix re-orientation occurs during branching. Representative BF and CRM of a branch from a mammary explant at hour 28 and 39 (dashed black insert), showing dramatic matrix alignment proximal to branch tip (upper panel), confirmed via FFT analysis (dashed red insert, scale bar 50μm). Inhibition of ROCK via Y27632 shows no significant changes in matrix orientation (lower).

4.3.7 – Pre-aligned matrices direct branch orientation

While previous experiments demonstrated that the surrounding matrix is oriented during branching, it was unclear whether matrix orientation played a role during the process. To elucidate this point and discern between the correlative versus causative role of matrix orientation during branching morphogenesis, a simple though novel method was developed in which an axial bias is induced within collagen matrices via application of a modest compression (~10% strain), as seen in Figure 4.8. Initial characterization was performed using the standard collagen concentration (3 mg/ml) and the orientation visualized before and after compression. FFT analysis showed a dramatic increase in matrix orientation upon compression. Moreover, lowering collagen concentration (1.5 mg/ml) did not significantly alter the efficiency of alignment induction, as depicted in Figure 4.8.

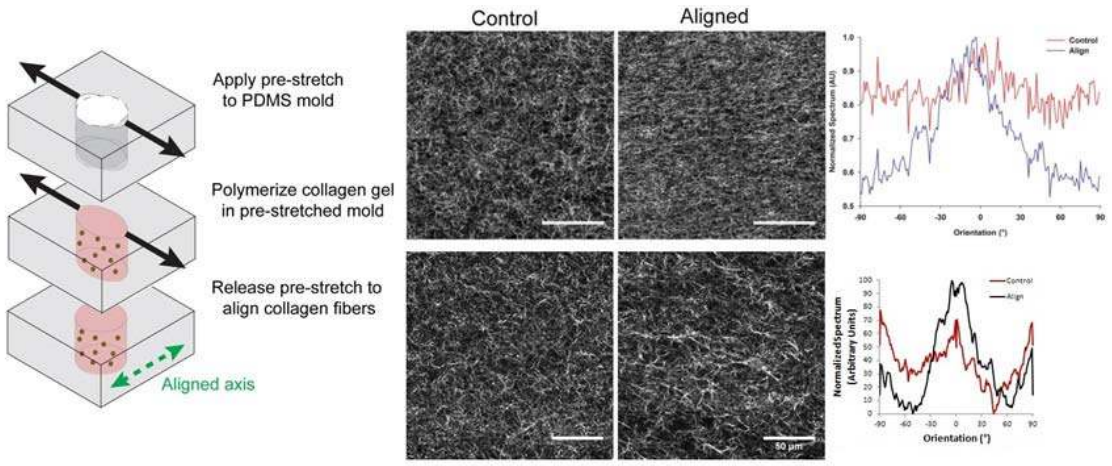

Figure 4.8. Aligning three-dimensional matrices for in culture assays via compression. Schematic of method, in which a malleable well is pre-stretched then released after gelation, aligning the matrix perpendicular to the axis of compression (left). CRM of matrices before and after compression for 3 (upper) and 1.5 (lower) mg/ml, respectively, with subsequent FFT quantification showing significant uni-axial orientation upon compression.

Next, both mammary explants and aggregates were embedded into both control and aligned matrices. After three days of branching, 50 explants/aggregates were imaged and branch orientation measured, which averages of 100-150 branches per condition. Measurements of branches with a length shorter than the radius of the explant/aggregate are discarded. The resulting orientation data are shown in a rose plot in figure 4.9. As expected, both organoids and aggregrates show no signifcatnt orientation bias in control matrices. Strikingly, both organoids and aggregates in pre-aligned matrices showed significant orientation towards the axis of collagen alignment. These results indicate collagen alignment can impart directional cues during branching morphogenesis.

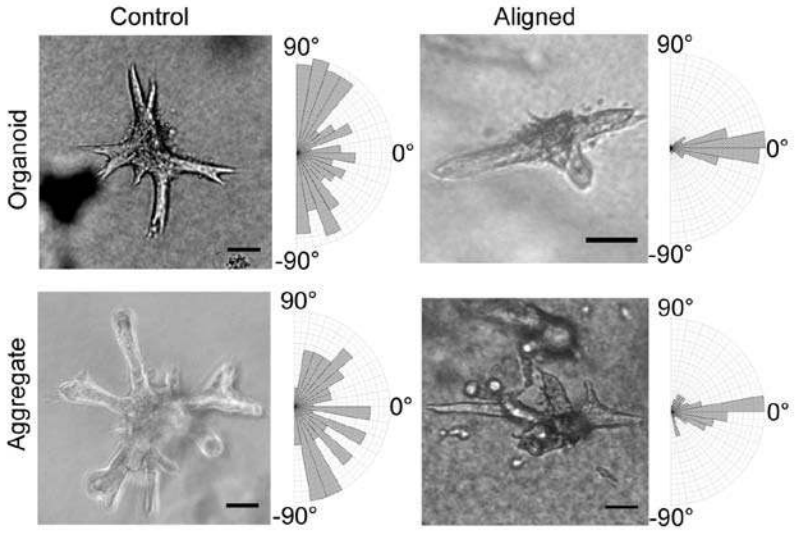

Figure 4.9. Matrix pre-alignment orients branching epithelium. Representative phase images of organoids and aggregates either in control or aligned matrices with corresponding rose plots (scale bar 50μm). Dramatic branch orientation is observed in both aggregate and organoid assays.

4.3.8 – The actomyosin machinery is dispensable for alignment sensing

While previous experiments demonstrated the strength of collagen alignment in influencing epithelial orientation during branching morphogenesis, the mechanism by which epithelial cells sense extracellular collagen alignment remained to be determined. Towards this goal, EpH4 cell lines expressing either a control construct, mYPet or a dominant negative RhoA construct, mYPet-RhoAT17, were generated suing standard molecular techniques and selected via puromyocin resistance then aggregated and used in alignment studies. As illustrated in Figure 4.10, deactivation of RhoA, the small GTPase implicated in regulating actomyosin contractions, had no significant effect compared to the control in branch orientation. To further rule out the actomyosin machinery, inhibitors of ROCK (Y27632) and MLCK (ML-7) activity as well as of binding affinity of type II non-muscle myosin to actin (Blebbistatin) were used in the alignment assay. Interestingly, while in some cases disrupting branching morphology (Blebbistatin), all conditions still followed extracellular alignment cues.

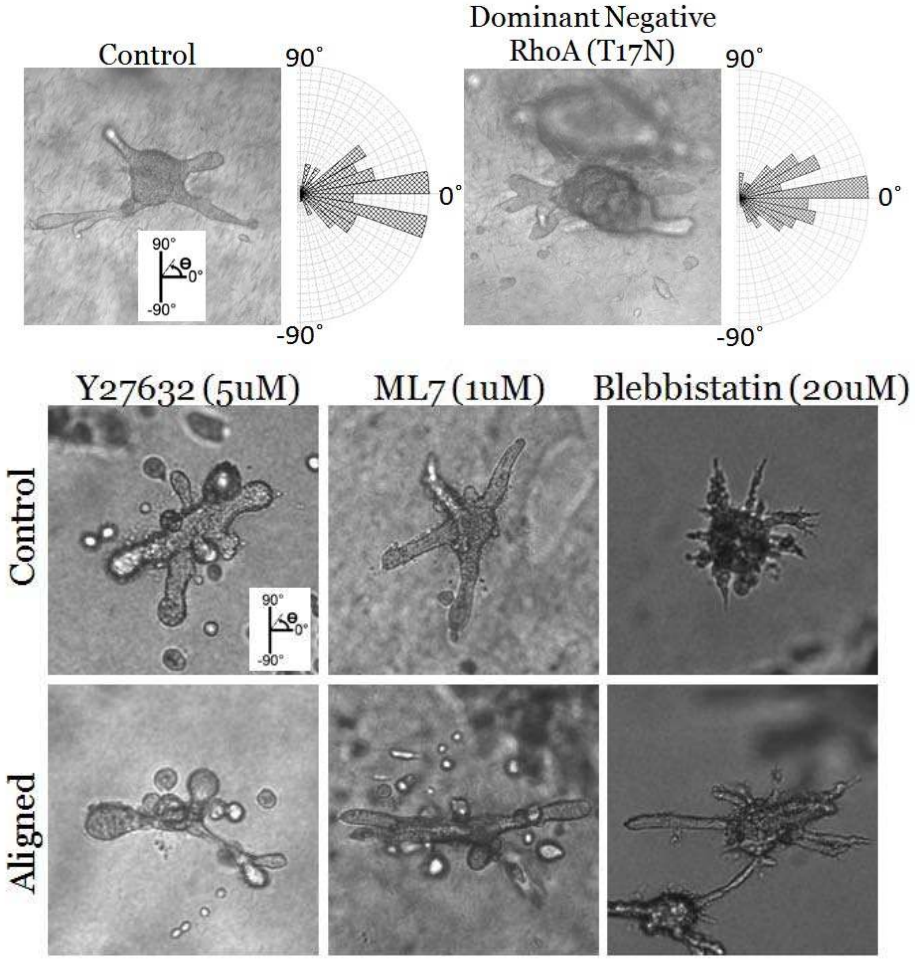

Figure 4.10. Alignment sensing does not require actomyosin machinery. Neither deactivation of RhoA (upper) nor inhibition of downstream components ROCK, MLCK, and type II non-muscle myosin led to disruption of alignment sensing in oriented collagen matrices.

4.3.9 – Matrix and epithelial orientation in the mammary gland

It was necessary to determine if observations found in our three-dimensional culture assay were relevant in the mammary gland, mainly to see whether there an orientation bias existed in the mammary epithelium and stromal collagen, as well as co-orientation between both. To determine if stromal collagen was pre-oriented prior to branching morphogenesis, confocal sections of mammary glands from 3 week Balb/c mice were stained with a novel probe specific for type I collagen. Significant fibrillar, collagen rich structures were observed enveloping the fat pad, both proximal and distal to the branching epithelium as seen in Figure 4.11. Moreover, the fibers demonstrated a significant uni-axial bias parallel the horizontal axis depicted below. Fibers proximal to the epithelium showed significant co-orientation to the epithelium, irrespective to the horizontal axis. Orthogonal section of the fat pad shows intense collagen I signal towards either exterior surface of the fat pad which corresponds to areas of greatest collagen orientation.

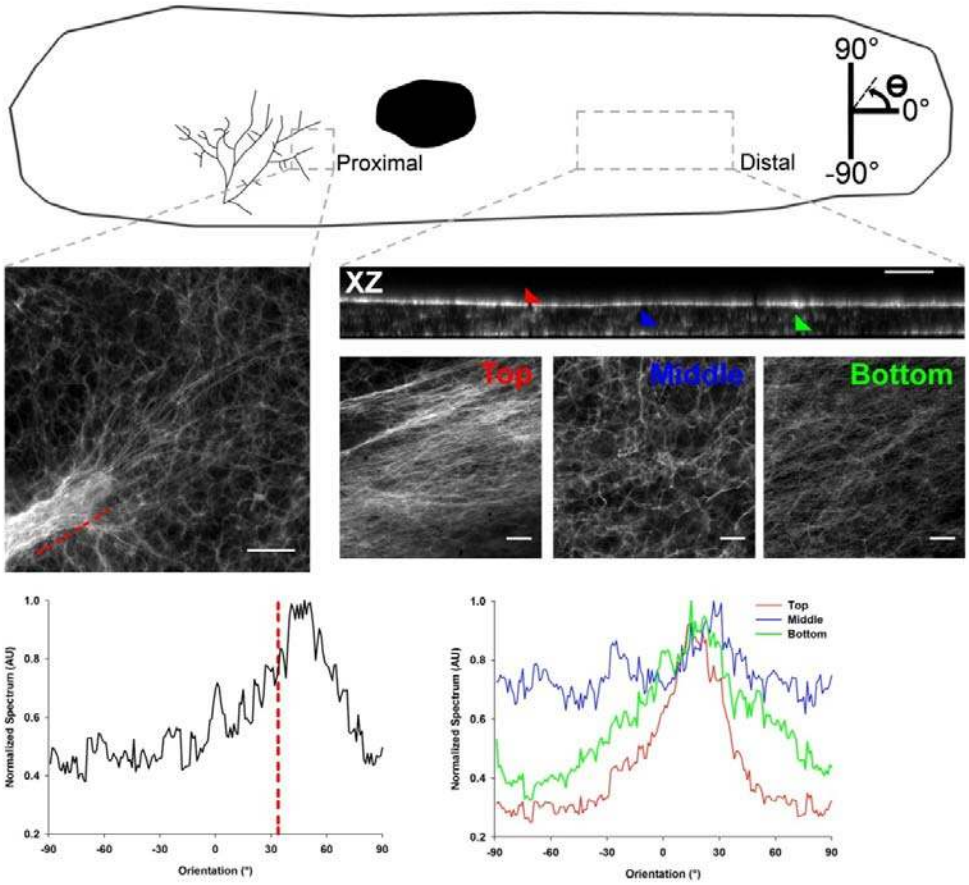

Figure 4.11. Collagen I orientation in the mammary gland. Model of a 3 week old inguinal mammary gland, showing fibers proximal to the epithelium (lower left) co-orient to the branch (dashed red line) while distal fibers (lower right) are mainly located to the exterior surface (red and green arrows) of the fat pad and are uni-axially oriented with the horizontal axis (scale bar, 100μm).

Finally, the epithelial orientation within the mammary gland was measured, specifically at the initiation (~3 week) and termination (~8 week) of branching morphogenesis. In order to quantify orientation, whole mounts were imaged via a stereoscope and the epithelium traced using ImageJ. Generated traces were analyzed using a novel matlab script that segments the traces into evenly space 50μm segments whose orientation was calculated, leading to measurement numbers in the 100's for 3 week samples and 1000's for 8 week samples. For 3 week mammary glands, no repeatable axial bias is observed, with most glands having unique distributions of unbiased orientation as observed in Figure 4.12. In contrast, the epithelia from 8 week glands were dramatically and repeatedly oriented towards the horizontal axis. Moreover, the axis of epithelia bias observed at 8 weeks is the same for the collagen-fibers observed distally from the epithelia of 3 week mammary glands, strongly inferring that collagen I is utilized as a directional cue during branching morphogenesis.

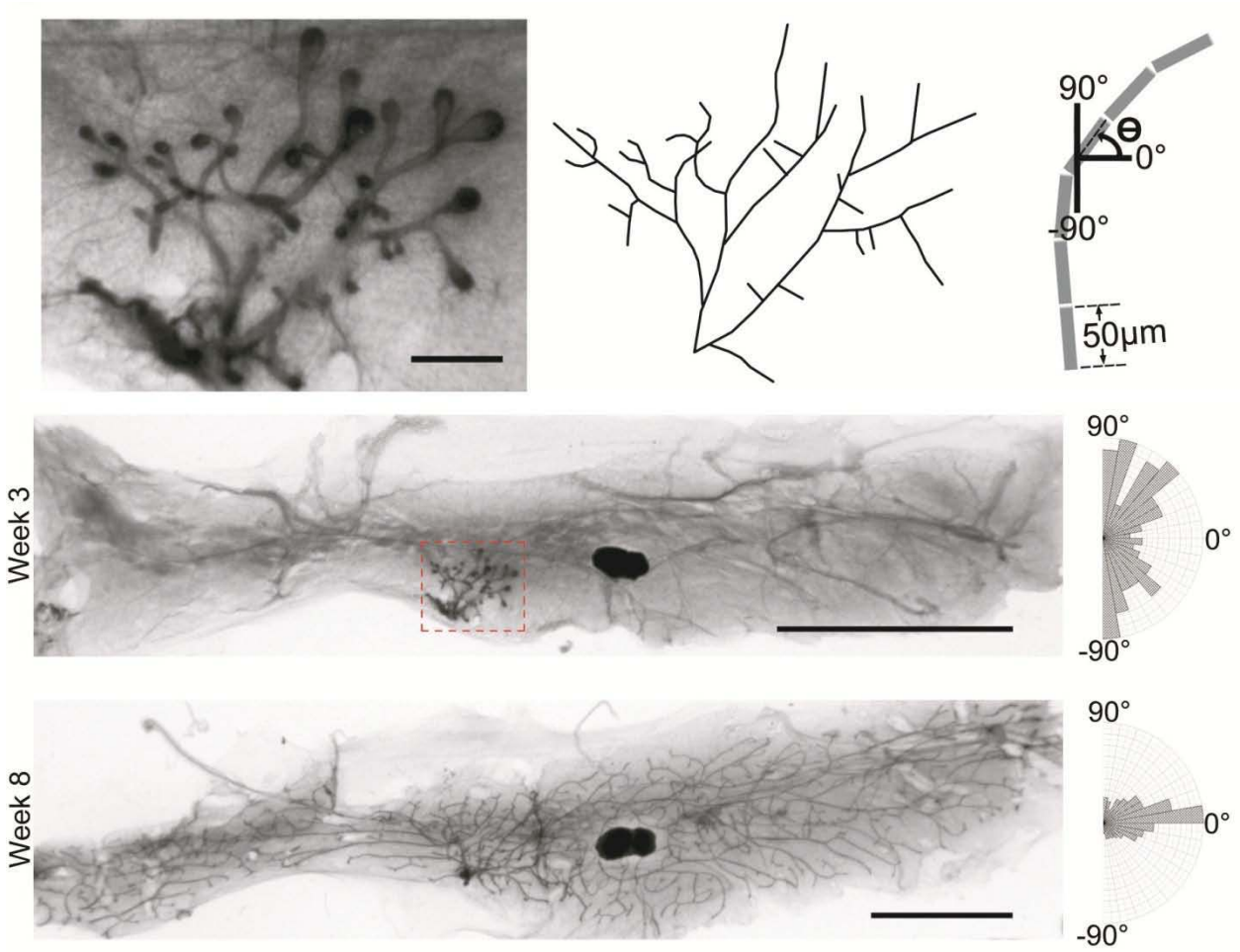

Figure 4.12. Orientation of the mammary epithelium during and after branching morphogenesis. Depiction of orientation analysis (upper,), in which an image of the mammary epithelium is traced then orientation measured in evenly spaced, 50μm segments. Representative whole mounts (lower) of 3 and 8 week mammary glands with corresponding orientation analysis, showing a significant axial bias of th epithelium in 8 week samples (scale bar, 5mm).

4.4 – Discussion

4.4.1 – Interrelationship between ECM composition and stiffness with functional differentiation

When considering the interface between the ECM and the mammary epithelium, it is important to remember in vivo signals from the microenvironment are essential for normal development and organ homoeostasis, and abnormalities in these signals contribute to various pathologies including tumorigenesis [186, 261]. Nevertheless, the detailed mechanochemical signaling by which the microenvironment controls these processes are still ill-defined [256]. Previous studies using cultured cells have examined the effects of extracellular biochemical or biophysical cues on differentiation [255], morphology [262] and mechanics [263], each in isolation. Here, we used a comprehensive approach to demonstrate quantitatively the intimate connection among LM1 binding, ECM elasticity, cell shape and cell elasticity in controlling tissue-specific gene expression in single epithelial cells. In addition, we found that variations of these properties from biomimetic values induce a loss of functional differentiation, which could potentially be linked to loss of differentiation during tumorigenesis.

4.4.2 – ECM softening during branching morphogenesis

We observed localized ECM degradation and softening at invasive fronts, in agreement with a long-standing hypothesis in the field [239, 243]. In this context it is worth noting that this localized ECM remodeling may facilitate branching through separate processes that may occur coincidentally. First, collagen degradation removes steric obstacles at invasive fronts, thereby increasing the room available to accommodate the thickness of the invasive body (i.e., a path clearing function), and/or facilitating the assembly of tracks that are filled by following cells (i.e., path-generating function) [264]. Second, because opposing F_{el} increases linearly with E of the collagen gel, a reduction of E will have a direct and proportional impact in reducing opposing elastic forces. Third, local gel softening creates a stiffness gradient within the ECM, which may act as a migratory cue [265]. Finally, there is evidence that degraded fibrillar collagens per se can stimulate growth.

4.4.3 – ECM organization directs epithelial orientation during branching morphogenesis

Initially we observed branching mammary explants in collagen matrices and found substantial re-organization, specifically local matrix alignment that the branching epithelium co-orients with the collagen tracks, the generation of which required ROCK activity. Interestingly, further work in aligned matrices showed that the actomyosin machinery was dispensable for alignment sensing. Taken together, these results indicate the role cellular contractions could be positively reinforcing directional decisions. Since oriented collagen had a strong impact on branch direction in culture, we next observed collagen organization in the fat pad. Areas of aligned collagen fibers were observed distal to the epithelium oriented along a main axis in 3 week old

mammary fat pads, well before significant ductal branching occurs. Next, measuring orientation during branching morphogenesis 3-8 weeks after birth, we observed the mouse mammary epithelium is dramatically oriented along the same axis of pre-oriented collagen fibers.

Chapter 5 – Conclusions and future directions

This chapter will outline both the results and conclusions drawn from this dissertation while providing thoughts on future experiments and directions. First a quick recitation of key experimental results for each chapter corresponding to which aims being addressed, with specific criticism and analysis covered later in the conclusion and future direction section.

5.1 – Results Summary

The overall goal of this dissertation was to characterize the interface between the microenvironment and the developing mammary epithelium. To pursue specific aspects of the interface, the project is first divided into the two main components of the microenvironmental interface, the cell-cell interface and the cell-ECM interface. From this distinction, the dissertation focuses on three main aims: 1) First, characterization of the lineage-dependent sorting between human mammary epithelial cells. 2) Next, characterization of the extracellular stiffness in mammary gland development. 3) Last, characterization of matrix organization during branching morphogenesis.

For Aim A, HMECs were found to undergo lineage dependent sorting that was mainly dependent on levels of E-cadherin. Other molecular components involved in the cytoskeleton as well as junction stability such as MLCK and ROCK, though further studies demonstrated MLCK was necessary for generation and maintenance of sorting, while ROCK was dispensable after successful sorting was established.

In Aim B, the role of extracellular stiffness was explored using two models for different stages of mammary gland development. First, ECM stiffness was studied with respect to functional differentiation, in which the promoter activity for the gene encoding the milk protein β-casein was used the main metric. It was found that maintenance of β-casein expression required both laminin signaling and a 'soft' extracellular matrix, as is the case in normal tissues in vivo, as well as physiological intracellular elasticity, as is the case in primary mammary epithelial organoids. Next, the relationship of extracellular stiffness was explored in a three-dimensional collagen culture model for branching morphogenesis and identified stiffness of the collagenous ECM is reduced at invasive fronts due to its degradation by MMPs.

Finally, Aim C was plummeted with both a novel variant of aforementioned collagen three-dimensional culture model as well as extracted mammary glands. Results in culture inferred the mammary epithelium follows oriented collagen tracks, either pre-existing or self-generated via local contractions. While contractions are necessary to generate local alignment, it was dispensable for sensing and following aligned collagen. Oriented, collagen rich tracks were found in the mammary fat pad distal from the branching epithelium, strongly inferring the tissue encodes directional cues that direct branch orientation and shape overall epithelial architecture.

5.1.1 – Determination of HMEC self-organization

In this aim, we sought to observe and quantify the sorting of different HMECs. Towards that end, we developed a method to extract different epithelial lineages from normal human mammary tissue as well as a three dimensional culture model to visualize and quantify sorting between lineage mixtures. From there we crafted experiments to determine which cell surface molecules are involved in lineage-specific sorting. Further characterization was carried out to test the role of cellular stiffness in sorting, as well as to test whether regulators of the actomyosin cytoskeleton were also implicated in self organization. Finally, experiments to discern between mechanisms necessary for the establishment versus maintenance of sorting were carried out.

Here it was demonstrated that self-organization of mammary epithelial cells is a lineage-specific process that is principally E-cadherin driven; however, P-cadherin also may play a role in organizing the MEP layer. Unaltered normal finite-lifespan HMEC and the microwell assay were used together with recombinant proteins and antibodies that blocked specific adherens junction proteins. Previous, elegant proof-of-principal experiments, which that showed differential levels of cell–cell adhesion molecules can drive self-organizing, were performed using fibroblasts and other immortal cell lines that were engineered to express different levels of adherens junction proteins. It is remarkable, given the undoubted complexity of the LEP and MEP cell surfaces, that E-cadherin plays so central a role in the process of self-organization in those cells. It has been hypothesized that self-organizing is not simply the result of differential levels of cadherin expression or of binding affinities, but rather that adhesion energy and the ability to remodel cell–cell junctions are crucial determinants.

Dynamic analysis of HMEC in the microwell assay platform in the presence of actomyosin inhibitors provided support for that hypothesis in the context of mammary gland, in which MLCK inhibition (ML-7) prevented self-organization as well maintenance of sorted phenotype, while ROCK inhibition (Y27632) was dispensable for said maintenance. Elegant time-lapse imaging studies from others of mouse mammary organoid morphogenesis also revealed that the actomyosin inhibitors Y27632 and ML-7 disrupted the clean bilayered organization [226], but not to the catastrophic extent observed in the HMEC microwell assay. Because the mouse mammary organoids were developed in vivo, a number of additional cellular interconnectivities crucial for tissue stability may have formed that were absent in our recombined system. Although the focus was on cell–cell E-cadherin junctions, other adhesive and physical interactions, such as desmosomal interactions between LEPs and MEPs [232], undoubtedly are important in maintaining mammary gland organization and bear further dissection. Cell–ECM interactions also will likely affect sorting in vivo. Because the microwell assay uses a nonfouling coating to prevent cell adhesion, the adherens junction proteins may have had a more pronounced effect on self-organizing than they would have had in the presence of ECM. Atomic force microscopy analysis of LEP and MEP on plastic dishes indicated that LEP tended to be softer than MEP. However, a cultured murine epithelial cell line became less stiff in contact with LM1, a principal component of basement membrane, than when in contact with plastic [2]. Therefore, MEPs in vivo may be less

or equally as stiff as LEPs because of their direct contact with basement membrane. Future iterations of the microwell platform will help elucidate more of the factors involved in making stable and organized tissues.

5.1.2 – Characterization of extracellular stiffness during functional differentiation

Next the focus adjusted to the cell-ECM component of the interface, specifically the relationship of stiffness with respect to functional differentiation. Towards that end, both biological and synthetic substrata were used to test the hypothesis that robust functional differentiation in culture requires substrata exhibiting elasticity within the range observed in normal mammary tissue, which are defined here as physiological or biomimetic elasticity. The elastic modulus of the substrata was measured at the micro- and macroscopic scales by AFM and rheometry, respectively. In agreement with previous findings on synthetic gels [262], the two techniques provided comparable values for biological gels, indicating that either method is suitable to probe the mechanics of compliant materials.

In support of this hypothesis, it was found that β-casein expression was maximal in MECs cultured on LM1-rich ECM gels containing ~40% LM1 or more and exhibiting elastic moduli values within 75–120 Pa, a range comparable with normal mammary tissue. Conversely, dramatic reduction in β-casein expression (<3-fold) was observed in gels with less than 10% LM1 and a non-biomimetic elasticity of 4250 Pa. Similarly, increasing the stiffness of synthetic polyacrylamide gels close to mammary tumour values was sufficient to downregulate functional differentiation induced by overlaying 2% Matrigel in the medium. However, the corresponding degree of β-casein expression on polyacrylamide gels was less than that observed on the biological gel assays. This lower β-casein induction is not surprising if one considers the important differences between the biological gels and the polyacrylamide gel assay in terms of how laminin is presented to the cell, that is, physically cross-linked within a gel versus in soluble form, and at what time point during the assay, that is, at plating time versus after 24 hours. It is remarkable that all experiments conducted consistently reveal that LM1-dependent functional differentiation is modulated by extracellular elasticity, and that, for a given LM1 concentration, β-casein expression is enhanced when the substrata exhibits biomimetic elasticity.

In addition to a requirement for biomimetic extracellular elasticity, it was observed that strong β-casein expression (~10–100-fold) was tightly associated with biomimetic cell elastic moduli (400–800 Pa), whereas β-casein expression was lost when values fell outside this range. Collectively, these findings reveal that functional differentiation of MECs is programmed to be highly responsive only in a narrow range of extra- and intercellular elasticity. These findings are qualitatively similar to recent findings on mechanically dependent stem cell commitment [266]. These results also suggest that the high compliance of the mammary tissue in vivo is essential for its functional differentiation as well as morphogenesis.

5.1.3 – Localized, MMP-dependent collagen I softening during branching morphogenesis

Next, ECM stiffness was observed in a different context, particularly the modulation of stiffness of three-dimensional type I collagen matrices during branching morphogenesis. Previous work inferred that it is conceivable that MECs could minimize F_{el} further by locally degrading the ECM, thereby down-regulating E of the collagenous gel at invasive fronts. To test this hypothesis, AFM was used to locally measure the E of gels either at invasive fronts or >100 μm away from cell clusters in the absence or presence of the broad spectrum MMP inhibitor and found that the average E at invasive fronts was nearly half the average E measured far from cell clusters. Furthermore, this dramatic ECM softening at the edge of invasive bodies was abrogated with GM6001, supporting the hypothesis that ECM softens locally at invasive fronts, and that this softening is driven by MMP-dependent local degradation.

To analyze the extent of this local collagenous degradation, similar branching experiments were conducted with cell clusters embedded instead within collagen-I mixed with DQ-Collagen, from which was observed areas void of DQ-collagen signal at the invasive front in control branching conditions, while areas were barely observed or were randomly distributed in non-branching clusters treated with GM6001. Morphometric analysis of the areas void of DQ-signal revealed an average width of 25–40 μm, which is slightly larger than the depth of invasive bodies probed with AFM. These findings indicate that the local ECM softening measured at invasive fronts spatially matched the appearance of areas void of fluorescent signal, which is indicative of degradation of filamentous collagens.

To understand quantitatively how local collagen degradation leads to gel softening a cell-free 3 mg/ml collagen-I gel with was treated with exogenous bacterial collagenase up to 60 minutes, which led to a dramatic disappearance of collagen filaments as revealed by CRM as well as a five-fold decrease in E as measured by AFM. Therefore, as in our branching assay, we observed that collagenase-dependent gel softening was associated with loss of fluorescence signal indicative of degradation of collagen filaments. Second, we measured E on gels prepared at different collagen concentrations (1–4 mg/ml), and observed a marked gel stiffening with increasing c. The average E of cell-free collagen gels measured with AFM was consistent with bulk measurements reported elsewhere at similar semi-diluted concentrations [267] and fell within the physiological range reported for mouse mammary tissue [175].

5.1.4 – Collagen I directs epithelial orientation during branching morphogenesis

Finally, specific Aim C was addressed in the context of collagen I matrix organization during branching morphogenesis. Initial studies of time lapse microscopy of embedded organoids revealed significant matrix re-organization at the invasive fronts described previously as being implicated with local matrix degradation [1]. Regarding organization, orientation analysis revealed significantly increased alignment compared

to farther away from the organoids. Similar bias in collagen I alignment proximal to epithelium was observed in the mammary gland as well, of both 3 week and 8 week old mice, with subsequent co-orientation of the epithelium to the collagen tracks. Treatment with an inhibitor of ROCK in culture demonstrated a significant loss in generated local alignment in the collagen matrix, inferring the dependence of actomyosin contraction machinery in creating alignment.

Next the role of matrix alignment during branching was directly assessed by the development of a novel method to generate collagen pre-alignment in three-dimensional cultures via compression. Once the method was verified to work via FFT analysis, independent of collagen concentrations used in standard culture experiments, organoids and aggregates were embedded in pre-aligned matrices. Strikingly, a substantial bias in branch orientation was observed (~5 fold bias) in both aggregates and organoids. Further work utilizing inhibitors of actomyosin machinery, such as ROCK (Y27632), MLCK (ML-7), and nonmuscle type II myosin (Blebbistatin) as well as a lentiviral expression of a dominant negative form of RhoA demonstrated no dramatic impact on the orientation bias of branching aggregates, implying the dispensability of actomyosin machinery and contractions in sensing collagen I alignment.

Finally, the possibility of collagen I pre-orientation is explored in mouse mammary fat pads. Visualizing collagen I in 3-week mice, in which very little branching has occurred, showed significant collagen I orientation at sites distal to the epithelium, especially towards the exterior surfaces of the fat pad. Epithelial orientation also was measured and while 3-week glands show no repeatable bias, there is a significant uniaxial bias in 8-week glands, a time when branching morphogenesis has terminated. Taken together, these results infer that collagen I tracks are to some extent prepatterned into the fat pad well before the start of branching morphogenesis and guide epithelial orientation.

5.2 – Conclusions and future directions

In characterizing the interface between the mammary epithelium and the microenvironment, it is necessary to define specific components and context for focused studies. The cell-cell component of the interface could be researched with respect to several developmental processes, such as milk production, collective cell migration, as well as lumen formation. Studying self-organizing behavior of a human epithelium generally is challenging because results cannot be extrapolated easily to in vivo conditions. However, observations of breast cancer pathogenesis suggest the basic mechanisms described here are important for maintaining mammary gland organization. E-cadherin expression and localization frequently are misregulated in breast cancers [233, 234], and loss of E-cadherin is a hallmark of the epithelial-to-mesenchymal transition, which is associated with invasive and aggressive breast cancer [236]. The mechanisms governing self-organization also are important in the context of regenerative tissue maintenance. As MEPs and LEPs are produced anew by mammary progenitor cells in vivo, they must adopt their appropriate place within the tissue, or,

alternatively, the progenitors must be able to move to receive instructive microenvironments that direct cell-fate decisions [237]. Understanding tissue self-organization mechanisms may help explain how stem cell differentiation and maintenance of tissue architecture in adults are coordinated.

There is much future work to be completed with regards to lineage dependent sorting of adult MECs. While initial microwells were fabricated from PDMS of fairly high rigidity and treated to become a non-fouling surface, future studies focused on the interrelationship of cell-cell and cell-ECM interactions could incorporate coatings of various ECM molecules, possibly restriction the localization as well, in order to capture dynamics of sorting in a more biologically relevant context. Moreover, microwells could be fabricated out of materials whose stiffness can be finely tuned to further probe interrelationships between cell-cell stiffness as well as cell-ECM stiffness during sorting. Of course this novel technique could be used to study other biological processes in better detail, such as lumen formation, as well be used in conjunction with other techniques, such as AFM to accurately capture mechanical behavior in the context of the assay [202]. Further characterization studies could also be carried out, in which the localization of other junction or cytoskeletal proteins are visualized during the sorting process as well functional perturbed to determine potential mechanism.

Transitioning from characterization of cell-cell interactions to cell-ECM, this dissertation sought to better understand the role of extracellular stiffness on functional differentiation, also known as milk production. From studies in which extracellular stiffness was tightly controlled and cellular stiffness measured, a strong association between extra- and intracellular elasticity and functional differentiation in MECs was found. Specifically, this work demonstrated that LM1 signaling and biomimetic extracellular elasticity are clearly necessary for functional differentiation of MECs; these cells in turn exhibit a strong correlation with biomimetic cellular elasticity, although the proof of a mechanistic relation between the latter and β-casein expression remains to be elucidated. As these signaling pathways go awry in tumorigenesis [175, 258], it is tempting to speculate that, in addition to LM1 signaling, physiological tissue mechanics and/or its underlying homoeostatic mechanisms would have protective, that is, tumour suppressor, functions associated with maintenance of functional differentiation in vivo.

Future work would either focus on underlying mechanisms of how stiffness regulates or misregulates functional differentiation or further explore regulatory roles of dimensionality and/or geometry. Mechanistic studies would take the form of time-course experiments, determining the timing between cellular elasticity reaching biomimetic ranges to the increase of β-casein production. In combination with images showing composition/structure of the cytoskeleton while in different moduli or while the cellular elasticity is transitioning from/into the biomimetic range. Dimensionality could dramatically modulate both magnitude and time-response from MECs with respect to functional differentiation. What remains to be determined is whether LM1 rich matrices of increasing stiffness would affect magnitude, speed, or both of β-casein expression. Such information would be critical in gaining mechanistic insight into microenvironmental regulation of milk production. Since previous work has shown

micropatterned cells undergo specific tension dictated in part by the pattern's geometry, it can be hypothesized that β-casein production would vary cell to cell by its particular position on the micropattern. The possibility that geometry regulates functional differentiation via the differential generation of intracellular tension begs the question whether the developmental state between branching morphogenesis and functional differentiation, named alveologenesis and involves the formation of flowering buds that become main sites for later milk production, is necessary in part to generate a geometry that is permissive for MECs to exist in a 'soft' state that is optimal for β-casein production. Softening of the microenvironment for functional differentiation may also be a secondary role for the work described below, in which collagen I is locally degraded during branching morphogenesis which precedes functional differentiation.

Next the mechanical nature of ECM resistance during branching morphogenesis was studied to identify efficient strategies to overcome this resistance using a three-dimensional culture model of mammary epithelial branching morphogenesis in collagen-I gels. Modeling work by collaborators [1] theorized that any increase in exogenous ECM elastic resistance must be counterbalanced by reducing this resistance, increasing cell intrinsic forces, or both. In support of this prediction, two strategies were identified that can independently reduce the elastic resistance imposed by the collagenous ECM on cells. The first strategy is based on adopting a narrow tube-like invasive geometry, not covered in this dissertation, which minimizes elastic forces according to the theory of contact elasticity. The second strategy is based on locally degrading the ECM at invasive fronts, thereby inducing a local softening of the ECM gel and a concomitant reduction of at least 50% of the ECM stiffness and elastic resistance. This latter observation is of particular interest because it provides experimental evidence of a long-standing hypothesis in the field. Local ECM softening at invasive fronts was largely driven by MMP activity, in agreement with previous studies supporting a prominent role for a collagenase, MMP14 in particular, in physiologic and pathologic collective cell migration. In contrast, shape accommodation was discarded as an efficient strategy to overcome ECM barriers, instead focusing on that invasive geometries permissive for lumen formation such as those involved in ductal formation are subjected to increased ECM elastic resistance, and predicted that cells must employ additional strategies to compensate for this raise in ECM resistance, including increased cell layers, building up fluid pressure within a sealed lumen, or strengthening of the basement membrane. Collectively, these findings shed new light on how cells overcome ECM mechanical resistance during branching morphogenesis via local matrix degradation via MMPs.

Future work, possible as well as ongoing, focuses on the relationship of extracellular stiffness on invasion as well the expression and activation of MMPs. It is likely that the stiffness dependent malignant and/or invasive phenotypes observed by others are in part mediated by MMPs [175], so the remaining direction would be to determine by what mechanism, such as transcriptional regulation or mechanical activation, certain MMPs are regulated by extracellular stiffness. Another interesting direction would be to reconcile discrepancies between the in culture model and the in vivo process of branching morphogenesis, the most obvious of all being the end bud,

which has yet to be reproduced morphologically in culture. While much work in the mammary development field has learned much from using such models that shows biological relevance in the mammary gland [259, 268], others have inferred such models are inaccurate regarding migratory or other morphogenic processes [226]. Future studies in which an end bud can be recapitulated in culture would be instrumental in understanding the context of sensing extracellular stiffness as well as local MMP-dependent matrix remodeling.

In studying the role of extracellular stiffness at the cell-ECM interface [1], it became apparent that matrix organization was critical during branching in collagen I matrices. Initial time course studies demonstrated that local, ROCK-dependent, contractions generated aligned collagen I tracks at invasive front that the multicellular branch co-orients with. Later work using a novel approach demonstrated collagen I alignment was a strong directional cue during branching and that alignment sensing/following was independent from actomyosin machinery previously mentioned. Orientation analysis in extracted mammary glands provided strong evidence that pre-oriented collagen I tracks exist in the fat pad prior to onset of branching morphogenesis. Moreover, the orientation of the mammary epithelial tree formed during branching morphogenesis is uni-axially biased and co-oriented with the collagen I tracks previously described. Taken together, this study strongly implies the possibility that the fat pad encodes the orientation of the epithelial tree well before branching morphogenesis.

The possibility of mesenchymal patterning that directs epithelial architecture opens many new avenues for future studies. Since the pre-oriented collagen I tracks observed were more localized towards the exterior surfaces, such as the fascia or skin though it was a separate layer from the fat pad, one possibility is that the construction and orientation of these tracks occurs earlier in development, specifically when the dermis and mesenchyme start to show dramatic differentiation. Future studies would focus on embryological time points to observe the start of these collagen I tracks. Another possibility, since the no SEM images were taken, is that other components are involved and possibly their patterning precedes collagen deposition, such as fibrillin, which is the earliest expressed fibrous ECM molecule in the embryo. Fibrillin is also known to bind TGF-β, which has been known to promote collagen fibrillogenesis. Future studies could also focus on the mechanism for sensing/following alignment cues. Initial studies strongly dissuade the possibility that cellular contractions, mediated by the canonical actomyosin machinery, mediate such sensing. Current work focuses on the role of molecules known to regulate adhesion and filopodia formation/stabilization, mainly β1-integrin, fascin-1, and myosin-X. While initial knockdown studies has shown a dramatic decrease in % branching, inferring this machinery is generally critical for branching and migration, future studies will focus of fascin-1 overexpression as well as time course studies visualizing filopodial components in aligned matrices.

REFERENCES

1. Alcaraz, J., Mori, H., Ghajar, C.M., Brownfield, D., Galgoczy, R., and Bissell, M.J. (2011). Collective epithelial cell invasion overcomes mechanical barriers of collagenous extracellular matrix by a narrow tube-like geometry and MMP14-dependent local softening. Integr. Biol.
2. Alcaraz, J., Xu, R., Mori, H., Nelson, C.M., Mroue, R., Spencer, V.A., Brownfield, D., Radisky, D.C., Bustamante, C., and Bissell, M.J. (2008). Laminin and biomimetic extracellular elasticity enhance functional differentiation in mammary epithelia. EMBO J *27*, 2829-2838.
3. Drife, J.O. (1986). Breast Development in Puberty. Annals of the New York Academy of Sciences *464*, 58-65.
4. Nelson, C.M., and Bissell, M.J. (2006). Of Extracellular Matrix, Scaffolds, and Signaling: Tissue Architecture Regulates Development, Homeostasis, and Cancer. Annual Review of Cell and Developmental Biology *22*, 287-309.
5. Turner, C., and Gomez, E. (1933). The normal development of the mammary gland of the male and female albino mouse. Mo. Agric. Exp. Stn. Res. Bull. *182*, 3-20.
6. Balinsky, B. (1950). On the pre-natal growth of the mammary gland rudiment in the mouse. J. Anat. *84*, 227-235.
7. Propper, A. (1978). Wandering epithelial cells in the rabbit embryo milk line. Dev. Biol. *67*, 225-231.
8. Parmar, H., and Cunha, G.R. (2004). Epithelial–stromal interactions in the mouse and human mammary gland in vivo. Endocrine-Related Cancer *11*, 437-458.
9. Nandi, S. (1959). Hormonal control of mammogenesis and lactogenesis in the C3H/He Crgl mouse. Univ. Calif. Publ. Zoology *65*, 1-128.
10. Sinha, Y., and Tucker, H. (1966). Mammary gland growth of rats between 10 and 100 days of age. Am J Physiol. *210*, 601-605.
11. Sternlicht, M.D., Kouros-Mehr, H., Lu, P., and Werb, Z. (2006). Hormonal and local control of mammary branching morphogenesis. Differentiation *74*, 365-381.
12. Affolter, M., Bellusci, S., Itoh, N., Shilo, B., Thiery, J.-P., and Werb, Z. (2003). Tube or Not Tube: Remodeling Epithelial Tissues by Branching Morphogenesis. Developmental cell *4*, 11-18.
13. Hinck, L., and Silberstein, G. (2005). Key stages in mammary gland development: The mammary end bud as a motile organ. Breast Cancer Research *7*, 245 - 251.
14. Sternlicht, M. (2006). Key stages in mammary gland development: The cues that regulate ductal branching morphogenesis. Breast Cancer Research *8*, 201.
15. Lu, P., Sternlicht, M., and Werb, Z. (2006). Comparative Mechanisms of Branching Morphogenesis in Diverse Systems. Journal of Mammary Gland Biology and Neoplasia *11*, 213-228.
16. Wiseman, B.S., and Werb, Z. (2002). Stromal Effects on Mammary Gland Development and Breast Cancer. Science *296*, 1046-1049.

17. Fata, J.E., Chaudhary, V., and Khokha, R. (2001). Cellular Turnover in the Mammary Gland Is Correlated with Systemic Levels of Progesterone and Not 17β-Estradiol During the Estrous Cycle. Biology of Reproduction *65*, 680-688.
18. Oakes, S., Rogers, R., Naylor, M., and Ormandy, C. (2008). Prolactin Regulation of Mammary Gland Development. Journal of Mammary Gland Biology and Neoplasia *13*, 13-28.
19. Brisken, C., Kaur, S., Chavarria, T.E., Binart, N., Sutherland, R.L., Weinberg, R.A., Kelly, P.A., and Ormandy, C.J. (1999). Prolactin Controls Mammary Gland Development via Direct and Indirect Mechanisms. Developmental Biology *210*, 96-106.
20. Pang, W., and Hartmann, P. (2007). Initiation of Human Lactation: Secretory Differentiation and Secretory Activation. Journal of Mammary Gland Biology and Neoplasia *12*, 211-221.
21. Neville, M.C., McFadden, T.B., and Forsyth, I. (2002). Hormonal Regulation of Mammary Differentiation and Milk Secretion. Journal of Mammary Gland Biology and Neoplasia *7*, 49-66.
22. Walker, N., Bennett, R., and Kerr, J. (1989). Cell death by apoptosis during involution of the lactating breast in mice and rats. Am J Anat. *185*, 19-32.
23. Lund, L.R., Romer, J., Thomasset, N., Solberg, H., Pyke, C., Bissell, M.J., Dano, K., and Werb, Z. (1996). Two distinct phases of apoptosis in mammary gland involution: proteinase-independent and -dependent pathways. Development *122*, 181-193.
24. Alexander, C.M., Selvarajan, S., Mudgett, J., and Werb, Z. (2001). Stromelysin-1 Regulates Adipogenesis during Mammary Gland Involution. The Journal of Cell Biology *152*, 693-703.
25. Watson, C.J. (2006). Post-lactational mammary gland regression: molecular basis and implications for breast cancer. Expert Reviews in Molecular Medicine *8*, 1-15.
26. Hennighausen, L., and Robinson, G.W. (2005). Information networks in the mammary gland. Nat Rev Mol Cell Biol *6*, 715-725.
27. Alberts, B., Johnson, A., Lewis, J., Raff, M., Roberts, K., and Walter, P. (2002). Molecular Biology of the cell., (New York: Garland Science).
28. Folkman, J., and Moscana, A. (1978). Role of cell shape in growth control. Nature *273*, 345-349.
29. Hauschka, S., and Konigsberg, I. (1966). The influence of collagen on the development of muscle clones. Proceedings of the National Academy of Sciences *55*, 119-126.
30. Meier, S., and Hay, E.D. (1974). Control of corneal differentiation by extracellular materials. Collagen as a promoter and stabilizer of epithelial stroma production. Developmental Biology *38*, 249-270.
31. Emerman, J., Enami, J., Pitelka, D., and Nandi, S. (1977). Hormonal effects on intracellular and secreted casein in cultures of mouse mammary epithelial cells on floating collagen membranes. Proceedings of the National Academy of Sciences *74*, 4466-4470.
32. Bissell, M., Hall, H., and G, P. (1982). How does the extracellular matrix direct gene expression? J Theor Biol *99*, 31-68.

33. Ninomiya, Y., Showalter, A., and Olsen, B. (1982). In the Role of Extracellular Matrix in Development., (Alan R. Liss, Inc.).
34. Linsenmayer, T.F., Fitch, J.M., and Birk, D.E. (1990). Heterotypic Collagen Fibrils and Stabilizing Collagens. Annals of the New York Academy of Sciences *580*, 143-160.
35. Hemler, M. (1990). VLA proteins in the integrin family: structures, functions, and their role on leukocytes. Annu Rev Immunol. *8*, 365-400.
36. Huerre, C., Junien, C., Weil, D., Chu, M., Morabito, M., Van Cong, N., Myers, J., Foubert, C., Gross, M., Prockop, D., et al. (1982). Human type I procollagen genes are located on different chromosomes. Proceedings of the National Academy of Sciences *79*.
37. Junien, C., Weil, D., Myers, J., Van Cong, N., Chu, M., Foubert, C., Gross, M., Prockop, D., Kaplan, J., and Ramirez, F. (1982). Assignment of the human pro alpha 2(I) collagen structural gene (COLIA2) to chromosome 7 by molecular hybridization. Am J Hum Genet. *34*, 381-387.
38. Strom, C., Eddy, R., and Shows, T. (1984). Localization of human type II procollagen gene (COL2A1) to chromosome 12. Somat Cell Mol Genet. *10*, 651-655.
39. Solomon, E., Hiorns, L., Spurr, N., Kurkinen, M., Barlow, D., Hogan, B., and Dalgleish, R. (1985). Chromosomal assignments of the genes coding for human types II, III, and IV collagen: a dispersed gene family. Proceedings of the National Academy of Sciences *82*, 3330-3334.
40. Emanuel, B., Cannizzaro, L., Seyer, J., and Myers, J. (1985). Human alpha 1(III) and alpha 2(V) procollagen genes are located on the long arm of chromosome 2. Proceedings of the National Academy of Sciences *82*, 3385-3389.
41. Henry, I., Bernheim, A., Bernard, M., van der Rest, M., Kimura, T., Jeanpierre, C., Barichard, F., Berger, R., Olsen, B., and Ramirez, F. (1988). Mapping of a human fibrillar collagen gene, pro alpha 1 (XI) (COL11A1), to the p21 region of chromosome 1. Genomics *3*, 87-90.
42. Kimura, T., KS, C., Chan, S., Lui, V., Mattei, M., Van der Rest, M., Ono, K., Solomon, E., Ninomiya, Y., and Olsen, B. (1989). The human alpha 2(XI) collagen (COL11A2) chain. Molecular cloning of cDNA and genomic DNA reveals characteristics of a fibrillar collagen with differences in genomic organization. J Biol Chem. *264*, 13910-13916.
43. Kimura, T., Mattei, M., Stevens, J., Goldring, M., Ninomiya, Y., and Olsen, B. (1989). Molecular cloning of rat and human type IX collagen cDNA and localization of the alpha 1(IX) gene on the human chromosome 6. Eur J Biochem. *179*, 71-78.
44. Muragaki, Y., Mattei, M., Yamaguchi, N., Olsen, B., and Ninomiya, Y. (1991). The complete primary structure of the human alpha 1 (VIII) chain and assignment of its gene (COL8A1) to chromosome 3. Eur J Biochem. *197*, 615-622.
45. Muragaki, Y., Jacenko, O., Apte, S., Mattei, M., Ninomiya, Y., and Olsen, B. (1991). The alpha 2(VIII) collagen gene. A novel member of the short chain collagen family located on the human chromosome 1. J Biol Chem. *266*, 7721-7727.

46. Apte, S., Mattei, M., and Olsen, B. (1991). Cloning of human alpha 1(X) collagen DNA and localization of the COL10A1 gene to the q21-q22 region of human chromosome 6. FEBS Lett. *282*, 393-396.
47. Griffin, C., Emanuel, B., Hansen, J., Cavenee, W., and Myers, J. (1987). Human collagen genes encoding basement membrane alpha 1 (IV) and alpha 2 (IV) chains map to the distal long arm of chromosome 13. Proceedings of the National Academy of Sciences *84*, 512-516.
48. Killen, P., Francomano, C., Yamada, Y., Modi, W., and O'Brien, S. (1987). Partial structure of the human alpha 2(IV) collagen chain and chromosomal localization of the gene (COL4A2). Hum Genet. *77*, 318-324.
49. Solomon, E., Hall, V., and Kurkinen, M. (1987). The human alpha 2(IV) collagen gene, COL4A2, is syntenic with the alpha 1(IV) gene, COL4A1, on chromosome 13. Ann Hum Genet. *51*, 125-127.
50. Hostikka, S., Eddy, R., Byers, M., Hoyhtya, M., Shows, T., and Tryggvason, K. (1990). Identification of a distinct type IV collagen alpha chain with restricted kidney distribution and assignment of its gene to the locus of X chromosome-linked Alport syndrome. Proceedings of the National Academy of Sciences *87*, 1606-1610.
51. Kreis, T., and Vale, R. (1993). Guidebook to the Extracellular Matrix and Adhesion Proteins., (New York: Oxford University Press).
52. Sandell, L., and Boyd, C. (1990). In: Extracellular Matrix Genes, (Academic Press Inc).
53. Vuorio, E., and de Crombrugghe, B. (1990). The family of collagen genes. Annu Rev Biochem. *59*, 837-872.
54. Rauch, F., and Glorieux, F.H. (2004). Osteogenesis imperfecta. The Lancet *363*, 1377-1385.
55. Lawrence, E. (2005). The clinical presentation of Ehlers-Danlos syndrome. Adv Neonatal Care. *5*, 301-314.
56. Prockop, D.J., Olsen, A., Kontusaari, S., Hyland, J., Ala-Kokko, L., Vasan, N.S., Barton, E., Buck, S., Harrison, K., and Brent, R.L. (1990). Mutations in Human Procollagen Genes. Annals of the New York Academy of Sciences *580*, 330-339.
57. Byers, P., and Bonadio, J. (1989). In: Collagen - Molecular Biology, Volume IV, (CRC Press).
58. Superti-Furga, A., Steinmann, B., Ramirez, F., and Byers, P. (1989). Molecular defects of type III procollagen in Ehlers-Danlos syndrome type IV. Hum Genet. *82*, 104-108.
59. Ala-Kokko, L., Baldwin, C., Moskowitz, R., and Prockop, D.J. (1990). Single base mutation in the type II procollagen gene (COL2A1) as a cause of primary osteoarthritis associated with a mild chondrodysplasia. Proceedings of the National Academy of Sciences *87*, 6565-6568.
60. Lee, B., Vissing, H., Ramirez, F., Rogers, D., and Rimoin, D. (1989). Identification of the molecular defect in a family with spondyloepiphyseal dysplasia. Science *244*, 978-980.
61. Birk, D.E., Zycband, E.I., Winkelmann, D.A., and Trelstad, R.L. (1990). Collagen Fibrillogenesis in Situ. Annals of the New York Academy of Sciences *580*, 176-194.

62. Kadler, K.E., Hulmes, D.J.S., Hojima, Y., and Prockop, D.J. (1990). Assembly of Type I Collagen Fibrils de Novo by the Specific Enzymic Cleavage of pC Collagen. Annals of the New York Academy of Sciences *580*, 214-224.
63. Canty, E.G., and Kadler, K.E. (2005). Procollagen trafficking, processing and fibrillogenesis. Journal of Cell Science *118*, 1341-1353.
64. Timpl, R. (1989). Structure and biological activity of basement membrane proteins. European Journal of Biochemistry *180*, 487-502.
65. Yurchenco, P., and Schittny, J. (1990). Molecular architecture of basement membranes. The FASEB Journal *4*, 1577-1590.
66. Glanville, R. (1987). Structure and Function of Collagen Types, (Academic Press Inc).
67. Gordon, M.K., and Olsen, B.R. (1990). The contribution of collagenous proteins to tissue-specific matrix assemblies. Current Opinion in Cell Biology *2*, 833-838.
68. Olsen, B. (1989). The next frontier: molecular biology of extracellular matrix. Connect Tissue Res. *23*, 115-121.
69. Van der Rest, M., and Mayne, R. (1987). Structure and Function of Collagen Types., R. Mayne and R. Burgeson, eds. (Academic Press Inc), pp. 195-221.
70. Gordon, M.K., Gerecke, D.R., Dublet, B., van der Rest, M., and Olsen, B.R. (1989). Type XII collagen. A large multidomain molecule with partial homology to type IX collagen. Journal of Biological Chemistry *264*, 19772-19778.
71. Dublet, B., Oh, S., Sugrue, S.P., Gordon, M.K., Gerecke, D.R., Olsen, B.R., and van der Rest, M. (1989). The structure of avian type XII collagen. Alpha 1 (XII) chains contain 190-kDa non-triple helical amino-terminal domains and form homotrimeric molecules. Journal of Biological Chemistry *264*, 13150-13156.
72. Dublet, B., and van der Rest, M. (1991). Type XIV collagen, a new homotrimeric molecule extracted from fetal bovine skin and tendon, with a triple helical disulfide-bonded domain homologous to type IX and type XII collagens. Journal of Biological Chemistry *266*, 6853-6858.
73. Gordon, M.K., Castagnola, P., Dublet, B., Linsenmayer, T.F., Van Der Rest, M., Mayne, R., and Olsen, B.R. (1991). Cloning of a cDNA for a new member of the class of fibril-associated collagens with interrupted triple helices. European Journal of Biochemistry *201*, 333-338.
74. Lunstrum, G.P., Morris, N.P., McDonough, A.M., Keene, D.R., and Burgeson, R.E. (1991). Identification and partial characterization of two type XII-like collagen molecules. The Journal of Cell Biology *113*, 963-969.
75. Keene, D.R., Lunstrum, G.P., Morris, N.P., Stoddard, D.W., and Burgeson, R.E. (1991). Two type XII-like collagens localize to the surface of banded collagen fibrils. The Journal of Cell Biology *113*, 971-978.
76. Aumailley, M., Bruckner-Tuderman, L., Carter, W.G., Deutzmann, R., Edgar, D., Ekblom, P., Engel, J., Engvall, E., Hohenester, E., Jones, J.C.R., et al. (2005). A simplified laminin nomenclature. Matrix Biology *24*, 326-332.
77. Parsons, M.J., Campos, I., Hirst, E.M.A., and Stemple, D.L. (2002). Removal of dystroglycan causes severe muscular dystrophy in zebrafish embryos. Development *129*, 3505-3512.

78. Macdonald, P.R., Lustig, A., Steinmetz, M.O., and Kammerer, R.A. (2010). Laminin chain assembly is regulated by specific coiled-coil interactions. Journal of Structural Biology *170*, 398-405.
79. Yurchenco, P.D. (2011). Basement Membranes: Cell Scaffoldings and Signaling Platforms. Cold Spring Harbor Perspectives in Biology *3*.
80. Halfter, W., Dong, S., Schurer, B., and Cole, G.J. (1998). Collagen XVIII is a basement membrane heparan sulfate proteoglycan. J Biol Chem *273*, 25404-25412.
81. Groffen, A.J., Ruegg, M.A., Dijkman, H., van de Velden, T.J., Buskens, C.A., van den Born, J., Assmann, K.J., Monnens, L.A., Veerkamp, J.H., and van den Heuvel, L.P. (1998). Agrin Is a Major Heparan Sulfate Proteoglycan in the Human Glomerular Basement Membrane. Journal of Histochemistry & Cytochemistry *46*, 19-27.
82. Timpl, R., and Brown, J.C. (1996). Supramolecular assembly of basement membranes. Bioessays *18*, 123-132.
83. Wu, R.R., and Couchman, J.R. (1997). cDNA cloning of the basement membrane chondroitin sulfate proteoglycan core protein, bamacan: a five domain structure including coiled-coil motifs. J Cell Biol *136*, 433-444.
84. Miner, J.H., Patton, B.L., Lentz, S.I., Gilbert, D.J., Snider, W.D., Jenkins, N.A., Copeland, N.G., and Sanes, J.R. (1997). The laminin alpha chains: expression, developmental transitions, and chromosomal locations of alpha1-5, identification of heterotrimeric laminins 8-11, and cloning of a novel alpha3 isoform. J Cell Biol *137*, 685-701.
85. Marinkovich, M.P., Lunstrum, G.P., Keene, D.R., and Burgeson, R.E. (1992). The dermal-epidermal junction of human skin contains a novel laminin variant. J Cell Biol *119*, 695-703.
86. Leivo, I., Laurila, P., Wahlstrom, T., and Engvall, E. (1989). Expression of merosin, a tissue-specific basement membrane protein, in the intermediate trophoblast cells of choriocarcinoma and placenta. Lab Invest. *60*, 783-790.
87. Goldfinger, L.E., Stack, M.S., and Jones, J.C. (1998). Processing of laminin-5 and its functional consequences: role of plasmin and tissue-type plasminogen activator. J Cell Biol *141*, 255-265.
88. Giannelli, G., Falk-Marzillier, J., Schiraldi, O., Stetler-Stevenson, W.G., and Quaranta, V. (1997). Induction of cell migration by matrix metalloprotease-2 cleavage of laminin-5. Science *277*, 225-228.
89. Colognato, H., and Yurchenco, P.D. (2000). Form and function: the laminin family of heterotrimers. Dev Dyn *218*, 213-234.
90. Wu, T., Wan, Y., Chung, A., and Damjanov, I. (1983). Immunohistochemical localization of entactin and laminin in mouse embryos and fetuses. Dev Biol *100*, 496-505.
91. Thorsteinsdottir, S. (1992). Basement membrane and fibronectin matrix are distinct entities in the developing mouse blastocyst. Anat Rec *232*, 141-149.
92. Smyth, N., Vatansever, H.S., Murray, P., Meyer, M., Frie, C., Paulsson, M., and Edgar, D. (1999). Absence of Basement Membranes after Targeting the LAMC1 Gene Results in Embryonic Lethality Due to Failure of Endoderm Differentiation. The Journal of Cell Biology *144*, 151-160.

93. Shim, C., Kwon, H.B., and Kim, K. (1996). Differential expression of laminin chain-specific mRNA transcripts during mouse preimplantation embryo development. Mol Reprod Dev *44*, 44-55.
94. Dziadek, M., and Timpl, R. (1985). Expression of nidogen and laminin in basement membranes during mouse embryogenesis and in teratocarcinoma cells. Dev Biol *111*, 372-382.
95. Nissinen, M., Vuolteenaho, R., Boot-Handford, R., Kallunki, P., and Tryggvason, K. (1991). Primary structure of the human laminin A chain. Limited expression in human tissues. Biochem J *276 (Pt 2)*, 369-379.
96. Myers, C.A., Schmidhauser, C., Mellentin-Michelotti, J., Fragoso, G., Roskelley, C.D., Casperson, G., Mossi, R., Pujuguet, P., Hager, G., and Bissell, M.J. (1998). Characterization of BCE-1, a transcriptional enhancer regulated by prolactin and extracellular matrix and modulated by the state of histone acetylation. Mol Cell Biol *18*, 2184-2195.
97. Salmivirta, K., Sorokin, L.M., and Ekblom, P. (1997). Differential expression of laminin alpha chains during murine tooth development. Dev Dyn *210*, 206-215.
98. Schuger, L., Skubitz, A.P., Zhang, J., Sorokin, L., and He, L. (1997). Laminin alpha1 chain synthesis in the mouse developing lung: requirement for epithelial-mesenchymal contact and possible role in bronchial smooth muscle development. J Cell Biol *139*, 553-562.
99. Sorokin, L.M., Pausch, F., Frieser, M., Kroger, S., Ohage, E., and Deutzmann, R. (1997). Developmental regulation of the laminin alpha5 chain suggests a role in epithelial and endothelial cell maturation. Dev Biol *189*, 285-300.
100. Yurchenco, P.D., Tsilibary, E.C., Charonis, A.S., and Furthmayr, H. (1985). Laminin polymerization in vitro. Evidence for a two-step assembly with domain specificity. J Biol Chem *260*, 7636-7644.
101. Yurchenco, P.D., and Cheng, Y.S. (1993). Self-assembly and calcium-binding sites in laminin. A three-arm interaction model. J Biol Chem *268*, 17286-17299.
102. Paulsson, M., and Saladin, K. (1989). Mouse heart laminin. Purification of the native protein and structural comparison with Engelbreth-Holm-Swarm tumor laminin. J Biol Chem *264*, 18726-18732.
103. Kalb, E., and Engel, J. (1991). Binding and calcium-induced aggregation of laminin onto lipid bilayers. J Biol Chem *266*, 19047-19052.
104. Yurchenco, P.D., Cheng, Y.S., and Schittny, J.C. (1990). Heparin modulation of laminin polymerization. Journal of Biological Chemistry *265*, 3981-3991.
105. Paulsson, M., Aumailley, M., Deutzmann, R., Timpl, R., Beck, K., and Engel, J. (1987). Laminin-nidogen complex. Extraction with chelating agents and structural characterization. Eur J Biochem *166*, 11-19.
106. Fox, J.W., Mayer, U., Nischt, R., Aumailley, M., Reinhardt, D., Wiedemann, H., Mann, K., Timpl, R., Krieg, T., Engel, J., et al. (1991). Recombinant nidogen consists of three globular domains and mediates binding of laminin to collagen type IV. EMBO J *10*, 3137-3146.
107. Aumailley, M., Wiedemann, H., Mann, K., and Timpl, R. (1989). Binding of nidogen and the laminin-nidogen complex to basement membrane collagen type IV. European Journal of Biochemistry *184*, 241-248.

108. Battaglia, C., Mayer, U., Aumailley, M., and Timpl, R. (1992). Basement-membrane heparan sulfate proteoglycan binds to laminin by its heparan sulfate chains and to nidogen by sites in the protein core. Eur J Biochem *208*, 359-366.
109. Brown, J.C., Sasaki, T., Gohring, W., Yamada, Y., and Timpl, R. (1997). The C-terminal domain V of perlecan promotes beta1 integrin-mediated cell adhesion, binds heparin, nidogen and fibulin-2 and can be modified by glycosaminoglycans. Eur J Biochem *250*, 39-46.
110. Mayer, U., Nischt, R., Poschl, E., Mann, K., Fukuda, K., Gerl, M., Yamada, Y., and Timpl, R. (1993). A single EGF-like motif of laminin is responsible for high affinity nidogen binding. EMBO J *12*, 1879-1885.
111. Colognato-Pyke, H., O'Rear, J.J., Yamada, Y., Carbonetto, S., Cheng, Y.-S., and Yurchenco, P.D. (1995). Mapping of Network-forming, Heparin-binding, and 11 Integrin-recognition Sites within the -Chain Short Arm of Laminin-1. Journal of Biological Chemistry *270*, 9398-9406.
112. Colognato, H., MacCarrick, M., O'Rear, J.J., and Yurchenco, P.D. (1997). The Laminin α2-Chain Short Arm Mediates Cell Adhesion through Both the α1β1 and α2β1 Integrins. Journal of Biological Chemistry *272*, 29330-29336.
113. Hall, D.E., Reichardt, L.F., Crowley, E., Holley, B., Moezzi, H., Sonnenberg, A., and Damsky, C.H. (1990). The alpha 1/beta 1 and alpha 6/beta 1 integrin heterodimers mediate cell attachment to distinct sites on laminin. J Cell Biol *110*, 2175-2184.
114. Languino, L.R., Gehlsen, K.R., Wayner, E., Carter, W.G., Engvall, E., and Ruoslahti, E. (1989). Endothelial cells use alpha 2 beta 1 integrin as a laminin receptor. J Cell Biol *109*, 2455-2462.
115. Tomaselli, K.J., Hall, D.E., Flier, L.A., Gehlsen, K.R., Turner, D.C., Carbonetto, S., and Reichardt, L.F. (1990). A neuronal cell line (PC12) expresses two beta 1-class integrins-alpha 1 beta 1 and alpha 3 beta 1-that recognize different neurite outgrowth-promoting domains in laminin. Neuron *5*, 651-662.
116. Gee, S.H., Blacher, R.W., Douville, P.J., Provost, P.R., Yurchenco, P.D., and Carbonetto, S. (1993). Laminin-binding protein 120 from brain is closely related to the dystrophin-associated glycoprotein, dystroglycan, and binds with high affinity to the major heparin binding domain of laminin. J Biol Chem *268*, 14972-14980.
117. Sonnenberg, A., Modderman, P.W., and Hogervorst, F. (1988). Laminin receptor on platelets is the integrin VLA-6. Nature *336*, 487-489.
118. Lee, E.C., Lotz, M.M., Steele, G.D., Jr., and Mercurio, A.M. (1992). The integrin alpha 6 beta 4 is a laminin receptor. J Cell Biol *117*, 671-678.
119. Kramer, R.H., Vu, M.P., Cheng, Y.F., Ramos, D.M., Timpl, R., and Waleh, N. (1991). Laminin-binding integrin alpha 7 beta 1: functional characterization and expression in normal and malignant melanocytes. Cell Regul *2*, 805-817.
120. Ervasti, J.M., and Campbell, K.P. (1993). A role for the dystrophin-glycoprotein complex as a transmembrane linker between laminin and actin. J Cell Biol *122*, 809-823.
121. Aumailley, M., Timpl, R., and Sonnenberg, A. (1990). Antibody to integrin alpha 6 subunit specifically inhibits cell-binding to laminin fragment 8. Exp Cell Res *188*, 55-60.

122. Almeida, E.A., Huovila, A.P., Sutherland, A.E., Stephens, L.E., Calarco, P.G., Shaw, L.M., Mercurio, A.M., Sonnenberg, A., Primakoff, P., Myles, D.G., et al. (1995). Mouse egg integrin alpha 6 beta 1 functions as a sperm receptor. Cell *81*, 1095-1104.
123. Brandenberger, R., Kammerer, R.A., Engel, J., and Chiquet, M. (1996). Native chick laminin-4 containing the beta 2 chain (s-laminin) promotes motor axon growth. The Journal of Cell Biology *135*, 1583-1592.
124. Liesi, P., Narvanen, A., Soos, J., Sariola, H., and Snounou, G. (1989). Identification of a neurite outgrowth-promoting domain of laminin using synthetic peptides. FEBS Lett *244*, 141-148.
125. Matter, M.L., and Laurie, G.W. (1994). A novel laminin E8 cell adhesion site required for lung alveolar formation in vitro. J Cell Biol *124*, 1083-1090.
126. Graf, J., Ogle, R.C., Robey, F.A., Sasaki, M., Martin, G.R., Yamada, Y., and Kleinman, H.K. (1987). A pentapeptide from the laminin B1 chain mediates cell adhesion and binds the 67,000 laminin receptor. Biochemistry *26*, 6896-6900.
127. Hunter, D.D., Porter, B.E., Bulock, J.W., Adams, S.P., Merlie, J.P., and Sanes, J.R. (1989). Primary sequence of a motor neuron-selective adhesive site in the synaptic basal lamina protein S-laminin. Cell *59*, 905-913.
128. Chalazonitis, A., Tennyson, V.M., Kibbey, M.C., Rothman, T.P., and Gershon, M.D. (1997). The alpha1 subunit of laminin-1 promotes the development of neurons by interacting with LBP110 expressed by neural crest-derived cells immunoselected from the fetal mouse gut. J Neurobiol *33*, 118-138.
129. De Arcangelis, A., Neuville, P., Boukamel, R., Lefebvre, O., Kedinger, M., and Simon-Assmann, P. (1996). Inhibition of laminin alpha 1-chain expression leads to alteration of basement membrane assembly and cell differentiation. The Journal of Cell Biology *133*, 417-430.
130. Desban, N., and Duband, J.L. (1997). Avian neural crest cell migration on laminin: interaction of the alpha1beta1 integrin with distinct laminin-1 domains mediates different adhesive responses. Journal of Cell Science *110*, 2729-2744.
131. Schuger, L. (1997). Laminins in lung development. Exp Lung Res *23*, 119-129.
132. Sorokin, L.M., Pausch, F., Durbeej, M., and Ekblom, P. (1997). Differential expression of five laminin alpha (1-5) chains in developing and adult mouse kidney. Dev Dyn *210*, 446-462.
133. Wolff, Y. (1892). Das Gesetz der Transformation der Knochen (Berlin: Verlag von August Hirschwald).
134. Roux, W. (1895). Gesammelte Abhandlungen uber Entwicklungsmechanik, *Volume II* (Leipzig, Germany: W. Engelmann).
135. Thompson, D. (1917). On Growth and Form, (Cambridge: Cambridge University Press).
136. Bancroft, G.N., Sikavitsas, V.I., van den Dolder, J., Sheffield, T.L., Ambrose, C.G., Jansen, J.A., and Mikos, A.G. (2002). Fluid flow increases mineralized matrix deposition in 3D perfusion culture of marrow stromal osteoblasts in a dose-dependent manner. Proc Natl Acad Sci U S A *99*, 12600-12605.
137. Raab-Cullen, D., Thiede, M., Petersen, D., Kimmel, D., and Recker, R. (1994). Mechanical loading stimulates rapid changes in periosteal gene expression. Calcif Tissue Int. *55*, 473-478.

138. el Haj, A.J., Minter, S.L., Rawlinson, S.C., Suswillo, R., and Lanyon, L.E. (1990). Cellular responses to mechanical loading in vitro. J Bone Miner Res *5*, 923-932.
139. David, V., Martin, A., Lafage-Proust, M.H., Malaval, L., Peyroche, S., Jones, D.B., Vico, L., and Guignandon, A. (2007). Mechanical loading down-regulates peroxisome proliferator-activated receptor gamma in bone marrow stromal cells and favors osteoblastogenesis at the expense of adipogenesis. Endocrinology *148*, 2553-2562.
140. Sumpio, B.E., Banes, A.J., Levin, L.G., and Johnson, G., Jr. (1987). Mechanical stress stimulates aortic endothelial cells to proliferate. J Vasc Surg *6*, 252-256.
141. Yamawaki, H., Pan, S., Lee, R.T., and Berk, B.C. (2005). Fluid shear stress inhibits vascular inflammation by decreasing thioredoxin-interacting protein in endothelial cells. J Clin Invest *115*, 733-738.
142. Davies, P.F., Dewey, C.F., Jr., Bussolari, S.R., Gordon, E.J., and Gimbrone, M.A., Jr. (1984). Influence of hemodynamic forces on vascular endothelial function. In vitro studies of shear stress and pinocytosis in bovine aortic cells. J Clin Invest *73*, 1121-1129.
143. Haudenschild, C.C., Grunwald, J., and Chobanian, A.V. (1985). Effects of hypertension on migration and proliferation of smooth muscle in culture. Hypertension *7*, I101-104.
144. Tzima, E., Irani-Tehrani, M., Kiosses, W.B., Dejana, E., Schultz, D.A., Engelhardt, B., Cao, G., DeLisser, H., and Schwartz, M.A. (2005). A mechanosensory complex that mediates the endothelial cell response to fluid shear stress. Nature *437*, 426-431.
145. Harris, A.K., Wild, P., and Stopak, D. (1980). Silicone rubber substrata: a new wrinkle in the study of cell locomotion. Science *208*, 177-179.
146. Harris, A.K., Stopak, D., and Wild, P. (1981). Fibroblast traction as a mechanism for collagen morphogenesis. Nature *290*, 249-251.
147. Renkawitz, J., and Sixt, M. (2010). Mechanisms of force generation and force transmission during interstitial leukocyte migration. EMBO Rep. *11*, 744-750.
148. Civelekoglu-Scholey, G., and Scholey, J. (2010). Mitotic force generators and chromosome segregation. Cellular and Molecular Life Sciences *67*, 2231-2250.
149. Wang, N., Butler, J.P., and Ingber, D.E. (1993). Mechanotransduction across the cell surface and through the cytoskeleton. Science *260*, 1124-1127.
150. Sheetz, M. (1996). Microtubule Motor Complexes Moving Membranous Organelles. Cell Structure and Function *5*, 369-373.
151. Sims, J.R., Karp, S., and Ingber, D.E. (1992). Altering the cellular mechanical force balance results in integrated changes in cell, cytoskeletal and nuclear shape. J Cell Sci *103 (Pt 4)*, 1215-1222.
152. Vicente-Manzanares, M., Ma, X., Adelstein, R.S., and Horwitz, A.R. (2009). Non-muscle myosin II takes centre stage in cell adhesion and migration. Nat Rev Mol Cell Biol *10*, 778-790.
153. Dogterom, M., Kerssemakers, J.W.J., Romet-Lemonne, G., and Janson, M.E. (2005). Force generation by dynamic microtubules. Current Opinion in Cell Biology *17*, 67-74.

154. Vicente-Manzanares, M., Koach, M.A., Whitmore, L., Lamers, M.L., and Horwitz, A.F. (2008). Segregation and activation of myosin IIB creates a rear in migrating cells. J. Cell Biol. *183*, 543-554.
155. Zimerman, B., Volberg, T., and Geiger, B. (2004). Early molecular events in the assembly of the focal adhesion-stress fiber complex during fibroblast spreading. Cell Motil Cytoskeleton *58*, 143-159.
156. Choi, C.K. (2008). Actin and [alpha]-actinin orchestrate the assembly and maturation of nascent adhesions in a myosin II motor-independent manner. Nature Cell Biol. *10*, 1039-1050.
157. Krammer, A., Lu, H., Isralewitz, B., Schulten, K., and Vogel, V. (1999). Forced unfolding of the fibronectin type III module reveals a tensile molecular recognition switch. Proceedings of the National Academy of Sciences *96*, 1351-1356.
158. Wipff, P.-J., Rifkin, D.B., Meister, J.-J., and Hinz, B. (2007). Myofibroblast contraction activates latent TGF-β1 from the extracellular matrix. The Journal of Cell Biology *179*, 1311-1323.
159. Lammerding, J., Schulze, P.C., Takahashi, T., Kozlov, S., Sullivan, T., Kamm, R.D., Stewart, C.L., and Lee, R.T. (2004). Lamin A/C deficiency causes defective nuclear mechanics and mechanotransduction. The Journal of Clinical Investigation *113*, 370-378.
160. Chancellor, T.J., Lee, J., Thodeti, C.K., and Lele, T. (2010). Actomyosin Tension Exerted on the Nucleus through Nesprin-1 Connections Influences Endothelial Cell Adhesion, Migration, and Cyclic Strain-Induced Reorientation. Biophysical Journal *99*, 115-123.
161. Johnson, C.P., Tang, H.-Y., Carag, C., Speicher, D.W., and Discher, D.E. (2007). Forced Unfolding of Proteins Within Cells. Science *317*, 663-666.
162. del Rio, A. (2009). Stretching single talin rod molecules activates vinculin binding. Science *323*, 638-641.
163. Sawada, Y. (2006). Force sensing by mechanical extension of the Src family kinase substrate p130Cas. Cell *127*, 1015-1026.
164. Sadoshima, J., Takahashi, T., Jahn, L., and Izumo, S. (1992). Roles of mechano-sensitive ion channels, cytoskeleton, and contractile activity in stretch-induced immediate-early gene expression and hypertrophy of cardiac myocytes. Proceedings of the National Academy of Sciences *89*, 9905-9909.
165. Lansman, J.B., Hallam, T.J., and Rink, T.J. (1987). Single stretch-activated ion channels in vascular endothelial cells as mechanotransducers? Nature *325*, 811-813.
166. Matthews, D., Thodeti, C., Tytell, J., Mammoto, A., Overby, D., and Ingber, D. (2010). Ultra-rapid activation of TRPV4 ion channels by mechanical forces applied to cell surface β1 integrins. Integr Biol *2*, 435-442.
167. Parsons, J.T., Horwitz, A.R., and Schwartz, M.A. (2010). Cell adhesion: integrating cytoskeletal dynamics and cellular tension. Nat Rev Mol Cell Biol *11*, 633-643.
168. Zaidel-Bar, R., Milo, R., Kam, Z., and Geiger, B. (2007). A paxillin tyrosine phosphorylation switch regulates the assembly and form of cell-matrix adhesions. J Cell Sci *120*, 137-148.

169. Friedland, J.C., Lee, M.H., and Boettiger, D. (2009). Mechanically activated integrin switch controls [alpha]5[beta]1 function. Science *323*, 642-644.
170. Rid, R., Schiefermeier, N., Grigoriev, I., Small, J.V., and Kaverina, I. (2005). The last but not the least: the origin and significance of trailing adhesions in fibroblastic cells. Cell Motil Cytoskeleton *61*, 161-171.
171. Kirfel, G., Rigort, A., Borm, B., and Herzog, V. (2004). Cell migration: mechanisms of rear detachment and the formation of migration tracks. Eur J Cell Biol *83*, 717-724.
172. Wozniak, M.A., Desai, R., Solski, P.A., Der, C.J., and Keely, P.J. (2003). ROCK-generated contractility regulates breast epithelial cell differentiation in response to the physical properties of a three-dimensional collagen matrix. The Journal of Cell Biology *163*, 583-595.
173. Chen, C., Mrksich, M., Huang, S., Whitesides, G., and Ingber, D. (1997). Geometric control of cell life and death. Science *276*, 1425-1428.
174. Pirone, D.M., Liu, W.F., Ruiz, S.A., Gao, L., Raghavan, S., Lemmon, C.A., Romer, L.H., and Chen, C.S. (2006). An inhibitory role for FAK in regulating proliferation: a link between limited adhesion and RhoA-ROCK signaling. The Journal of Cell Biology *174*, 277-288.
175. Paszek, M.J., Zahir, N., Johnson, K.R., Lakins, J.N., Rozenberg, G.I., Gefen, A., Reinhart-King, C.A., Margulies, S.S., Dembo, M., Boettiger, D., et al. (2005). Tensional homeostasis and the malignant phenotype. Cancer Cell *8*, 241-254.
176. Paszek, M.J., and Weaver, V.M. (2004). The Tension Mounts: Mechanics Meets Morphogenesis and Malignancy. Journal of Mammary Gland Biology and Neoplasia *9*, 325-342.
177. Levental, K.R., Yu, H., Kass, L., Lakins, J.N., Egeblad, M., Erler, J.T., Fong, S.F.T., Csiszar, K., Giaccia, A., Weninger, W., et al. (2009). Matrix Crosslinking Forces Tumor Progression by Enhancing Integrin Signaling. Cell *139*, 891-906.
178. Ingber, D.E., Prusty, D., Sun, Z., Betensky, H., and Wang, N. (1995). Cell shape, cytoskeletal mechanics, and cell cycle control in angiogenesis. Journal of biomechanics *28*, 1471-1484.
179. Yamada, S., Pokutta, S., Drees, F., Weis, W.I., and Nelson, W.J. (2005). Deconstructing the Cadherin-Catenin-Actin Complex. Cell *123*, 889-901.
180. Smutny, M., Cox, H.L., Leerberg, J.M., Kovacs, E.M., Conti, M.A., Ferguson, C., Hamilton, N.A., Parton, R.G., Adelstein, R.S., and Yap, A.S. (2010). Myosin II isoforms identify distinct functional modules that support integrity of the epithelial zonula adherens. Nat Cell Biol *12*, 696-702.
181. Liu, Z., Tan, J.L., Cohen, D.M., Yang, M.T., Sniadecki, N.J., Ruiz, S.A., Nelson, C.M., and Chen, C.S. (2010). Mechanical tugging force regulates the size of cell-cell junctions. Proc Natl Acad Sci U S A *107*, 9944-9949.
182. le Duc, Q., Shi, Q., Blonk, I., Sonnenberg, A., Wang, N., Leckband, D., and de Rooij, J. (2010). Vinculin potentiates E-cadherin mechanosensing and is recruited to actin-anchored sites within adherens junctions in a myosin II-dependent manner. J Cell Biol *189*, 1107-1115.
183. Yonemura, S., Wada, Y., Watanabe, T., Nagafuchi, A., and Shibata, M. (2010). [alpha]-Catenin as a tension transducer that induces adherens junction development. Nat Cell Biol *12*, 533-542.

184. Nakagawa, M., Fukata, M., Yamaga, M., Itoh, N., and Kaibuchi, K. (2001). Recruitment and activation of Rac1 by the formation of E-cadherin-mediated cell-cell adhesion sites. J Cell Sci *114*, 1829-1838.
185. Wildenberg, G.A., Dohn, M.R., Carnahan, R.H., Davis, M.A., Lobdell, N.A., Settleman, J., and Reynolds, A.B. (2006). p120-catenin and p190RhoGAP regulate cell-cell adhesion by coordinating antagonism between Rac and Rho. Cell *127*, 1027-1039.
186. Nelson, C.M., Vanduijn, M.M., Inman, J.L., Fletcher, D.A., and Bissell, M.J. (2006). Tissue geometry determines sites of mammary branching morphogenesis in organotypic cultures. Science *314*, 298-300.
187. Gjorevski, N., and Nelson, C.M. (2010). Endogenous patterns of mechanical stress are required for branching morphogenesis. Integr Biol (Camb) *2*, 424-434.
188. Dembo, M., and Wang, Y.-L. (1999). Stresses at the Cell-to-Substrate Interface during Locomotion of Fibroblasts. Biophysical Journal *76*, 2307-2316.
189. Butler, J.P., Tolic-Norrelykke, I.M., Fabry, B., and Fredberg, J.J. (2002). Traction fields, moments, and strain energy that cells exert on their surroundings. Am J Physiol Cell Physiol *282*, C595-605.
190. Yang, Z., Lin, J.S., Chen, J., and Wang, J.H. (2006). Determining substrate displacement and cell traction fields--a new approach. J Theor Biol *242*, 607-616.
191. Tan, J.L., Tien, J., Pirone, D.M., Gray, D.S., Bhadriraju, K., and Chen, C.S. (2003). Cells lying on a bed of microneedles: An approach to isolate mechanical force. Proceedings of the National Academy of Sciences *100*, 1484-1489.
192. du Roure, O., Saez, A., Buguin, A., Austin, R.H., Chavrier, P., Siberzan, P., and Ladoux, B. (2005). Force mapping in epithelial cell migration. Proceedings of the National Academy of Sciences of the United States of America *102*, 2390-2395.
193. Balaban, N.Q., Schwarz, U.S., Riveline, D., Goichberg, P., Tzur, G., Sabanay, I., Mahalu, D., Safran, S., Bershadsky, A., Addadi, L., et al. (2001). Force and focal adhesion assembly: a close relationship studied using elastic micropatterned substrates. Nat Cell Biol *3*, 466-472.
194. Nelson, C.M., and Chen, C.S. (2002). Cell-cell signaling by direct contact increases cell proliferation via a PI3K-dependent signal. FEBS Letters *514*, 238-242.
195. Chanson, L., Brownfield, D., Garbe, J.C., Kuhn, I., Stampfer, M.R., Bissell, M.J., and LaBarge, M.A. (2011). Self-organization is a dynamic and lineage-intrinsic property of mammary epithelial cells. Proceedings of the National Academy of Sciences *108*, 3264-3269.
196. Alenghat, F.J., Fabry, B., Tsai, K.Y., Goldmann, W.H., and Ingber, D.E. (2000). Analysis of cell mechanics in single vinculin-deficient cells using a magnetic tweezer. Biochemical and Biophysical Research Communications *277*, 93-99.
197. Matthews, B.D., Overby, D.R., Alenghat, F.J., Karavitis, J., Numaguchi, Y., Allen, P.G., and Ingber, D.E. (2004). Mechanical properties of individual focal adhesions probed with a magnetic microneedle. Biochemical and Biophysical Research Communications *313*, 758-764.
198. Asbury, C.L., Fehr, A.N., and Block, S.M. (2003). Kinesin moves by an asymmetric hand-over-hand mechanism. Science *302*, 2130.

199. Altman, D., Sweeney, H.L., and Spudich, J.A. (2004). The mechanism of myosin VI translocation and its load-induced anchoring. Cell *116*, 737-749.
200. Gross, S.P., Welte, M.A., Block, S.M., and Wieschaus, E.F. (2000). Dynein-mediated cargo transport in vivo. The Journal of Cell Biology *148*, 945-956.
201. Choquet, D., Felsenfeld, D.P., and Sheetz, M.P. (1997). Extracellular matrix rigidity causes strengthening of integrin-cytoskeleton linkages. Cell *88*, 39-48.
202. Chaudhuri, O., Parekh, S.H., Lam, W.A., and Fletcher, D.A. (2009). Combined atomic force microscopy and side-view optical imaging for mechanical studies of cells. Nature Methods *6*, 383-387.
203. Rosenbluth, M.J., Lam, W.A., and Fletcher, D.A. (2006). Force microscopy of nonadherent cells: a comparison of leukemia cell deformability. Biophysical Journal *90*, 2994-3003.
204. Webster, K.D., Crow, A., and Fletcher, D.A. (2011). An AFM-based stiffness clamp for dynamic control of rigidity. PLoS ONE *6*, e17807.
205. Rief, M., Pascual, J., Saraste, M., and Gaub, H.E. (1999). Single molecule force spectroscopy of spectrin repeats: low unfolding forces in helix bundles1. Journal of molecular biology *286*, 553-561.
206. Puech, P.H., Poole, K., Knebel, D., and Muller, D.J. (2006). A new technical approach to quantify cell-cell adhesion forces by AFM. Ultramicroscopy *106*, 637-644.
207. Steinberg, M.S. (1962). On the mechanism of tissue reconstruction by dissociated cells. I. Population kinetics, differential adhesiveness. and the absence of directed migration. Proc Natl Acad Sci U S A *48*, 1577-1582.
208. Steinberg, M.S. (1962). On the Mechanism of Tissue Reconstruction by Dissociated Cells, Iii. Free Energy Relations and the Reorganization of Fused, Heteronomic Tissue Fragments. Proc Natl Acad Sci U S A *48*, 1769-1776.
209. Steinberg, M.S. (1962). Mechanism of tissue reconstruction by dissociated cells. II. Time-course of events. Science *137*, 762-763.
210. Townes, P., and Holtfreter, J. (1955). Directed movements and selective adhesion of embryonic amphibian cells. J Exp Zool *128*, 53-120.
211. Wei, C., Larsen, M., Hoffman, M.P., and Yamada, K.M. (2007). Self-organization and branching morphogenesis of primary salivary epithelial cells. Tissue Eng *13*, 721-735.
212. Krieg, M., Arboleda-Estudillo, Y., Puech, P.H., Käfer, J., Graner, F., Müller, D., and Heisenberg, C.P. (2008). Tensile forces govern germ-layer organization in zebrafish. Nature Cell Biology *10*, 429-436.
213. Foty, R.A., and Steinberg, M.S. (2004). Cadherin-mediated cell-cell adhesion and tissue segregation in relation to malignancy. International Journal of Developmental Biology *48*, 397-410.
214. Foty, R.A., and Steinberg, M.S. (2005). The differential adhesion hypothesis: a direct evaluation. Developmental Biology *278*, 255-263.
215. Manning, M.L., Foty, R.A., Steinberg, M.S., and Schoetz, E.M. (2010). Coaction of intercellular adhesion and cortical tension specifies tissue surface tension. Proceedings of the National Academy of Sciences *107*, 12517.
216. Garbe, J.C., Bhattacharya, S., Merchant, B., Bassett, E., Swisshelm, K., Feiler, H.S., Wyrobek, A.J., and Stampfer, M.R. (2009). Molecular distinctions between

stasis and telomere attrition senescence barriers shown by long-term culture of normal human mammary epithelial cells. Cancer research *69*, 7557.
217. Stampfer, M.R., and Bartley, J.C. (1985). Induction of transformation and continuous cell lines from normal human mammary epithelial cells after exposure to benzo [a] pyrene. Proceedings of the National Academy of Sciences *82*, 2394.
218. Tan, J.L., Liu, W., Nelson, C.M., Raghavan, S., and Chen, C.S. (2004). Simple approach to micropattern cells on common culture substrates by tuning substrate wettability. Tissue engineering *10*, 865-872.
219. Hertz, H. (1882). Uber die Beruhung fester elastischer Korper. [in German]. J. Reine Angew. Mathematik *92*, 156-171.
220. Bilodeau, G. (1992). Regular pyramid punch problem. J. Applied Mech *59*, 519-523.
221. Villadsen, R., Fridriksdottir, A.J., Ronnov-Jessen, L., Gudjonsson, T., Rank, F., LaBarge, M.A., Bissell, M.J., and Petersen, O.W. (2007). Evidence for a stem cell hierarchy in the adult human breast. J Cell Biol *177*, 87-101.
222. Gumbiner, B.M. (2005). Regulation of cadherin-mediated adhesion in morphogenesis. Nat Rev Mol Cell Biol *6*, 622-634.
223. Shimoyama, Y., Hirohashi, S., Hirano, S., Noguchi, M., Shimosato, Y., Takeichi, M., and Abe, O. (1989). Cadherin Cell-Adhesion Molecules in Human Epithelial Tissues and Carcinomas. Cancer research *49*, 2128-2133.
224. Shi, Q., Chien, Y.H., and Leckband, D. (2008). Biophysical properties of cadherin bonds do not predict cell sorting. Journal of Biological Chemistry *283*, 28454.
225. Vargo-Gogola, T., Heckman, B.M., Gunther, E.J., Chodosh, L.A., and Rosen, J.M. (2006). P190-B Rho GTPase-Activating Protein Overexpression Disrupts Ductal Morphogenesis and Induces Hyperplastic Lesions in the Developing Mammary Gland. Molecular Endocrinology *20*, 1391-1405.
226. Ewald, A.J., Brenot, A., Duong, M., Chan, B.S., and Werb, Z. (2008). Collective Epithelial Migration and Cell Rearrangements Drive Mammary Branching Morphogenesis. Developmental cell *14*, 570-581.
227. Makishima, M., Honma, Y., Hozumi, M., Sampi, K., Hattori, M., and Motoyoshi, K. (1991). Induction of differentiation of human leukemia cells by inhibitors of myosin light chain kinase. FEBS Lett *287*, 175-177.
228. Davies, S.P., Reddy, H., Caivano, M., and Cohen, P. (2000). Specificity and mechanism of action of some commonly used protein kinase inhibitors. Biochem. J. *351*, 95-105.
229. Fukata, M., and Kaibuchi, K. (2001). Rho-family GTPases in cadherin-mediated cell [mdash] cell adhesion. Nat Rev Mol Cell Biol *2*, 887-897.
230. Sahai, E., and Marshall, C.J. (2002). ROCK and Dia have opposing effects on adherens junctions downstream of Rho. Nat Cell Biol *4*, 408-415.
231. Borghi, N., and James Nelson, W. (2009). Chapter 1 Intercellular Adhesion in Morphogenesis: Molecular and Biophysical Considerations. In Current Topics in Developmental Biology, Volume Volume 89, L. Thomas, ed. (Academic Press), pp. 1-32.

232. Runswick, S.K., O'Hare, M.J., Jones, L., Streuli, C.H., and Garrod, D.R. (2001). Desmosomal adhesion regulates epithelial morphogenesis and cell positioning. Nat Cell Biol *3*, 823-830.
233. Zhang, X., Hashemi, S.S., Yousefi, M., Gao, C., Sheng, J., Ni, J., Wang, W., Mason, J., and Man, Y.-g. (2009). Atypical E-cadherin expression in cell clusters overlying focally disrupted mammary myoepithelial cell layers: Implications for tumor cell motility and invasion. Pathology - Research and Practice *205*, 375-385.
234. Korkola, J.E., DeVries, S., Fridlyand, J., Hwang, E.S., Estep, A.L., Chen, Y.Y., Chew, K.L., Dairkee, S.H., Jensen, R.M., and Waldman, F.M. (2003). Differentiation of lobular versus ductal breast carcinomas by expression microarray analysis. Cancer Res *63*, 7167-7175.
235. Moll, R., Mitze, M., Frixen, U.H., and Birchmeier, W. (1993). Differential loss of E-cadherin expression in infiltrating ductal and lobular breast carcinomas. Am J Pathol *143*, 1731-1742.
236. Cano, A., Perez-Moreno, M.A., Rodrigo, I., Locascio, A., Blanco, M.J., del Barrio, M.G., Portillo, F., and Nieto, M.A. (2000). The transcription factor snail controls epithelial-mesenchymal transitions by repressing E-cadherin expression. Nat Cell Biol *2*, 76-83.
237. LaBarge, M.A., Nelson, C.M., Villadsen, R., Fridriksdottir, A., Ruth, J.R., Stampfer, M.R., Petersen, O.W., and Bissell, M.J. (2009). Human mammary progenitor cell fate decisions are products of interactions with combinatorial microenvironments. Integr Biol (Camb) *1*, 70-79.
238. Provenzano, P.P., Eliceiri, K.W., Campbell, J.M., Inman, D.R., White, J.G., and Keely, P.J. (2006). Collagen reorganization at the tumor-stromal interface facilitates local invasion. BMC Med *4*, 38.
239. Wolf, K., Wu, Y.I., Liu, Y., Geiger, J., Tam, E., Overall, C., Stack, M.S., and Friedl, P. (2007). Multi-step pericellular proteolysis controls the transition from individual to collective cancer cell invasion. Nat Cell Biol *9*, 893-904.
240. Gudjonsson, T., Rønnov-Jessen, L., Villadsen, R., Rank, F., Bissell, M.J., and Petersen, O.W. (2002). Normal and tumor-derived myoepithelial cells differ in their ability to interact with luminal breast epithelial cells for polarity and basement membrane deposition. Journal of Cell Science *115*, 39-50.
241. Xu, R., Spencer, V.A., and Bissell, M.J. (2007). Extracellular matrix-regulated gene expression requires cooperation of SWI/SNF and transcription factors. J Biol Chem *282*, 14992-14999.
242. Streuli, C.H., Bailey, N., and Bissell, M.J. (1991). Control of mammary epithelial differentiation: basement membrane induces tissue-specific gene expression in the absence of cell-cell interaction and morphological polarity. The Journal of Cell Biology *115*, 1383-1395.
243. Gjorevski, N., and Nelson, C.M. (2010). Branch formation during organ development. Wiley Interdiscip Rev Syst Biol Med *2*, 734-741.
244. Desprez, P., Roskelley, C., Campisi, J., and Bissell, M. (1993). Isolation of functional cell lines from a mouse mammary epithelial cell strain: the importance of basement membrane and cell-cell interaction. Mol. Cell. Differ *1*, 99-110.

245. Pujuguet, P., Radisky, D., Levy, D., Lacza, C., and Bissell, M.J. (2001). Trichostatin A inhibits beta-casein expression in mammary epithelial cells. J Cell Biochem *83*, 660-670.
246. Muschler, J., Lochter, A., Roskelley, C.D., Yurchenco, P., and Bissell, M.J. (1999). Division of labor among the alpha6beta4 integrin, beta1 integrins, and an E3 laminin receptor to signal morphogenesis and beta-casein expression in mammary epithelial cells. Mol Biol Cell *10*, 2817-2828.
247. Pelham, R.J., and Wang, Y. (1997). Cell locomotion and focal adhesions are regulated by substrate flexibility. Proceedings of the National Academy of Sciences *94*, 13661.
248. Alcaraz, J., Buscemi, L., Grabulosa, M., Trepat, X., Fabry, B., Farré, R., and Navajas, D. (2003). Microrheology of human lung epithelial cells measured by atomic force microscopy. Biophysical Journal *84*, 2071-2079.
249. Roca-Cusachs, P., Alcaraz, J., Sunyer, R., Samitier, J., Farré, R., and Navajas, D. (2008). Micropatterning of single endothelial cell shape reveals a tight coupling between nuclear volume in G1 and proliferation. Biophysical Journal *94*, 4984-4995.
250. Fata, J.E., Mori, H., Ewald, A.J., Zhang, H., Yao, E., Werb, Z., and Bissell, M.J. (2007). The MAPKERK-1,2 pathway integrates distinct and antagonistic signals from TGFα and FGF7 in morphogenesis of mouse mammary epithelium. Developmental Biology *306*, 193-207.
251. Krahn, K.N., Bouten, C.V., van Tuijl, S., van Zandvoort, M.A., and Merkx, M. (2006). Fluorescently labeled collagen binding proteins allow specific visualization of collagen in tissues and live cell culture. Anal Biochem *350*, 177-185.
252. Boerboom, R.A., Krahn, K.N., Megens, R.T., van Zandvoort, M.A., Merkx, M., and Bouten, C.V. (2007). High resolution imaging of collagen organisation and synthesis using a versatile collagen specific probe. J Struct Biol *159*, 392-399.
253. Ng, C.P. (2005). Interstitial fluid flow induces myofibroblast differentiation and collagen alignment in vitro. Journal of Cell Science *118*, 4731-4739.
254. Roskelley, C.D., Desprez, P.Y., and Bissell, M.J. (1994). Extracellular matrix-dependent tissue-specific gene expression in mammary epithelial cells requires both physical and biochemical signal transduction. Proceedings of the National Academy of Sciences *91*, 12378-12382.
255. Le Beyec, J., Xu, R., Lee, S.Y., Nelson, C.M., Rizki, A., Alcaraz, J., and Bissell, M.J. (2007). Cell shape regulates global histone acetylation in human mammary epithelial cells. Experimental Cell Research *313*, 3066-3075.
256. Alcaraz, J., Nelson, C.M., and Bissell, M.J. (2004). Biomechanical approaches for studying integration of tissue structure and function in mammary epithelia. Journal of Mammary Gland Biology and Neoplasia *9*, 361-374.
257. Klinowska, T., Soriano, J.V., Edwards, G.M., Oliver, J.M., Valentijn, A.J., Montesano, R., and Streuli, C.H. (1999). Laminin and [beta] 1 integrins are crucial for normal mammary gland development in the mouse. Developmental Biology *215*, 13-32.
258. Wetzels, R., Holland, R., Van Haelst, U., Lane, E.B., Leigh, I., and Ramaekers, F. (1989). Detection of basement membrane components and basal cell keratin 14 in

noninvasive and invasive carcinomas of the breast. The American journal of pathology *134*, 571.
259. Simian, M., Hirai, Y., Navre, M., Werb, Z., Lochter, A., and Bissell, M.J. (2001). The interplay of matrix metalloproteinases, morphogens and growth factors is necessary for branching of mammary epithelial cells. Development *128*, 3117-3131.
260. MacKintosh, F., Käs, J., and Janmey, P. (1995). Elasticity of semiflexible biopolymer networks. Physical review letters *75*, 4425-4428.
261. Ingber, E. (2003). Mechanobiology and diseases of mechanotransduction. Annals of Medicine *35*, 564-577.
262. Engler, A., Bacakova, L., Newman, C., Hategan, A., Griffin, M., and Discher, D. (2004). Substrate compliance versus ligand density in cell on gel responses. Biophysical Journal *86*, 617-628.
263. Solon, J., Levental, I., Sengupta, K., Georges, P.C., and Janmey, P.A. (2007). Fibroblast adaptation and stiffness matching to soft elastic substrates. Biophysical Journal *93*, 4453-4461.
264. Friedl, P., and Wolf, K. (2003). Tumour-cell invasion and migration: diversity and escape mechanisms. Nature Reviews Cancer *3*, 362-374.
265. Pathak, A., and Kumar, S. (2011). Biophysical regulation of tumor cell invasion: moving beyond matrix stiffness. Integr. Biol.
266. Engler, A.J., Sen, S., Sweeney, H.L., and Discher, D.E. (2006). Matrix Elasticity Directs Stem Cell Lineage Specification. Cell *126*, 677-689.
267. Gehler, S., Baldassarre, M., Lad, Y., Leight, J.L., Wozniak, M.A., Riching, K.M., Eliceiri, K.W., Weaver, V.M., Calderwood, D.A., and Keely, P.J. (2009). Filamin A–β1 integrin complex tunes epithelial cell response to matrix tension. Molecular biology of the cell *20*, 3224-3238.
268. Montesano, R., Carrozzino, F., and Soulié, P. (2007). Low concentrations of transforming growth factor-beta-1 induce tubulogenesis in cultured mammary epithelial cells. BMC developmental biology *7*, 7.